Understanding avalanche systems through underlying interface dynamics

Chun-Chung Chen

A dissertation submitted in partial fulfillment
of the requirements for the degree of

Doctor of Philosophy

University of Washington

2002

Program Authorized to Offer Degree: Physics

University of Washington

Graduate School

This is to certify that I have examined this copy of a doctoral dissertation by

Chun-Chung Chen

and have found that it is complete and satisfactory in all respects,
and that any and all revisions required by the final
examining committee have been made.

Chair of Supervisory Committee:

_____

Marcel den Nijs

Reading Committee:

_____

Larry Sorensen

_____

Laurence Yaffe

Date: _____

In presenting this dissertation in partial fulfillment of the requirements for the Doctoral degree at the University of Washington, I agree that the Library shall make its copies freely available for inspection. I further agree that extensive copying of this dissertation is allowable only for scholarly purposes, consistent with "fair use" as prescribed in the U.S. Copyright Law. Requests for copying or reproduction of this dissertation may be referred to Bell and Howell Information and Learning, 300 North Zeeb Road, Ann Arbor, MI 48106-1346, to whom the author has granted "the right to reproduce and sell (a) copies of the manuscript in microform and/or (b) printed copies of the manuscript made from microform."

Signature_____

Date_____

University of Washington

Abstract

Understanding avalanche systems through underlying interface dynamics

by Chun-Chung Chen

Chair of Supervisory Committee:

Professor Marcel den Nijs
Department of Physics

Nonequilibrium systems are often described by dynamic rules instead of Hamiltonians. Among them are those defined by local dynamic rules, e.g., interface growth models; and those defined by nonlocal rules, e.g., avalanche models. In this thesis, a mapping between these two kinds of systems is presented so that one can make predictions for latter based on the knowledge the former. The nonlocal iterative dynamics of the specific models that are discussed here involve sizable corrections to finite-size scaling. It is established that these corrections are irrelevant in the sense of renormalization group transformation and the scaling behaviors of the avalanche systems in the thermodynamic limit are still described by their underlying interface dynamics. The implications of a directed percolation roughening phase transition in the underlying interface dynamics is investigated. It is found that this leads to a deepening transition in avalanche systems. The critical exponent relations remain valid in both the deep and the shallow avalanche phases. However, the hyperscaling relation for mass established through the compactness of the avalanche clusters is broken at the transition point due to the fractal structure of the avalanche clusters at the transition point.

TABLE OF CONTENTS

List of Figures **iv**

Chapter 1: Introduction **1**

1.1 Criticality in nature 5

1.1.1 Continuous phase transition 6

1.1.2 Gutenberg-Richter relation of earthquake distribution 7

1.1.3 Spring block model of earthquake fault 10

1.2 Sandpile as a paradigm to self-organized criticality 11

1.2.1 The BTW Sandpile model 11

1.2.2 Critical state of Abelian Sandpile model 14

1.2.3 Directed sandpile model 15

1.2.4 Stochastic directed sandpile model 17

1.3 Kinetic roughening of interface growth 21

1.3.1 Continuous equations for interface growth 24

1.3.2 Edwards-Wilkinson growth equation 24

1.3.3 Kardar-Parisi-Zhang growth equation 26

1.3.4 Renormalization flow for the KPZ equation 28

1.4 Directed percolation 30

1.4.1 Kinzel's model 30

1.4.2 DP scaling exponents 31

1.5 A Lattice model: step flow with random deposition 32

1.5.1 Numerical results 33

1.5.2 Corrections to scaling 35

1.6 A surface roughening transition in one dimension 36

1.6.1 Mapping to Kinzel's model . . . 37
1.6.2 Scaling at the transition point . . . 37
1.7 Propagation of avalanche front . . . 38
1.8 Summary and preview . . . 39

Chapter 2: Directed avalanche processes with underlying interface dynamics 41

2.1 Introduction . . . 41
2.2 An unloading sandbox . . . 44
2.3 Avalanches versus epitaxial interface growth . . . 48
2.4 KPZ growth . . . 49
2.5 Scaling properties of 2D avalanches . . . 53
2.6 Numerical results for 2D sandbox avalanches . . . 55
2.7 Avalanche-correlated MC runs . . . 59
2.8 Surface rounding in the 1D unloading sandbox . . . 66
2.9 Avalanche rounding near the driving edge in 2D . . . 69
2.10 Summary . . . 73

Chapter 3: Deepening transition of avalanches 75

3.1 Introduction . . . 75
3.2 Tunable parameter for cohesion . . . 76
3.3 Discrete height sandbox model . . . 77
3.4 Underlying interface dynamics . . . 78
3.5 Deterministic limits . . . 81
3.5.1 Domain walls at $p = 0$ . . . 81
3.5.2 Exact solution at $p = 1$ . . . 83
3.6 Shallow-avalanche phase . . . 85
3.7 DP roughening transition . . . 85
3.7.1 Breakdown of mass hyperscaling . . . 87

3.7.2 Interface roughness 91
3.8 Summary 93

Bibliography **94**

Appendix A: Active width at a slanted active boundary in directed percolation **106**

A.1 Introduction 106
A.2 Numerical results for the curtain width 109
A.3 Independent Cluster Approximation 112
A.4 Logarithmic corrections to scaling analysis 114
A.5 Finite-size scaling at the percolation threshold 115
A.6 Final Remarks 117

LIST OF FIGURES

1.1 A typical 2D phase-space and renormalization flows (for the Heisenberg model with uniaxial anisotropy from [20]); The black dots are the fixed points and arrows are the directions of renormalization flows. The dashed line represents the trace of a typical experiment as the temperature is varied. 8

1.2 Earthquake magnitude distributions for world average in a year (solid line) and in South California from 1987 to 1996 (dashed line) with data obtained from the South California Earthquake Data Center; Both are showing similar power-law decay. 9

1.3 A spring block system for the modeling of an earthquake fault; The blocks on a frictional fixed plate are connected to each other with coil springs while each block is connected to the slow moving top plate with a leaf spring. . . . 10

1.4 Cluster size (a) and lifetime (b) distributions of avalanches, coarse grained, on a 50×50 array, averaged over 200 samples of the BTW model; The dashed line in (a) shows a power-law decay of s^{-1} and the dashed line in (b) shows a power-law decay of $t^{-}0.43$. These plots are taken from [5] 13

1.5 A typical avalanche cluster (sites participated in the toppling) in stochastic directed sandpile model; It's essentially compact in the sense that while holes of inactive regions are visible near the boundary, their sizes do not scale with the cluster size. The size of the box shown is $L_x \times L_y = 360 \times 8833$. 18

1.6 Growth of a Eden cluster from the bottom $y = 0$ row on a strip geometry: $0 \leq x < L_x$, $y \geq 0$ with $L_x = 800$; Each separately shaded region represents the growth of an area of 20000 lattice sites. As the interface grows upward, it becomes rougher and rougher. 23

1.7 Lattice structure of Kinzel's model [68]; Circles are the sites while the arrows represent bonds. It is a square lattice tilted diagonally with activities propagate upward. 31
1.8 Two stage growth rule for the step flow + random deposition model; a. The step flow, from solid line to dashed line ; b. The deposition, from dashed line to solid line; before the growth step, heights are defined on even number sites while after the growth step, heights are defined on odd number sites 34
1.9 Finite-size-scaling (FSS) estimates of the α exponent, defined by Eq. (1.18) and the β exponent, defined by Eq. (1.17) from Monte Carlo (MC) results of the step-flow random-deposition (SFRD) model; Solid lines are of the continuous height version which dashed lines are of the discrete height version 35

2.1 Sandbox with a slowly lowering retaining wall. 45
2.2 Lattice structure of sandbox model in 2D. 46
2.3 The interface growth dynamics described by Eq. (2.3) with upper panel showing movement of steps (from the drawn to dashed line) and lower panel random depositions (shaded area) to the interface. 50
2.4 MC results for the global interface width: left, finite-size (L_x, in the unit of lattice spacing) estimates for the saturated surface width exponent α; right, finite-time (t, in MC time steps) estimates for the transient interface width exponent β from a flat initial configuration. The solid (dashed) curves are for continuous (discrete) height model. 52
2.5 FSS plots for the τ exponents of 2D sandbox model. The solid (dashed) lines are for continuous (discrete) height model. 56
2.6 Effective scaling exponents derived from stationary avalanche distributions of sandbox systems. The solid (dashed) lines are for continuous (discrete) height model. 58
2.7 Effective scaling exponents derived from the distributions of first avalanches on fresh sandbox surface for the continuous height model. 61

2.8 Upper panel: The interface width (squared) for sandbox surface (solid lines) and the same for an ensemble of fresh surface (dashed lines); Lower panel: The difference between the two, with $L_x = 8$, 16, 32, 64, 128 and ∞ (from bottom up) the box size in the direction parallel to the driving edge. 62

2.9 A typical configuration of the scars on the sandbox created by the avalanches. The driving edge is located at the bottom of the graph while avalanches propagate upward in the y (or t) direction. The system sizes are $L_x = 256$ and $L_y = 512$. 63

2.10 Finite-size approximates of the scaling exponents for stationary surface of sandbox (or correlated MC runs for the interface model) with α^* defined by Eq. (2.21) and β by Eq. (2.7). The solid (dashed) curves are for the continuous (discrete) height model. 64

2.11 Traces of stable sand surface over 256 avalanches for 1D sandbox model with $L_y = 256$. The system is driven from the left at $y = 0$. 68

2.12 Scaling exponent for boundary correction to the local slope of fresh 2D sandbox surface (or, in the interface language, transient growth rate from a flat interface), $s_f(y) - s_f(\infty) \sim y^{-\kappa_f}$, and its correction due to the iterated avalanche process, $\Delta s = s(y) - s_f(y) \sim y^{-\kappa}$. 70

2.13 Two possible cases at a boundary of an avalanche cluster (the shaded area): (a) avalanche expands; (b) avalanche shrinks. The local slopes along the arrow marks is reduced in (a) while increased in (b). 71

3.1 Lattice structure of the two dimensional discrete-height sandbox model. . . . 77

3.2 A typical configuration of the discrete-height sandbox model before (left) and after (right) a system spanning avalanche trigger at the boundary site marked by the white dot; The system size $L_x \times L_y$ is 32×64. 79

3.3 Two-step growth of the discrete-height step-flow random-deposition interface growth model; (a) Steps flow by one unit to the right (left) when its size Δh is negative (positive); (b) Each site increases by one unit with a probability p. 80

3.4 Scar (edge lines of avalanche clusters) configurations of DHSB avalanches at the two deterministic limits; (a) $p = 0$; (b) $p = 1$. 82
3.5 The domains of odd (shaded region) and even (light region) sites on a DHSB surface at $p = 0$, separating them are domain walls that no avalanche will penetrate at this deterministic limit. 84
3.6 Finite-size scaling (FSS) estimates of the scaling exponents versus inverse width $(1/w)$ of avalanche clusters for the DHSB avalanches in the shallow-avalanche phase (measured at $p = 0.1$). They are consistent with $\alpha = 0$ and $z = 1$. 86
3.7 A typical large avalanche cluster for DHSB at the DP transition point; The size of the box is $L_x \times L_y = 455 \times 10000$. 88
3.8 The FSS plot of the area density $a/(lw)$ (solid line) and the mass density $m/(lw\delta)$ (dashed line) versus inverse length $(1/l)$ for the avalanche clusters at the DP transition point. While the area density converges to a finite value at the thermodynamic limit, the mass density converges to 0. 89
3.9 FSS estimates of the scaling exponents derived from the avalanche exponents τ_l, τ_w, τ_δ for the discrete height sandbox model versus the inverse width $(1/w)$ at the DP transition point. The z exponent is consistent with dynamic exponent of DP universality class $z_{\rm DP} \simeq 1.582$. The combination $\sigma - z - 2\alpha < 2$ indicates a violation of mass hyperscaling relation (3.7). 90
3.10 The roughness of a stationary DHSB surface(dotted line) compared with the roughness of the SFRD model (solid line) versus the double logarithm of time t at the DP transition point. The iterated avalanche process makes the surface rougher. The dashed line shows the increase of the roughness by the iterated avalanche process. 91

3.11 FSS of the γ exponents of the logarithmic scaling of SFRD roughness (solid line) and $\Delta W^2 \equiv W^2_{\mathrm{DHSB}} - W^2_{\mathrm{SFRD}}$ (dashed line), assuming the scaling form $(\ln t)^\gamma$, versus the inverse of the logarithm of time. The change in roughness ΔW^2 scales with a smaller exponent than the scaling exponent of W^2. . . . 92

A.1 The curtain of active sites at the active slanted boundary. 108

A.2 Lattice structure near the active boundary. 110

A.3 Log plot of active width versus $p_c - p$ from straight Monte Carlo simulations on unlimited system sizes. The solid line represents the data. The dashed straight lines of slopes -2 and -1.734 are guides to the eyes. 111

A.4 Estimates for the active width exponent, x. In fit (a), W is assumed to scale as $W \sim \epsilon^{-x}$, in (b), as $W \sim \epsilon^{-x} \ln \epsilon$ and in (c), as $W \sim \epsilon^{-x}(\ln \epsilon + \ln 2)$. 112

A.5 Finite-size-scaling exponent z for ($\times$) the characteristic active width, $W \sim L^z$, and for ($+$) the time to reach the stationary state, $t \sim L^z$, at the percolation threshold in the transfer matrix setup. The data virtually coincide. . . 117

ACKNOWLEDGMENTS

I would like to thank my advisor, Marcel den Nijs, for his valuable advises and guidance. I would like thank Chen-Shan Chin, Mee-Soon Ha, Deok-Sun Lee, Hyunggyu Park, Jae Dong Noh, Douglas Davidson, and John Neergaard for the stimulating discussions in the group meetings. I would like to thank David Thouless and Gerald Seidler for their valuable comments and suggestions. I would like to thank Laurence Yaffe and Larry Sorensen for their critical reading of the manuscripts. I would like to thank Jian-Ming Tang, Li-Jen Chen, Dah-An Luh, Wen-Chi Chiang for their long-standing friendship. I would like to thank Cheng-Pang Liu, Chia-Lin Huang, Chia-Ping Chen for their company. I would like to thank Ting-Wai Chiu for his early guidance. I would like to thank many more people for their help and kindness. And, finally, I would like to thank my family for their love and support.

DEDICATION

To my grandfather.

Chapter 1

INTRODUCTION

Interest in critical phenomena dates back to, at least, the 19th century with the discovery of gas-liquid critical points, in particular due to the work of Andrews [3], and has been at the center of attention ever since the last quarter of the 20th century. An interesting observation is that at these transition points, systems exhibit long range correlations and lack a characteristic length scale, in other words, they are scale invariant. The latter means that systems look similar at different magnifications and that one can not find any characteristic feature to tell them apart at large length scales. This might at first seem peculiar, but physicists soon realized that examples are actually abundant in nature. Even more, systems in nature that lack characteristic scales often appear to do so naturally without evident controlling agents; unlike conventional phase transitions, which generally require the fine tuning of control parameters to reach the so-called critical points and consequently scale invariance only happens in a very small part of the phase diagram. This contrast between naturally occurring criticality and the criticality at continuous phase transitions has prompted many physicists to the search of possible mechanisms that can bring about criticality in spontaneous ways.

One of the attempts to understand the naturally occurring criticality is the so-called self-organized criticality (SOC) as proposed by Bak, Tang, and Wiesenfeld (BTW) in 1987 [5, 6] as an abstraction of their earlier study of coupled nonlinear oscillators [109]. Their nonlinear model actually bears some resemblance to a spring-block array introduced by Burridge and Knopoff [17] in 1967 for the purpose of modeling an earthquake fault. Earthquakes, as known by Gutenberg and Richter already before their published work in 1941 [51], follow a power-law distribution in the intensities of energy releases. This is a nice example, showing that

seismic activities of the earth are critical phenomena in the sense of the lack of characteristic intensity scales.

BTW's automatons, also known as deterministic sandpiles, are very simple models that capture the essence of the above nonlinear processes that exhibit critical distributions of avalanchelike events. Namely, these are systems with fast relaxation dynamics being driven under slow external forces. Since BTW's work, the idea of SOC has been applied to a broad array of fields ranging from studies of biological evolution [4], to river networks, to vortex avalanches in superconductors [8, 9], and to fluctuations in financial markets [77, 28], in addition to the original geological manifestations in earthquake faults [21].

Even though the sandpile models are already strong simplifications of their counterparts in nature, our current understanding of their behavior unfortunately still remains mostly numerical. Among the few exact results, the most notable ones are Dhar's analytic work based on the Abelian properties of the BTW model [30, 31] and also Dhar and Ramaswamy's exact solution to a two-dimensional (2D) directed version of the original BTW model [32] which is known as the DR model. One of the reasons that Dhar and Ramaswamy were able to achieve these results is that they were able to show that in these specific models there are no correlations in the stationary state and that the propagation of an avalanche is governed only by the dynamics of the two edges of the avalanche cluster which simply follow the dynamics of one-dimensional (1D) random walkers.

Directed sandpile models might at first seem much more restrictive than regular isotropic processes. Nonetheless, recent studies of the original BTW isotropic sandpile models show that the avalanche propagation in regular sandpile models can be decomposed into waves of toppling which propagate directly across the system, with each site participating at most once in each wave, until they damp away or reach the system boundary [98]. This realization points to the understanding of waves as a possible foundation for the understanding of the more general models. In this direction, directed models provide a simplification in which each avalanche consists only of one single wave.

However, the simplistic random-walk-type soluble models by Dhar and Ramaswamy are not very satisfactory. Following their work, physicists have been trying to expand the model and the results to a broader range of dynamic rules. Notable extensions are the inclusion of

stochasticity in the toppling process [81, 106, 76, 95], various parameters controlling, e.g., bulk dissipation [108], and assorted asymmetries and extra degrees of freedom in the piling configuration of grains [25]. Along these lines Paczuski and Bassler [91] and also Kloster *et al.* [69] found an exact solution to a stochastic directed sandpile model. They were able to link the scaling exponents of avalanche distributions to the critical exponents of the Edwards-Wilkinson (EW) universality class [35] which describes the fluctuating growth of an interface.

Interface growth models were motivated as a tool to understand the dynamics of interfaces in nature. These include coast lines and mountain shapes in geography [104], cluster boundaries of bacteria colonies [103, 82, 112, 83], crystal-melt interfaces of solidifying metals [71], suspension-aggregate interfaces for colloid sedimentation [27], meandering fire front propagation in a forest [50], and solid state surface growth under molecular beam epitaxy [29]. In the rough phase of such growing interfaces, physicists found random fluctuations of all length scales. This actually gives us another type of intrinsic critical phenomena, that is, the system exhibits long range correlations and scale invariance over a large part of the parameter space. Considerable efforts have been put into the study of these kinds of critical behavior [52, 7]. This makes it a relatively well-understood field with more analytical results and better established universality classes [7]. Therefore, this suggests a route of improving our understanding of sandpile models through an understanding of their relationship with interface models.

In interface growth, the EW universality class is for those systems whose growth is governed by a linear growth equation that takes into account the surface relaxation by desorption as well as random deposition onto a surface [35]. The equation can be solved exactly due to its linearity. However, the predicted results didn't seem to account for the early numerical simulations of low-dimensional lattice growth models such as Eden's model [34], ballistic deposition [113, 105, 40, 86], and random deposition with surface diffusion [39, 85]. As it turned out, the EW scaling behavior is unstable in one plus one dimensions (one space plus one time dimension) with respect to a nonlinearity which was to be accounted for by the Kardar-Parisi-Zhang (KPZ) growth equation [64]. Since nonlinear higher order terms generally arise in discrete height and lattice versions of growth dynamics, the scaling

behaviors of lattice models is generically controlled by the KPZ fixed point unless the nonlinear KPZ term in the growth equation can be made to disappear by some symmetry requirements [90].

Growth models generally result in rough interfaces in 1+1 dimensions (one space dimension and one time dimension), but in some discrete models of interface growth, long-range order (LRO) can be restored by the propagation of order parameters. In some cases LRO is induced by a limiting factor, like a maximum speed for the growth at sites [65] and in others by the surface height at a site being stuck at the lowest exposed level [1, 2]. Then, the dynamics of the propagation is those of absorbing states and is hierarchical. That is, when the order parameter vanishes from the system, it will never come back. However, when that happens, we can redefine the order parameter to, e.g., being sites of the new lowest level and it again will follow the same dynamics. In the ordered phase, the interface is *pinned* to a certain level and is macroscopically flat. The transition can be from a KPZ rough phase [101, 65, 1] or a EW rough phase [75] to a flat phase through a directed percolation (DP) [68, 102, 45, 46, 115] transition or through a directed Ising [49, 47, 62, 66] type transition [57, 94].

Another field of research inspired by BTW's sandpile models is the study of granular avalanches in real sandpiles. The early experiments involves rotating drums [61, 100, 38, 15, 18] or deposition onto a circular cone-shape sandpile [54]. However, no signals of power-law distributions of avalanches were found in these experiments except over some small regions of the avalanches [55, 15]. This remained the case until Frette *et al.* performed some experiments on a pile of elongated rice grains [42] sandwiched between glass plates. They attributed the observed power-law scalings of the avalanches to the asymmetries of the grains that allowed more friction and randomness in the packing configuration [42, 25]. This partly inspired the search for SOC in cohesive granular materials, e.g., the toner powders used in xerography [99].

Granular avalanches in cohesive materials were recently investigated by Valverde *et al.* [111]. They made an observation which is contrary to their noncohesive counterparts that that the avalanches for cohesive granular materials penetrate deeper into the surface. Noncohesive avalanches only involve a few surface layers. Since cohesion between sand

grains can be induced by adding moisture into the system [89], their observation leaves open the question of whether there exists a phase transition between the avalanches of dry sand and wet sand.

The scope of this thesis is to understand the relation between self-organized critical phenomena and the interface models. I will focus on directed sandpile models and on the specifics of low-dimensional systems to establish a mapping between directed sandpile models and interface growth model in one lower dimension. While interface models are usually defined by local updating rules, sandpile models are defined by iterated avalanche processes over local relaxation dynamics. This gives rise to the caveat that a large correction to scaling which is due to this distinction might change the scaling behavior of the avalanches. I will address this issue, and I will show that the correction is irrelevant in the thermodynamic limit.

The roughening transitions in 1+1-dimensional interface models lead to the interesting quest to understand its implications on the corresponding avalanche system. I will show that it gives rise to a deepening transition in the resulting conformations of the avalanche clusters to a flat avalanche region where only surface layers are involved in the toppling dynamics. However, the discrete nature of the models plays an important role in the existence of this transition, and I will leave open the question of whether the transition will exist in real sandpiles.

1.1 Criticality in nature

In statistical physics, a system is critical when it has long-range correlations and it is scale invariant. One example of scale invariance is the shape of a coast line as was pointed out as early as 1967 by Mandelbrot [79]. When a coast line is shown on a map, it's impossible for us to estimate the scale of magnification used in the map without previous knowledge of the area shown. One always sees similar wiggles at all scales of magnification and there is no characteristic feature allowing one to tell them apart. Also, the length of the coast line between two points on the coast is not well defined without choosing a lower limit of the minimum geographically meaningful features of the coast G. The measured length $L(G)$ will

then greatly depend on the actual value of G chosen, that is, it will depend on the length of the ruler one uses to carry out the measurement. Mandelbrot found L to be proportional G^{1-D}, with $D \approx 1.25$, which actually diverges as $D \to 0$. The exponent D here describes how two measurable quantities of the system will scale with respect to each other and is called the fractal dimension of the coast line. Deterministic fractals, like the Sierpinsky Gasket, are created by deterministic rules, while many random structures, such as a coast line or liquids droplets at the gas-liquid critical point, are statistically self-similar at different scales when ensemble averaged, and are therefore referred to as statistical fractals.

Scale invariance is often associated with long-range correlations in the systems. This means that the correlation dies out slower than any exponential, in particular, it decays as a power law, thus the correlation lengths diverges. In the example of the coast line, one may consider the orientational correlations between two segments of the coast separated by a certain distance. One finds that it decays as a power law in the distance. However, not all scale invariance we find in nature is associated with long-range correlations. For example, the path of a suspending particle in liquid follows a three dimensional random walk [36]. Its distance d from a given starting point and the path length l that it traces are related by $d = l^{1/2}$. The path is scale invariant in that it is self-similar at all magnifications. However, in this specific case, there are no correlations in the path and we generally do not consider the system critical.

1.1.1 Continuous phase transition

The interest in critical phenomena stems from the study of continuous phase transitions in equilibrium statistical mechanics, such as the critical opalescence of water at the endpoint of the liquid-gas boiling line, the zero field magnetic properties of iron near the Curie temperature, and the fractal shapes of the remaining conducting pathway in a grid of deteriorating wires at the threshold of losing its system-wide conduction. In these situations, criticality manifests itself as power-law dependence between the observable quantities in the system; for example, how much time it takes for a local excess water density to dissipate to half the original value as function of the amount of initially introduced excess water; or how

the zero field magnetization depends on the temperature deviation from the Curie point; or how many wire segments the shortest conduction pathway contains as a function of the distance between the two electrodes.

These examples from continuous phase transitions all share a common feature. They all require the tuning of some control parameters to reach criticality. For water, we need to tune the temperature to $T = 647.14$ (K) and the pressure to $p = 22.06$ (MPa) [74]; for the magnetization of iron, we need to tune the temperature to $T = 1043$ (K) [74]; while in a two-dimensional square grid of good and bad wires, the fraction of good wires needs to be exactly $1/2$ [80] in order to make the system critical.

The most important lesson that we learned from equilibrium critical phenomena is the existence of universality. For the vast varieties of physical systems, those found in nature as well as the model systems invented by physicists, the critical behaviors can be classified into so-called universality classes. They state how specific observed quantities in the systems behave at large length scales when we reduce the magnification of our measurement system. These universality classes turn out to be rather insensitive to the microscopic details, but instead, to depend only on the symmetries of the systems and the conservation laws obeyed by the systems. Decades of study have made these universality classes quite well understood. Especially in two dimensions, the postulate of conformal invariance limits the possible forms of the correlation functions in critical systems and allows us to identify the universality classes with different topological charges. Additionally, the development of renormalization group theory helps us understand the origin of these universality classes as fixed points in more general parameter phase spaces, such as that illustrated in Fig. 1.1. These fixed points trap the long-range behaviors of various systems.

1.1.2 Gutenberg-Richter relation of earthquake distribution

Criticality in nature in addition to the continuous phase transitions was noted as early as the 1930s. The Gutenberg-Richter relation for the distribution of earthquakes is the famous example. In a seminal paper published in 1941 [51], Gutenberg and Richter showed that on an annual basis the number of earthquakes of certain magnitudes is about ten times more

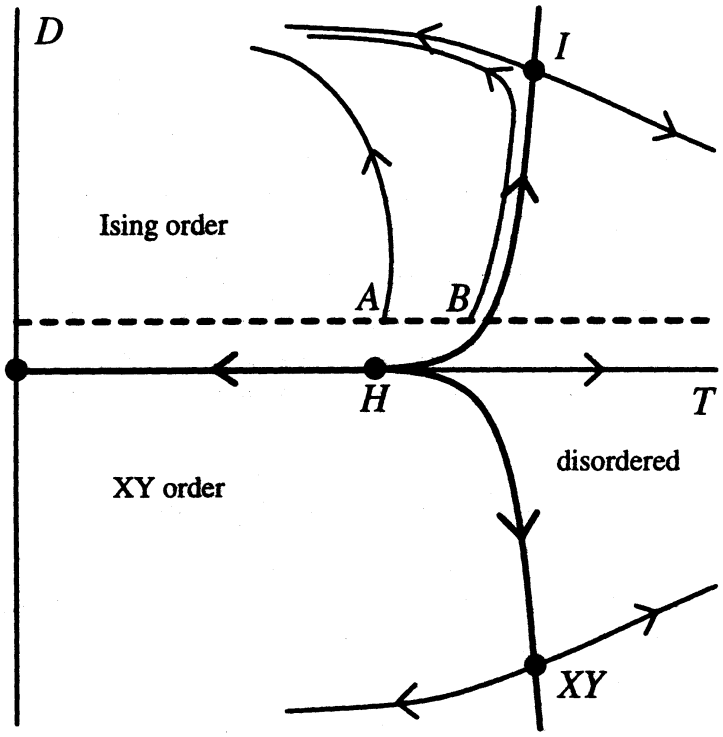

Figure 1.1: A typical 2D phase-space and renormalization flows (for the Heisenberg model with uniaxial anisotropy from [20]); The black dots are the fixed points and arrows are the directions of renormalization flows. The dashed line represents the trace of a typical experiment as the temperature is varied.

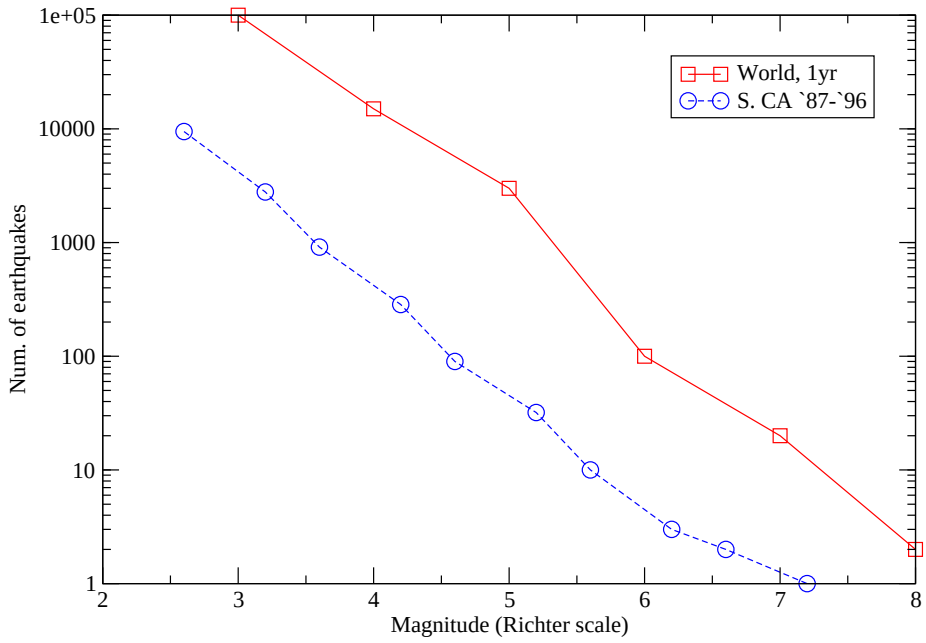

Figure 1.2: Earthquake magnitude distributions for world average in a year (solid line) and in South California from 1987 to 1996 (dashed line) with data obtained from the South California Earthquake Data Center; Both are showing similar power-law decay.

frequent as those of one magnitude higher. That is, they follow the relation

$$\log N(M) = a - bM \tag{1.1}$$

with the constant b being roughly 1. The magnitude M of an earthquake is measured on a log scale in terms of the energy release (Richter's scale). This demonstrates a nice power-law relation between the frequency of earthquakes and the released energy in each one. The most notable aspect of this relationship is its robustness. In Fig. 1.2, the data from different sources show similar power-law behavior.

The simplicity and robustness of this relationship suggest the existence of a general mechanism that might be underlying the seemingly complicated earthquake dynamics. That is, while the formation of individual quakes might be specific to the microscopic details of the local conditions of the system, the general statistical features of the earthquake distribution should be robust to variations in the implementing mechanism.

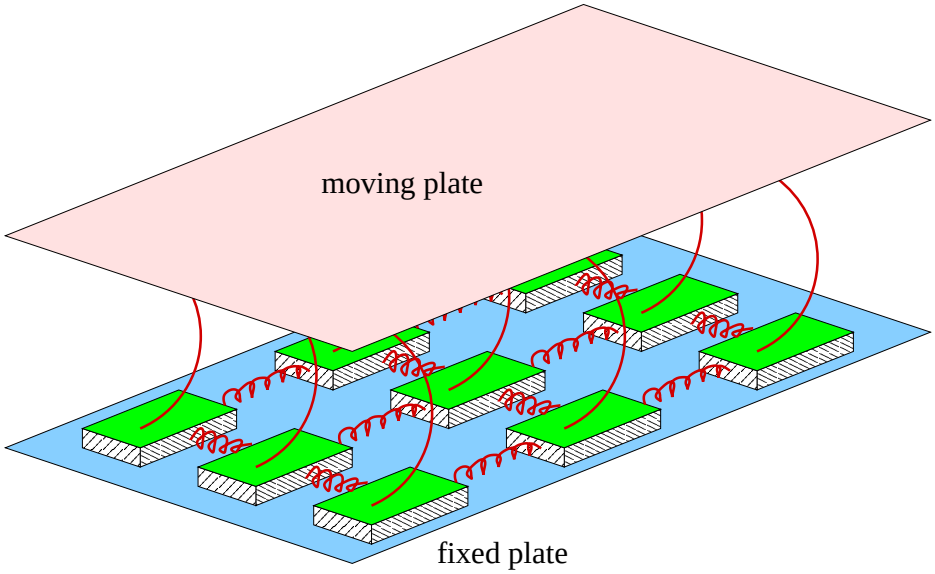

Figure 1.3: A spring block system for the modeling of an earthquake fault; The blocks on a frictional fixed plate are connected to each other with coil springs while each block is connected to the slow moving top plate with a leaf spring.

1.1.3 Spring block model of earthquake fault

This prompted Burridge and Knopoff to construct a spring-block system similar to that illustrated in Fig. 1.3 to model an earthquake fault [17]. What they built was an array of massive blocks resting on a frictional surface. Coil springs were used to connect each block to its neighbors. A leaf spring was used to connect each block to a slow moving plate hanging above. The static and dynamic friction between the surface and the blocks provide a highly nonlinear interaction. As the moving plate displaces gradually, the stress increases on each block through its connecting leaf spring. When the force on a given block exceeds its static friction with the bottom surface, it slides forward and stops at a position when its net stress is less than its kinetic friction. Through the coil springs connecting to the neighboring blocks, this change of position also increases the stress value of the neighboring blocks and it is thereby likely to create more sliding blocks among the neighbors. This earthquake like event stops when all the stresses on the blocks are less than their static

friction. As the slidings happen much faster than the stress build up by the hanging plate, we can distinguish each event as an isolated avalanche.

Counting the number of sliding blocks in each of the avalanches, Burridge and Knopoff were able to obtain a distribution of event sizes resembling the Gutenberg-Richter relation of earthquakes. Their result shows that the Gutenberg-Richter relation is a universal aspect of earthquakelike dynamics which can be captured by simple models with very limited degrees of freedom. However, even though the Burridge-Knopoff system is much simpler than a realistic earthquake fault, the highly nonlinear nature of the interaction makes attempts to obtain an analytical solution extremely difficult [21].

1.2 Sandpile as a paradigm to self-organized criticality

In the context of chaos theory, BTW studied the phase organization for a chain of nonlinear oscillators [109] coupled with each other through coil springs. This system is similar to the spring-block model made by Burridge and Knopoff and it is also difficult to treat analytically. However, BTW recognized that some of the behaviors of the system are more generic than these in the specific model. They later constructed a considerably simplified model that consists only of integer variables and cellular automaton dynamics that exhibits interesting behavior [5], i.e., the system exhibits power-law scaling in the avalanchelike events without the fine tuning of any control parameters. This has become known as the BTW sandpile model.

1.2.1 The BTW Sandpile model

Consider an integer height variable z defined on a square lattice with the sites $\{i\}$. The system is stable when all the heights are less than a given critical value z_c,

$$z_i < z_c. \tag{1.2}$$

An unstable site i is toppled with the rule

$$z_i \rightarrow z_i - 2d, \tag{1.3}$$

where $2d$ is for the coordination number of d dimensional system, while each of its $2d$ neighbors $\{j, \langle i, j\rangle\}$ have their heights increase by 1,

$$z_j \to z_j + 1. \tag{1.4}$$

The toppling process conserves height or particles except at the boundary sites which have less than $2d$ neighbors.

The system is driven by randomly choosing a site and increasing its height by 1, i.e., by the deposition of a particle. An avalanche is defined as the subsequent topplings of the unstable sites that are required to bring the system back to a stable configuration. The next deposition take places only after the system is completely stabilized.

The easiest way of understanding the rules in the BTW model is to think of it as a discrete version of the Burridge-Knopoff spring-block model. Think of the stress on each block as an integer with a critical value. When the stress on a block exceeds this value, the block's releasing and redistributing its stress to its neighbors are implemented by reducing the integer stress value it has by the number of its neighbors while each of its neighbor increases its stress value by one. The boundary of the system is implemented by surrounding the whole system with special blocks that will never release stress to their neighbors. The slow moving plate that is driving the system uniformly is implemented by randomly increasing the stress value of one of the blocks by one. This driving process is slow so that all blocks will return to a stable value of stress before the next increment by the driving plate is applied. An avalanche event is just the system's response to such an increment.

The BTW model has a simple set of dynamic rules that is very easy to implement on a computer. And, it's easy to observe the critical behavior of the system via the statistics of the avalanche events as shown in Fig. 1.4. The dashed lines are linear fits to the observed distributions. They show that the size s (the number of sites participate in an avalanche) distribution $D(s)$ scales as $s^{-\tau}$ and the duration t (how many times we need to topple all the unstable sites in the system to bring it back to a stable configuration) distribution $D(t)$ scales as $t^{-\alpha}$ with the exponents $\tau \approx 1$ and $\alpha \approx 0.43$. Nonetheless, the exact value for the scaling exponents remains unknown. The original result of BTW was supported by Zhang's

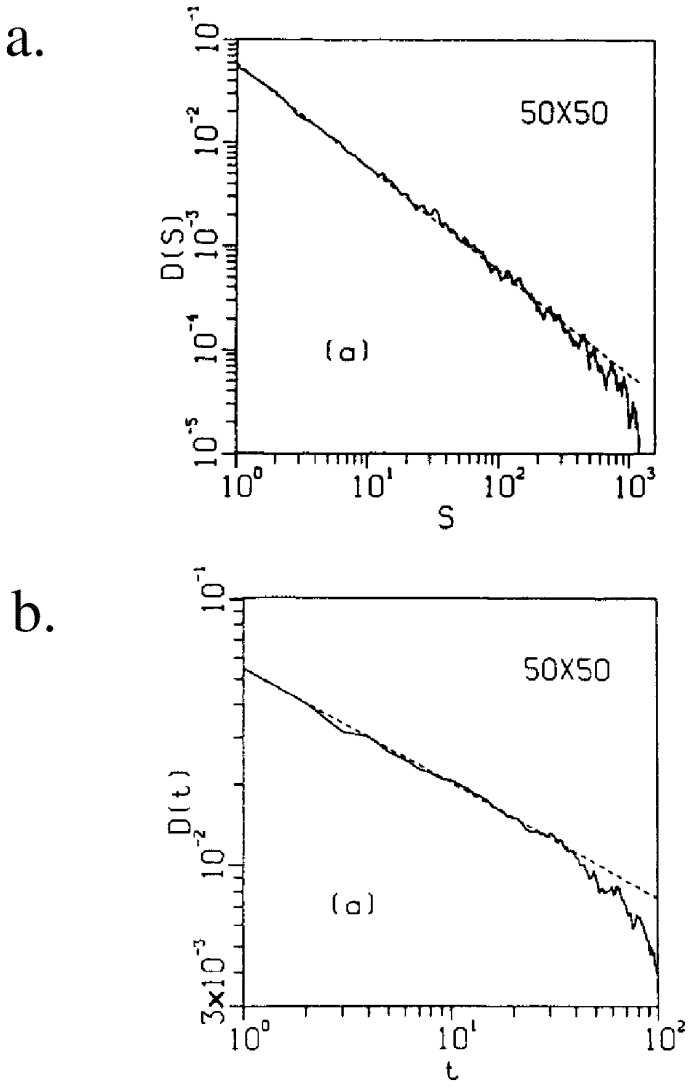

Figure 1.4: Cluster size (a) and lifetime (b) distributions of avalanches, coarse grained, on a 50×50 array, averaged over 200 samples of the BTW model; The dashed line in (a) shows a power-law decay of s^{-1} and the dashed line in (b) shows a power-law decay of $t^{-}0.43$. These plots are taken from [5]

prediction based on a continuous energy model [114] but later numerical studies put the τ value at roughly 7/6 [78] and a mean-field-type model suggests the value 23/21 for the τ exponent [26]. A study using a renormalization scheme by Pietronero *et al.* [97] shows $\tau \approx 1.253$.

1.2.2 Critical state of Abelian Sandpile model

A significant property of the BTW model is that the toppling rule of the model is Abelian in the sense that when multiple unstable sites are present in the system, the final stable system configuration before the next deposition of a particle is independent of the order in which the unstable sites are toppled. The Abelian property of the BTW model allows some analytical conclusions to be drawn. Dhar first showed that some of the configurations of the system will never show up in the stationary state of the system whereas all of the possible configurations of the stationary state will appear with equal probability [30]. Majumdar and Dhar later introduced a "toppling from the sink" algorithm to determine if a given configuration is a possible configuration of the stationary state [78]. This leads to a one-to-one mapping between the possible configurations of the stationary state and all possible spanning trees covering the lattice.

The Abelian property also allows a simple view of the particle movements in the system. Each of them can be considered as making a random walk on the lattice until they reach the boundary. The original toppling process is deterministic under the condition that we don't keep track of the identity of each particle. The stochasticity of the random walk enters by adding an imaginary label to each particle and having the particles participating in each toppling event randomly mixed before distributing them to the neighbors so that when one particle is tracked, we'll find that it moves in a random direction each time it participates in a toppling. From this random walk nature of the process, a particle will participate on the average in $O(L^2)$ toppling events before it reaches the system boundary and falls off the edge, given that the linear size of the system is very large, $L \gg 1$. As a consequence, the average number of topplings that results from a single deposition of particle also scales as L^2. The same random walk prospective also leads to the exact form of the correlation G_{ij} between

the deposition of a particle at site i and the number of consequent topplings at site j. In the continuous limit, it should simply follow the Poisson's equation $\nabla^2 G(x_j - x_i) = \delta(x_j - x_i)$ with a point source [30].

However, while these exact results are encouraging, when it comes to the exact values of the scaling exponents which characterize the distribution of avalanche sizes, and thus the possible universality classes, the problem becomes extremely elusive and, even for the original BTW model, there remain many open questions today.

1.2.3 Directed sandpile model

In trying to understand the dynamics of the BTW model and searching for a more analytically manageable model, Dhar and Ramaswamy found an exactly solvable variant of the BTW model which is called the directed sandpile model [32]. This differs from the BTW model in its toppling rule, in that, when a site reaches the critical height, its toppling only transfers its stress to half of its neighbors in a given direction such that the toppling activity only propagates in one-way through the system. This allows us to perform the toppling process in a row-by-row fashion. In d dimensional space, the system is defined on a square lattice tilted at 45° with critical height $z_c = d$ and the toppling of an unstable site transfers its d grains to its d downward neighbors. Consider $d = 2$ and use y for the downward direction and x for the transverse direction. The tilted square lattice is defined on the sites with $x + y$ being even numbers. A site (x, y) topples when $z(x, y) \geq 2$ with the rule

$$z(x, y) \to z(x, y) - 2 \tag{1.5}$$

and its two downward neighbors receive the displaced grains

$$z(x \pm 1, y + 1) \to z(x \pm 1, y + 1) + 1. \tag{1.6}$$

The system is driven by the deposition of a single grain to a randomly chosen site at the top $y = 0$ row,

$$z(x_i, 0) \to z(x_{i,}0) + 1 \tag{1.7}$$

where x_i is an even number randomly chosen as the triggering site for the i-th avalanche.

A special property can be found in the toppling rule of the DR model. When a site is inside a compact group of active sites, it will receive the exact number of grains that it will lose in its subsequent toppling to its downward neighbors. This guarantees its toppling and leaves its final configuration unchanged. There are two consequences of this. One is that the toppling rule can not create a hole of untoppled sites inside an avalanche cluster. While, in three or higher dimensions, holes of untoppled sites still can be embedded in an avalanche cluster by enclosing them within its meandering boundaries, in two dimensions (2D), where the boundaries are just the traces of two point-objects, an avalanche cluster remains compact. The other special property is that the configuration of the system is only changed at the boundary sites of an avalanche cluster. With the same Abelian property as in the isotropic model, Dhar and Ramaswamy were able to show that all the configurations of the system are allowed, and that each one will occur with equal probability in the stationary state of the system. From the symmetry of the stationary state, it is easy to show that there are no correlations between sites in a stationary sandpile. This makes the propagation of the two boundaries independent random walks in 1+1 dimensions with y as the time and where an avalanche cluster is given by the separation of the two walkers before their first and only encounter that stops the avalanche.

From the random walk nature, the distribution of the merging times for two walkers gives the distribution of the avalanche length l, which is defined as the maximum y coordinate of the avalanche cluster, and we have

$$P_l(l) \sim l^{\tau_l} \tag{1.8}$$

with $\tau_l = 3/2$. This leads also to $\tau_w = 2$ for the scaling exponent of the width w distribution, since $w \sim l^{1/2}$ follows directly from the random walk characteristics. (The width is measured as the transverse maximum x size of the avalanche cluster.)

With this exact solution, the directed sandpile model becomes a nice test bed for various numerical schemes, such as dynamical real space renormalization [11, 53, 60], and also for the concept of universality [12]. Additionally, it becomes interesting to investigate how various complications such as dissipation and stochasticity modify the scaling behaviors of the avalanches. One of these attempts was made by Tadić and Dhar [107]. They introduced

a toppling probability p for unstable sites. For $p < 1$, this leaves some chance for particles to pile up on a site i even when $z_i \geq z_c$. The product of the density ρ of sites with height of $z_c - 1$ and greater, which are pro-active in that they will be active once they receive a particle, with the toppling probability p becoming an effective parameter $\bar{p} = \rho p$ for the propagation probability of toppling activities. When p is greater than a critical threshold p_c of directed percolation (DP) on the lattice, the effective parameter $\bar{p}$ will self-tune to the critical point. This results in DP-like scaling behavior for the avalanche clusters. Tadić and Dhar were able to derive various scaling exponents for the avalanches from the known DP exponents.

Another attempt to introduce stochasticity into the model was proposed by Pastor-Satorras and Vespignani [95] which we will discuss in the next section.

1.2.4 Stochastic directed sandpile model

Considering the toppling rule in the DR model, we see that the stochasticity may be introduced by allowing each sand grain to make an independent choice of which downward neighbor it wants to go to [95, 96]. This is equivalent to replacing the toppling rule (1.6) with a stochastic one in which rule (1.6) applies for 1/2 of the time, while for 1/4 of the time

$$z(x+1, y+1) \to z(x+1, y+1) + 2 \tag{1.9}$$

and for the remaining 1/4 of the time

$$z(x-1, y+1) \to z(x-1, y+1) + 2. \tag{1.10}$$

The other site remains unchanged. This gives us the so-called stochastic directed sandpile model (SDSM). In the SDSM, the downward neighbors won't necessarily receive the same number of grains even if they have the same number of upward neighbors toppling in the same avalanche. This allows the possibility of opening up holes of inactive region in an avalanche cluster in contrast with the DR model. This can be confirmed by inspecting the typical avalanche cluster shown in Fig. 1.5, which contains holes of inactive regions near the boundaries of the cluster. However, nonetheless, the avalanches remain essentially compact

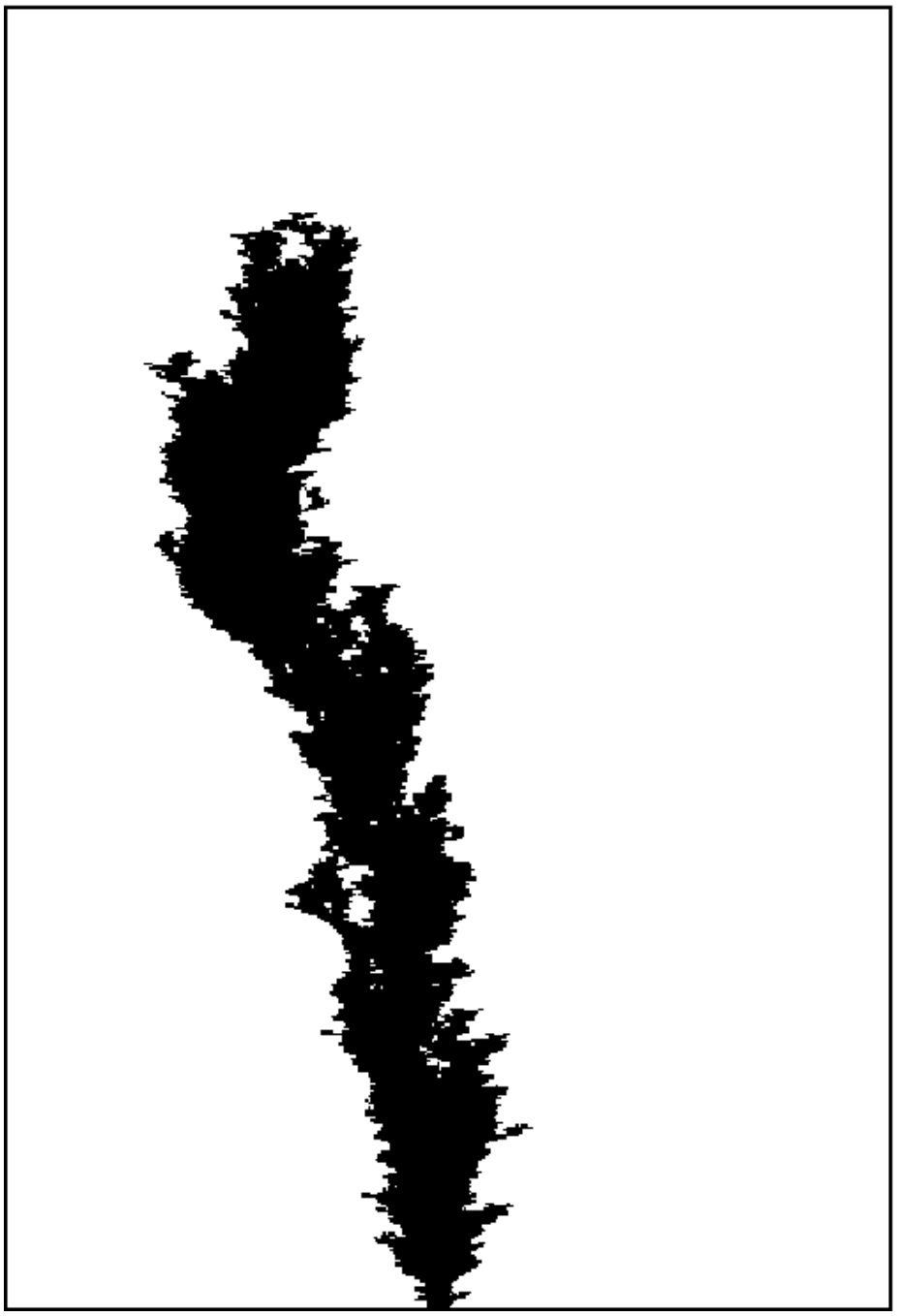

Figure 1.5: A typical avalanche cluster (sites participated in the toppling) in stochastic directed sandpile model; It's essentially compact in the sense that while holes of inactive regions are visible near the boundary, their sizes do not scale with the cluster size. The size of the box shown is $L_x \times L_y = 360 \times 8833$.

as the sizes of the holes of inactive sites do not seem to scale with the size of clusters themselves. This allows us to consider the avalanche cluster as a compact object in the thermodynamic limit.

It's easy to see, using the independent random walkers' picture, that this model remains Abelian. That representation also leads to the conclusion that all stable configurations of the system are possible and equally likely in the stationary state of the system [91, 69]. Just as in the deterministic model, this implies that the stationary state is not correlated and each avalanche can be considered as the propagation of toppling activities in uncorrelated random media.

However, unlike the deterministic model, the existence of multiple topplings leads to nontrivial propagation dynamics inside the avalanche cluster. Paczuski and Bassler [91] and also Kloster *et al.* [69] were able to show that, within an avalanche cluster, the number of particles received at each site (or the number of particles it has to loose for the site to become stable) is described by the Edwards-Wilkinson [35] equation of interface growth.

Define the quantity $n(x, y)$ to be the number of grains received by the site (x, y) in a given avalanche event. Since each toppling takes two particles, the number of grains it will transfer to its downward neighbors n_{out} will be the same as n with the probability $1/2$ while it will differ from n by ± 1 each with probability $1/4$. The randomness comes from whether the site is originally occupied by a particle or not. Since the stationary state of the system is uncorrelated, this results in an uncorrelated noise of limited amplitude whenever a site receives grains in an avalanche. We can describe this by

$$\begin{aligned} \langle \eta(x, y) \rangle &= 0 \\ \langle \eta(x, y) \eta(x', y') \rangle &= \theta[n(x, y)] \delta(x, x') \delta(y, y'), \end{aligned} \tag{1.11}$$

where $\theta(n)$ is a step function with $\theta(n > 0) = 1$ and $\theta(n \leq 0) = 0$ while $\delta(x, x')$ is the Kronecker delta function. On the average, each of it's downward neighbor receives $n_{\text{out}}/2$ particles from the site. However, as each grain is randomly making independent choices of which neighbor it's heading for, the actual number of grains that one of its downward neighbors receives is given by the sum of the random variables $\eta_i = 0$ or 1, $i = 1 \cdots n_{\text{out}}$. The fluctuations in the evenness of the grain distribution introduces an uncorrelated random

current j in the transverse direction with the amplitude $\sqrt{n}$,

$$\begin{aligned} \langle j(x,y)\rangle &= 0 \\ \langle j(x,y)j(x',y')\rangle &= n(x,y)\delta(x,x')\delta(y,y'). \end{aligned} \tag{1.12}$$

For the site (x,y), the contribution of this current comes from its two upward neighbors and it is given by $j(x-1,y)-j(x+1,y)\approx 2\partial j(x,y)/\partial x$. The continuous form of the equation of motion for n is then given by [91]

$$\frac{\partial n(x,y)}{\partial y} = \frac{1}{2}\nabla^2 n(x,y) - 2\frac{\partial j(x,y)}{\partial x} + \eta(x,y). \tag{1.13}$$

From dimensional analysis, the conservative random current is irrelevant compared to the nonconservative noise η. Ignoring the conservative random current, Eq. (1.13) is the EW equation with a threshold noise, which turns off when $n=0$. The compactness of the avalanche clusters allows the propagation dynamics to be described by the EW equation and the threshold nature of the noise only comes into play at the boundaries of an avalanche cluster. Therefore, the scaling of the characteristic lengths of the avalanches can be expected to follow that of the EW universality class, that is, the correlation lengths $\xi_n \sim \xi_x^\alpha$ and $\xi_y \sim \xi_x^z$ with $\alpha = 1/2$ and $z=2$.

Just as in the BTW model, we can imagine tracking each particle by labelling it. In a directed sandpile, a particle will participate in L_y topplings before leaving the system with L_y being the size of the system in the longitudinal direction. This gives the expected total number of topplings m for each avalanche,

$$\langle m\rangle = L_y/2. \tag{1.14}$$

Together with the EW scaling and the general formulation to be described in the next chapter, this determines all of the scaling exponents, $\tau_l = 7/4$ and $\tau_w = 5/2$, for the distribution $P_l(l) \sim l^{\tau_l}$ of the avalanche length l (the maximum y size of an avalanche), and the distribution $P_w(w) \sim w^{\tau_w}$ of the avalanche width w (the maximum x size of an avalanche).

1.3 Kinetic roughening of interface growth

Growing interfaces are yet another class of interesting phenomena in nonequilibrium systems that can exhibit critical behavior without the tuning of a control parameter. This refers to an evolving interface driven by a finite external force so that it won't settle into a equilibrium state. General observations of these systems have shown so-called kinetic roughening where an initially flat interface that is being driven through a random medium becomes rougher and rougher in as time progresses. Here are some examples. (i) Consider a liquid being pumped into a random porous media. The liquid-air interface develops an irregular shape as it penetrates faster and deeper at places where the path is easier while it moves slower or stands still at places where the path is blocked. (ii) Consider a growing bacteria colony on a nutritious agar plate where food is abundant. While the colony maintains a solid and roughly circular shape as it expands, the boundary of the colony becomes rougher and richer in structure. (iii) Consider the slow combustion of paper [84, 88]. The initially straight burning front wiggles more and more as it progresses through the randomness and fluctuations in the paper texture.

Simple models for understanding the dynamics of such growing interfaces have long been studied. Among the earliest and the simplest ones is the so-called Eden's model [34] which can be regarded as a lattice model describing the growth of a bacteria colony on a agar plate. The system starts with a single occupied site representing the source of bacteria. The cluster then expands by randomly occupying empty sites neighboring the occupied cluster. After a long period of expansion, the resulting geometry of the cluster is a compact and roughly circular object. It is not a fractal. The boundary of the cluster develops into a roughened interface with self-affine structure which means that it looks alike after rescaling with different factors in different directions.

Just as for the sandpile models, the dynamic rules for Eden's model appear very simple, but a field-theoretical description of the process yields a stochastic nonlinear equation of motion [93],

$$\frac{\partial \rho(\mathbf{x},t)}{\partial t} = \nabla^2 \rho + \rho - \rho^2 + \rho\eta(\mathbf{x},t), \tag{1.15}$$

where the variable ρ represents the density of occupied sites. Equation (1.15) proves to

be too difficult for analytical treatments. However, numerical simulations and physical observations show that the interesting dynamics of the system actually happen only at the boundary of the cluster, that is, on the interface. Therefore, we can hope to understand this growth process by focusing on the dynamics of its boundary.

Instead of the growth from a single seed, consider the growth from a line source in a strip geometry. The system is finite in the x direction with $0 \leq x < L$ and is semi-infinite in the y direction with $y \geq 0$. The initial cluster occupies the whole $y = 0$ row. We can describe the boundary using a single-valued function $h(x)$ that represents the maximum y of the occupied sites in column x. We call h the *position* of the interface at the *location* x. A growth process that follows the dynamics of Eden's model is illustrated in Fig. 1.6.

Heuristically, the roughness of an interface depends on the length scale over which we view it. For example, the surface of the moon looks smooth from the earth, but it is full of craters and marks when we approach it with the lunar lander. To have a definition of being rough in the thermodynamic limit, we need a criterion that is scale independent. Here we define the roughness of an interface to be the second moment of its position h with respect to the average position over all locations x,

$$W^2 \equiv \overline{(h - \bar{h})^2}. \tag{1.16}$$

This h variable can be considered as the distance of the interface position relative to some reference line while the roughness is independent of this choice. The interface is considered to be in the so-called rough phase when the roughness W^2 diverges as the system size L goes to infinity. Generally, in the rough phase of the growth, an initially flat interface will roughen in time. And, if the system size is finite, its roughness will eventually reach a stationary value that depends on the size of the system. The way that it roughens from a initially flat configuration is characterized by the roughening exponent β which is defined through the equation

$$W \sim t^{\beta}, \tag{1.17}$$

where t is the time over which it has grown since the initial flat state. The stationary value of the interface roughness is characterized by the roughness exponent α which is defined

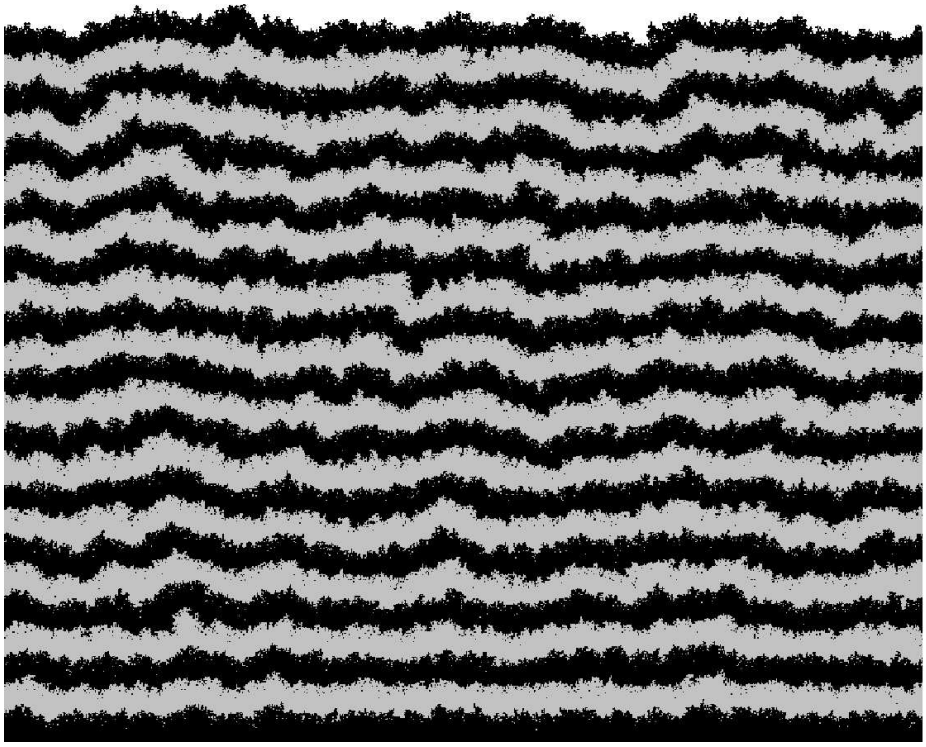

Figure 1.6: Growth of a Eden cluster from the bottom $y = 0$ row on a strip geometry: $0 \leq x < L_x$, $y \geq 0$ with $L_x = 800$; Each separately shaded region represents the growth of an area of 20000 lattice sites. As the interface grows upward, it becomes rougher and rougher.

through the equation

$$W \sim L^{\alpha} \tag{1.18}$$

that describes how it scales with respect to the interface length L.

1.3.1 Continuous equations for interface growth

The dynamics of a rough growing interface can be described by the so-called Langevin equation which in its simplest form is given by

$$\frac{\partial h(x,t)}{\partial t} = V_0 + \eta(x,t). \tag{1.19}$$

Here V_0 is a constant that represents the growth rate of the interface, and η is a random variable that accounts for the noise in the growth process. To simplify the problem, we assume η to have zero mean

$$\langle \eta(x,t) \rangle = 0, \tag{1.20}$$

and to be uncorrelated

$$\langle \eta(x_1,t_1)\eta(x_2,t_2) \rangle = D\delta(x_1 - x_2)\delta(t_1 - t_2). \tag{1.21}$$

Here D is a constant that characterizes the magnitude of the noise. The brackets indicate an ensemble average. This set of equations describes an interface growing with a velocity that's independently fluctuating in time at each location. In fact, for each location the interface position is just a random walk process biased with a mean velocity V_0 in the h direction. Equations (1.19)–(1.21) define the so-called random deposition model for which it's obvious from the random walk aspect that the second moment of the position h grows as the square root of time, and consequently, will never saturate for any system size. As a result, the roughening exponent $\beta = 1/2$ while the roughness exponent α is not well defined.

1.3.2 Edwards-Wilkinson growth equation

Growth with a random velocity at each location in space is not very realistic since we certainly expect that the growth is influenced by what's happening at neighboring locations.

In addition, the growth can only be well characterized by an interface when it's a well-defined continuous line, that is, $h(x)$ needs to be a continuous function. To preserve its continuity and to account for the coupling between the neighbors, we can introduce a surface-relaxation-type curvature term into the Langevin equation

$$\frac{\partial h}{\partial t} = \nu \nabla^2 h + V_0 + \eta. \tag{1.22}$$

Here ν is a parameter that controls the strength of the relaxation process. This gives us the Edwards-Wilkinson equation [35]. Because Eq. (1.22) is linear in h, it can be solved via Fourier transformation into momentum space. Also, the average growth rate can be made to vanish by transforming into a moving frame in the h direction, $h \to h - V_0 t$. Consequently, we can just consider the case $V_0 = 0$ without any loss of generality.

In momentum space, all of the modes decouple and the parameters in Eq. (1.22) will not be modified by the renormalization process. So, we can derive the scaling exponents from a simple scaling ansatz. Consider measuring the space using a scale which is larger by a factor of b than the original scale, $x = bx'$. We introduce the corresponding adjustments in the scale for time $t = b^z t'$ and for the interface position $h = b^\alpha h'$. The simple scaling ansatz requires that the rescaled system has the same physical description, that is, the new variables should also satisfy Eq. (1.22) with the same value of ν and with the same value of D for the noise as that defined in Eq. (1.21). This leads to the rescaled noise $\eta = b^{-(d+z)/2}\eta'$, where d is the dimension of x space, and to the equation

$$\frac{\partial h'}{\partial t'} = \nu b^{z-2} \nabla'^2 h' + b^{z-\alpha-(d+z)/2} \eta'. \tag{1.23}$$

Setting the exponents for the b factors to zero leads to

$$z = 2 \tag{1.24}$$

and

$$\alpha = \frac{z-d}{2}. \tag{1.25}$$

This indicates that the interface is rough for $d < 2$ and flat for $d > 2$.

1.3.3 Kardar-Parisi-Zhang growth equation

In describing a growing interface by a position variable h relative to some reference line, we are picking up a preferred direction for the growth process. However, for some interfaces, the growth dynamics is rotationally invariant and it only depends on the local orientation of the interface. Both the boundary of a bacteria colony on a uniform substrate and the cluster in Eden's model expand in all directions and therefore are examples in which each segment of their cluster boundaries should have the same dynamics when we choose any reference frame relative to the local orientation of the segment. When an interface segment is growing with a given velocity v perpendicular to its orientation, the growth rate measured in a reference frame slightly misaligned with the surface is given by [10]

$$\frac{\partial h}{\partial t} = v\sqrt{1+(\nabla h)^2} \approx v + \frac{v}{2}(\nabla h)^2 . \tag{1.26}$$

This shows the presence of a nonlinearity in the growth of this kind of interface and it becomes necessary to consider a more general equation which includes such a nonlinearity. This is the so-called Kardar-Parisi-Zhang (KPZ) equation [64]

$$\frac{\partial h}{\partial t} = \nu\nabla^2 h + \frac{\lambda}{2}(\nabla h)^2 + \eta. \tag{1.27}$$

In additional to providing rotational invariance, the additional λ term in Eq. (1.27) can also be used to account for a component of gradient-dependent growth rate in the growing process.

Applying the same rescaling argument as we did for Eq. (1.23), we find that the λ term in Eq. (1.27) scales like

$$\lambda b^{z-2+\alpha}(\nabla h)^2 . \tag{1.28}$$

This diverges with b for $d < 2$ if we assume EW scaling. This indicates that the EW scaling is unstable to the KPZ nonlinearity below two dimensions. As we have shown in Eq. 1.26, the coefficient λ is generally proportional to the growth velocity. Thus, this nonlinearity should be present in growing interfaces and we should expect them to be belong to the KPZ universality class.

The KPZ equation is also related to the so-called Burgers' equation [16]

$$\frac{\partial \mathrm{v}}{\partial t} = -\lambda \mathrm{v}\cdot\nabla \mathrm{v} + \nu\nabla^2 \mathrm{v} - \nabla\eta \tag{1.29}$$

with the constraint

$$\nabla \times \mathrm{v} = 0 \tag{1.30}$$

that describes a randomly stirred vorticity-free fluid by the change of variable

$$\mathrm{v} = -\nabla h. \tag{1.31}$$

The λ term in Eq. (1.29) comes from the total derivative of the velocity v,

$$\frac{D\mathrm{v}}{Dt} = \frac{\partial \mathrm{v}}{\partial t} + \mathrm{v} \cdot \nabla \mathrm{v}, \tag{1.32}$$

and it sets the value of the coefficient $\lambda = 1$ in order to respect Galilean invariance of the system, i.e., the fluid should be described by the same equation for all observers moving at constant velocity with respect to each other. This symmetry can not be broken by changing the scale used to measure the system. Therefore, $\lambda = 1$ should be invariant under a renormalization transformation that preserves this invariance and thus it represents a fixed point for the KPZ renormalization flow. Applying this to the KPZ equation, this suggests that the exponent of the scale factor b in Eq. (1.28) should be zero and it leads to the scaling relation [41, 87]

$$\alpha + z = 2. \tag{1.33}$$

This leaves us with only one independent scaling exponent between α and z at the $\lambda = 1$ fixed point.

In 1D, the value of this remaining independent scaling exponent, say, α can be found by showing that the probability $\Pi[h(x)]$ for the system to be in the configuration $h(x)$ has a stationary solution

$$\Pi\left[h(x)\right] = \exp\left(-\int dx \left[\frac{\nu}{2D}\left(\nabla h\right)^2\right]\right) \tag{1.34}$$

to the Fokker-Planck equation

$$\frac{\partial \Pi}{\partial t} = -\int dx \frac{\delta}{\delta h}\left[\left(\nu \nabla^2 h + \frac{\lambda}{2}\left(\nabla h\right)^2\right)\Pi\right] + D\int dx \frac{\delta^2 \Pi}{\delta h^2} \tag{1.35}$$

which is derived from Eq. (1.27). Equation (1.34) has a Gaussian distribution in ∇h which suggests that in the stationary state, there is no correlation between whether the interface height is going up or down at different locations as we trace it along the x direction. In

other words, it's a random walk if we consider x to be the time and h to be the position of the walker. This implies that the fluctuations in h scale as the root square of the interface length and gives us

$$\alpha = \frac{1}{2}. \tag{1.36}$$

This leads to

$$z = 2 - \alpha = \frac{3}{2}. \tag{1.37}$$

However, this solution is only applicable to 1D interfaces and the $\lambda = 1$ fixed point is only stable for $d < 2$. As will be discussed below, in 2D, the KPZ term is a marginal operator, which is known to change the scaling exponents of the EW equation to $\alpha \approx 0.4$ and $z \approx 1.6$. The exact values still remain unknown [24].

1.3.4 Renormalization flow for the KPZ equation

Following the success of equilibrium critical phenomena, Forster *et al.* [41] generalized the technique of renormalization group to dynamical systems and they applied it to the noisy Burgers' equation (1.29), i.e., they applied it to the equation that later became known as the KPZ equation. Their results were reformulated in interface language by Kardar *et al.* [64].

There the idea is to transform the equation to momentum space and to write down perturbative corrections to the parameters in the equation. The lattice spacing which is a lower cutoff in position space is represented by an upper cutoff Λ in momentum space. The renormalization is done by integrating over a thin shell of thickness $l\Lambda$ next to the cutoff in momentum space and then rescaling the system down by a factor of $b = e^l$, $x \to bx$ to restore the original cutoff. In order to preserve the same description of the system, we also need to make adjustments in the time $t \to b^z t$ and the height $h \to b^\alpha h$ scales.

Up to the order of λ^2 in the perturbative expansion, to obtain the same KPZ equation requires us to adjust the parameters according to the equations [64]

$$\frac{d\nu}{dl} = \nu \left[z - 2 + K_d g^2 \frac{2-d}{4d} \right] \tag{1.38}$$

$$\frac{dD}{dl} = D \left[z - d - 2\alpha + K_d \frac{g^2}{4} \right] \tag{1.39}$$

$$\frac{d\lambda}{dl} = \lambda\left[\alpha + z - 2\right], \tag{1.40}$$

where $g^2 \equiv \frac{\lambda^2 D}{\nu^3}$ and $K_d \equiv S_d/(2\pi)^d$ with S_d being the surface area of the d-dimensional unit sphere. These are the flow equations in the KPZ phase-space that show us how the parameters will appear to be changing when we change the scale of our measurements. The fixed points of these flow equations, which are found by setting the derivatives to zero, represent the asymptotic properties of the system in the thermodynamic limit and characterize the universality classes.

As mentioned previously, Galilean invariance requires that $\lambda = 1$ not be modified. Respecting that in Eq. (1.40), we need to have $\alpha + z = 2$ because otherwise we lose the invariance. A linear combination of the flow equations (1.38)–(1.40) gives the flow equation for the parameter g,

$$\frac{dg}{dl} = \frac{2-d}{2}g + K_d\frac{2d-3}{4d}g^3 \tag{1.41}$$

which is found to have the two fixed points,

$$g_1^* = 0 \tag{1.42}$$

and

$$g_2^* = \sqrt{\frac{2d(d-2)}{K_d(2d-3)}}. \tag{1.43}$$

The g_1^* fixed point corresponds to the $\lambda = 0$ case of the KPZ equation. This reduces the KPZ equation to the EW equation discussed previously. However, this is only stable for $d > 2$ and from Eq. (1.25), it gives us a flat phase. The g_2^* fixed point is unstable for $d > 2$. It represents the transition point between the EW flat phase and the KPZ rough phase. The characteristics of the KPZ rough phase in dimensions $d > 2$ are still being actively pursued by physicists. It is described by a strong-coupling fixed-point that lies outside the control of this renormalization transformation where the perturbative expansion is only valid for small λ.

In one dimension, $g_2^* = \sqrt{2/\pi}$ is an attractive fixed point. This means that for any system described with a nonzero λ term by the KPZ equation we'll eventually observe KPZ scaling behavior in the thermodynamic limit. At the KPZ fixed point, the EW surface relaxation term is actually also nonzero. The ratio ν^3/D is given by $\lambda^2\pi/2$. In practice,

the microscopic description of the system will not coincide with this ratio; i.e., we will not be at this renormalization-transformation fixed-point. All points at $\lambda \neq 0$ flow to the fixed point, and belong to the same universality class. However, we must expect to find so-called corrections to scaling with an amplitude proportional to the distance to the fixed point, i.e., the scaling of the system at small length scales or the scaling of a finite system of small size will appear different from that of the KPZ universality class, if fitted with a single power law. Moreover, strong crossover scaling effects will be present, both in length and time, that are associated with the EW fixed point if λ is small.

1.4 Directed percolation

Directed percolation (DP) emerged as one of the generic absorbing-state-type dynamic processes. It models the propagation of epidemics, e.g., forest fires and various types of surface catalysis processes [68, 102, 45, 46, 115]. Such processes involve an activity field $\rho(x) \geq 0$ and a so-called absorbing state $\rho(x) = 0$, typically the vacuum, from which it cannot escape. The relevant tunable parameter is the propagation probability q. The system undergoes a phase transition from the absorbing phase at small q, where the stationary state is the absorbing state, into an active stationary phase at large q, where the activities have a finite probability to last forever.

In the situations with more than one equivalent absorbing state or when the n module of the particle number is conserved by the dynamics of the system, a different type of absorbing-state phase transition might take place. In particular, the so-called *directed Ising* or *parity conserving* universality class [49, 47, 62, 66] can occur. However, most variations of the propagation rules put the transitions into the DP universality class [66]. It is now realized that DP critical behavior is the generic universality class for dynamic absorbing state type processes.

1.4.1 Kinzel's model

Consider the lattice shown in Fig. 1.7. The percolation activities only propagate upward in the directions shown by the arrows. The vertical upward direction can be considered as the

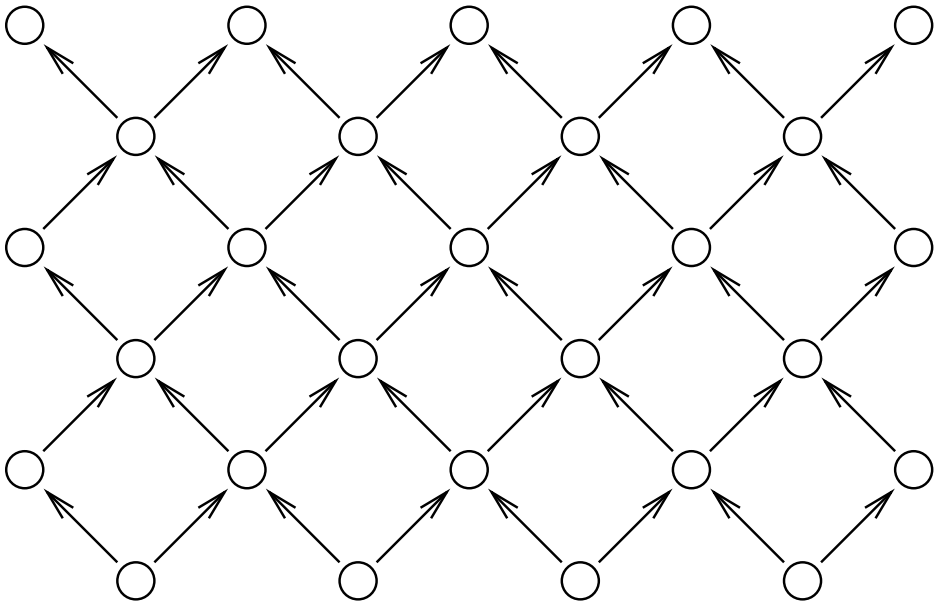

Figure 1.7: Lattice structure of Kinzel's model [68]; Circles are the sites while the arrows represent bonds. It is a square lattice tilted diagonally with activities propagate upward.

time direction. The full model consists of both the lattice sites and the bonds connecting the sites. A site in the system can only be active with a probability q when either one of the two bonds below it is present; and, a bond can only be present with a probability p when the site it's connecting to below is active. Setting $p = 1$ and using q as a control parameter leads to site percolation while setting $q = 1$ and using p as a control parameter leads to bond percolation [68, 33].

1.4.2 DP scaling exponents

At DP type critical points the correlation length in the time direction or the equilibration time $\xi_{\parallel}$ diverges. It's related to the spatial correlation length $\xi_{\perp}$ as $\xi_{\parallel} \sim \xi_{\perp}^{z}$ with the dynamic exponent $z \approx 1.581$ [63]. For example, starting from a single seed in the absorbing phase, the survival probability of the activities in the system obeys the scaling form

$$P_s(\epsilon, t) = b^{-x_s} P_s(b^{1/\nu_{\perp}}\epsilon, b^{-z}t) \tag{1.44}$$

with $\epsilon = q_c - q$ the distance from the critical point. This leads to

$$P_s \sim \epsilon^{\beta} \exp(\frac{-t}{\xi_{\|}}), \tag{1.45}$$

with the critical exponent $\beta = x_s \nu_{\perp}$. The exponential factor reflects the fact that deep inside the absorbing phase P_s decays exponentially in time. The equilibration time diverges at the DP critical point as $\xi_{\|} \sim \epsilon^{-\nu_{\|}}$ with $z = \nu_{\|}/\nu_{\perp}$. At the critical point, the survival probability decays as a power law, $P_s(t) \sim t^{-\delta}$ with $\delta = x_s/z = \beta/\nu_{\|}$.

The various scaling exponents of the DP universality class have been determined quite accurately. For example, using the method of low density series expansions, Jensen has studied several models in the DP universality class. He pushed the numerical accuracies for the values of the critical exponents to more than four decimal places with $\nu_{\|} \approx 1.7338$, $\nu_{\perp} \approx 1.0968$ and $\beta \approx 0.2765$ [63].

While these numerical results are encouraging, the exact scaling exponents of the DP universality class still remain unknown. Kwon *et al.* studied the dynamics of an interface between different absorbing regions in models with two absorbing ground states in 1D [70]. Consider an initial sharp interface separating the two absorbing state. The interface will grow from a single point to an active region where sites of the two ground states are intermixed.

Their numerical simulations of the system yield a scaling exponent $x \approx 2$ of the width of the active region $W \sim \epsilon^{-x}$, where $\epsilon = p_c - p$ near the DP critical point. While this seems to suggest a new simple exponent for the DP universality class, it will be shown in appendix A that the scaling behavior of the width is consistent with $W \sim \epsilon^{-\nu_{\|}} \ln(\epsilon_0/\epsilon)$.

1.5 A Lattice model: step flow with random deposition

Beside Eden's model which was mentioned previously, various model systems have been proposed to simulate kinetic roughening phenomena. Without going into the complete list of models that are relevant to kinetic roughening, I will focus on the details of a specific model that will be useful for the later discussion.

Consider an interface characterized by a height variable $h(x,t)$ defined on a one dimensional integer lattice $\{x\}$ with the strange rule that $h(x,t)$ is only defined on even

(odd) x sites when the time t is even (odd). This leaves the interface steps, the difference $h(x+1,t) - h(x-1,t)$, defined only on even (odd) x sites when the time t is odd (even). The system starts from a flat configuration with $h(x,0) = 0$ and evolves with a two-step rule as illustrated in Fig. 1.8. Consider the evolution from an even time t to the odd time $t+1$, as the height and step swap, the surface steps defined on the odd sites move by one unit to the even sites so that material is always removed. This amounts to having positive steps move to the right and the negative steps move to the left. This leaves the odd sites with no steps and with well defined heights. The steps meeting at even sites have their values added up and form one single step at each even site. Material is then deposited onto the odd sites so that each of them have its height value increased by the random amount $\eta(x,t+1)$, that is uncorrelated to other sites. The evolution from an odd time to an even time is done similarly.

We define two versions of the dynamics, using discrete or continuous height variables. In the continuous height version, h is a real number and the random variable η has an uniform distribution between 0 and a given constant s_c. As s_c is the only length scale in the h direction, we can set it equal to 1 without losing generality. For the discrete height model, h is an integer and $\eta = 0$ or 1 with probability $1-p$ or p respectively.

The complicated growth rule described above actually has the simple mathematical form

$$h(x,t+1) = \min\left[h(x-1,t), h(x+1,t)\right] + \eta(x,t+1) \tag{1.46}$$

or equivalently,

$$h(x,t+1) = \frac{h(x-1,t)+h(x+1,t)}{2} - \left|\frac{h(x-1,t)-h(x+1,t)}{2}\right| + \eta(x,t+1) \tag{1.47}$$

which can be regarded as a discretization of the KPZ equation (1.27).

1.5.1 Numerical results

My numerical results confirm the KPZ scaling for the both versions of the model as shown in Fig. 1.9. The figure also shows the finite-size-scaling (FSS) estimates of the scaling exponents α and β. The FSS plots reveal a correction to scaling to the exponents of the

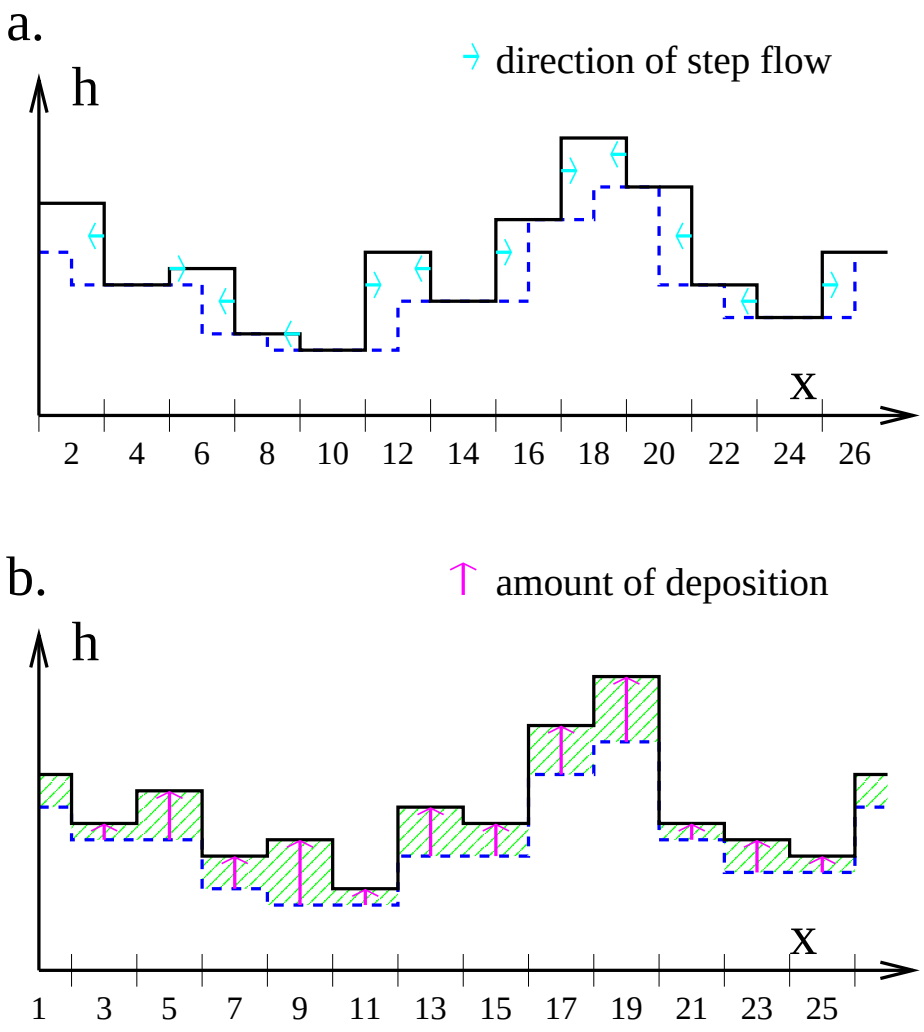

Figure 1.8: Two stage growth rule for the step flow + random deposition model; a. The step flow, from solid line to dashed line ; b. The deposition, from dashed line to solid line; before the growth step, heights are defined on even number sites while after the growth step, heights are defined on odd number sites

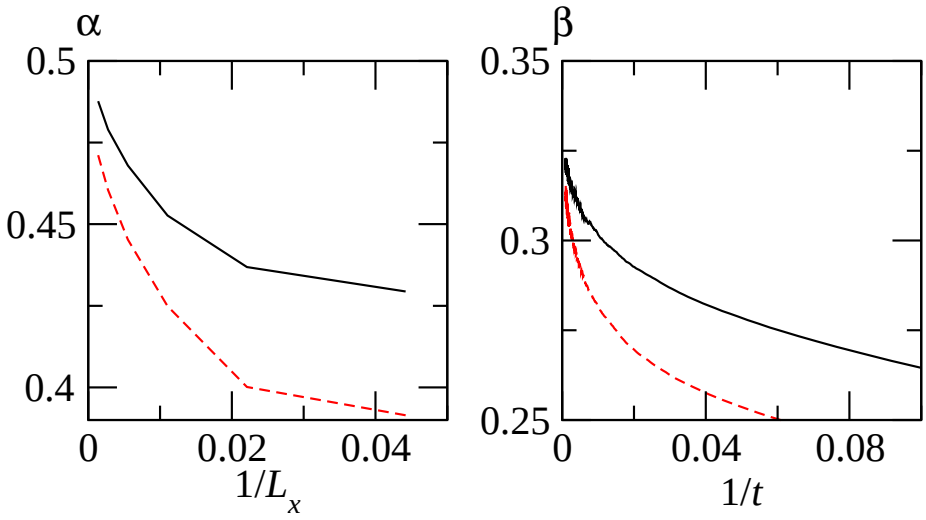

Figure 1.9: Finite-size-scaling (FSS) estimates of the α exponent, defined by Eq. (1.18) and the β exponent, defined by Eq. (1.17) from Monte Carlo (MC) results of the step-flow random-deposition (SFRD) model; Solid lines are of the continuous height version which dashed lines are of the discrete height version

form, e.g.,

$$\alpha(L) = \alpha_{\mathrm{KPZ}} + AL^{-x} \tag{1.48}$$

with $x \approx 1/3$. This suggests that the correction comes from the EW curvature term in the KPZ equation and that it presents a crossover effect between the two universality classes as will be elaborated below.

1.5.2 Corrections to scaling

For a finite system size L at a finite time t, the roughness is a function of the parameters $1/t$, $1/L$, and some irrelevant scaling field ν that represents the magnitude of the irrelevant operator in the equation,

$$w^2(t^{-1}, L^{-1}, \nu) = b^{2\alpha} w^2(b^z t^{-1}, bL^{-1}, b^{y_\nu}\nu). \tag{1.49}$$

For infinite systems, we can set $b = t^{1/z}$ so that the function can be expanded to give us

$$w^2(t^{-1}, 0, \nu) \simeq t^{2\alpha/z} \left[c_0 + c_1 t^{y_\nu/z} \right]. \tag{1.50}$$

For $y_\nu < 0$, the correction to the β exponent would be given by

$$\begin{aligned} \beta &= \beta_{\mathrm{KPZ}} + \frac{\ln\left(c_0 + c_1 t^{y_\nu/z}\right)}{\ln t} \\ &\simeq \beta_{\mathrm{KPZ}} + \frac{c_1 \ln c_0}{c_0 \ln t} t^{y_\nu/z}. \end{aligned} \tag{1.51}$$

For the KPZ equation (1.27), invariance under the renormalization transformation requires

$$\alpha - z = -y_\nu + \alpha - 2 = -y_\lambda + 2\alpha - 2. \tag{1.52}$$

Since at the KPZ fixed point, $y_\lambda = 0$, we have $y_\nu = 2 - z = 1/2$. This leads to the observed exponent $x = y_\nu/z = 1/3$ as the correction to scaling. This is the generic leading correction of the scaling exponent for lattice models which belong to the KPZ universality class.

1.6 A surface roughening transition in one dimension

For the discrete height version of the step-flow random-deposition (SFRD) model, we can vary the control parameter p corresponding to the deposition rate onto the interface. Since the steps move at unit speed over the interface, at low deposition rates, the lowest height level $h = h_0$ is stable in the sense that any single particle falling onto it will be evaporated away shortly in the following time step. Under this situation, the interface is said to be *pinned* at the bottom layer. The interface roughness is finite and doesn't scale with system size. Thus the system is in a flat phase. On the other hand, if the deposition rate is high, there is a sizable chance for islands to nucleate on the bottom layer. As the size of an island can only decrease from the edges, before these islands can be evaporated, they'll aggregate and fill up the whole bottom layer. When that happens, the $h = h_0 + 1$ layer becomes the new bottom layer until it also vanishes. The growth rate of the interface is thus governed by how fast a new bottom layer gets filled up.

There exists a DP type roughening transition between these two phases just as there does in the models studied by Savit and Ziff [101], Kertész and Wolf [65], and Alon *et al.* [1].

1.6.1 Mapping to Kinzel's model

The directed percolation aspect of the SFRD model comes from the dynamics of the bottom layer. We can define a density function $\rho_0(x,t)$ which is 1 when $h(x,t) = h_0$ and 0 otherwise. Since steps flow at unit speed and the depositions happen independently, the dynamics of $\rho_0(x,t)$ is independent of the other degrees of freedom in the system. In fact, it's a directed percolation process in the t direction. As shown in Fig. 1.7, the swap of even and oddness makes a diagonally placed square lattice in the x-t plane which is identical to the *site* directed percolation model studied by Kinzel *et al.* [68, 33]. The deposition rate p translates into $1-q$, the probability that a site is not present, in Kinzel's model. Since it is one of the models that have been extensively studied, the critical point of Kinzel's model is known to high accuracy $q_c = 0.7054850(15)$ [63]. This releases us from the burden of locating the transition point.

1.6.2 Scaling at the transition point

At the DP roughening transition, the interface width diverges logarithmically. Numerical investigations of poly-nucleation growth model by Kertész and Wolf reported [65] that the roughness $W^2 \sim \ln t$. However, the studies of a class of sequential solid-on-solid models by Alon *et al.* [2] showed that $W \sim (\ln t)^\gamma$ with a seemingly nonuniversal γ that has the values of about 0.24 for their unrestricted model and 0.43 for their restricted one. Numerical results on the SFRD model shows that the roughness scales as $W^2 \sim \ln t$. This agrees with Kertész's model.

As the dynamics of bottom layer density ρ_0 decouples from the rest of the degrees of freedom, its DP nature is in no doubt. This has been confirmed repeatedly by various numerical investigations [2, 110, 14]. Attempts to understand this transition have been made by putting the height variable into a hierarchy of fields ρ_k each representing the density of sites at height level $h_0 + k$ which is unidirectionally coupled through $\rho_{k-1} \to \rho_k$. As the upper critical dimension of the DP process is $d_c + 1 = 4 + 1$, Taüber *et al.* [110] and Goldschmidt *et al.* [44] performed $\epsilon = d_c - d$ expansion to first order and showed that the critical exponents $\beta^{(k+1)}$ which corresponds to the stationary density ρ_k in the active

phase for $k > 0$ are highly reduced with $\beta_1 = 1 - \epsilon/6 + O(\epsilon^2)$, $\beta_2 = 1/2 - \epsilon/8 + O(\epsilon^2)$, and $\beta_3 = 1/4 - O(\epsilon)$. The dynamic exponent z, as well as the transition point, are found to remain identical for all ρ_k.

However, our understanding of the scaling behavior for the interface roughness W^2 at the transition point remains only numerical. No theoretical explanation has been offered for what gives rise to the logarithmic divergence in time, and the logarithmic dependence on the sizes of finite systems has not been confirmed.

1.7 Propagation of avalanche front

Imagine an avalanche event in a sandpile model. Although the avalanche cluster can be large and span the entire system, the actual toppling activities at any given moment in time are usually more localized. The toppling fronts are usually objects of lower dimensionality and involve only a few degrees of freedoms. This motivates the approach to understanding the properties of the avalanches through the understanding of front propagation. In the regular sandpiles, a single avalanche often generates more than one of such front, each is sweeping through the system just once. These fronts are recognized as the so-called toppling waves by Priezzhev *et al.* [98]. They showed that in the BTW sandpile model one can decompose an avalanche into waves of topplings and they proved that in each of these waves, a given site will only topple once while the activity propagates away from the triggering point just like the ripple of a stone thrown into a pond. However, unlike the latter, the shape of the front might distort and fragment in time.

In directed avalanche systems, the causal nature in the propagation direction allows us to perform the toppling in a row-by-row fashion and this effectively leads to just one single front for each avalanche. While the dynamics of self-organized criticality is iterative and nonlocal, the evolution of a single front line is local owing to the toppling dynamics. Additionally, the propagation of a front line only depends on the configuration of the toppling row y and the receiving row $y + 1$, with no dependence on positions before y. Thus the process can be considered to be Markovian in this respect. To make this idea concrete, let's consider a system configuration at the y-th row that is given by $z_i^{(y)}$ and $\hat{z}_i^{(y)}$ after and before the i-th

avalanche. That is, in the i-th avalanche, the configuration at row y makes the transition

$$\hat{z}_i^{(y)}(x) \to z_i^{(y)}(x). \tag{1.53}$$

For directed local toppling rules, the pre-toppling configuration $\hat{z}_i^{(y)}$ only locally depends on the pre-toppling configuration $\hat{z}_i^{(y-1)}$ of the previous row and the post-toppling configuration $z_{i-1}^{(y)}$ in the previous avalanche. This allows to write down a general discrete Langevin equation of the form

$$\hat{z}_i^{(y)} - \hat{z}_i^{(y-1)} = F[\hat{z}_i^{(y-1)}, z_{i-1}^{(y)}, \eta_i^{(y)}] \tag{1.54}$$

where η accounts for the randomness in the toppling process. Since $z_{i-1}^{(y)}$ is already determined by the previous avalanche, it can combined with η to give an effective noise function $\tilde{\eta}$ in Eq. (1.54). In continuous form, Eq. (1.54) can be rewritten as

$$\frac{\partial \hat{z}_i^{(y)}}{\partial y} = \tilde{F}[\hat{z}_i^{(y)}, \tilde{\eta}_i^{(y)}] \tag{1.55}$$

which gives us the general form of Eq. (1.13).

The caveat in the above approach is that the effective noise $\tilde{\eta}$ in Eq. (1.55) is not always as simple as it is in the case of Eq. (1.11) where it's uncorrelated. Since the effective noise is related to the previous stable configuration of the system, if the stationary state of the system is nontrivial, we should expect to have a nontrivial effective noise, too. Under the situation, large corrections to the scaling behavior from the naïve local interface dynamics will result. But, we shall show that for avalanche systems with essentially compact avalanche clusters, this correction is irrelevant in the thermodynamic limit. Thus it does not hinder the validity of classifying these directed avalanche systems by the universality classes of their underlying interface dynamics.

1.8 Summary and preview

The theme of this thesis is to establish a mapping between avalanche systems and interface growth models as outline in the previous section. In the next chapter, I will formulate this mapping using a sandbox system as a paradigm. The interface dynamics that underlies the lattice sandbox model is that of the step-flow random-deposition model which we discussed

in Sec. 1.5 where we also established that it belongs to the Kardar-Parisi-Zhang universality class with typical corrections to scaling coming from the influence of the Edwards-Wilkinson fixed point.

This mapping allows us to predict the scaling exponents of the avalanche distributions based on those of the underlying interface model. However, the numerical results of the exponents show a small but significant deviation from their predicted values. I will address the issue of this deviation in chapter 2 and show that it is a large correction to scaling due to the scarring of the the sand surface by the iterative avalanche process. In the thermodynamic limit, the scaling exponents of the avalanches should remain as predicted.

The underlying interface model of the discrete-height sandbox model undergoes a continuous phase transition of directed percolation nature as described in Sec. 1.6. In chapter 3, I will show that this model can be used to describe the avalanches of granular materials with variable cohesiveness. The continuous phase transition in the interface model corresponds to the transition in a granular system from a phase of shallow avalanches to a phase of deep avalanches when the cohesiveness is increased. I will also show that the prediction based on the mapping between avalanche systems and interface models remains valid in both phases and also at the transition point. However, the mass hyperscaling relation, which is established in chapter 2, based on the compactness of the avalanche clusters is broken at the transition point due to the fractal property of the avalanche clusters.

Chapter 2

DIRECTED AVALANCHE PROCESSES WITH UNDERLYING INTERFACE DYNAMICS

In this chapter, we describe in more details the directed avalanche model; a slowly unloading sandbox driven by lowering a retaining wall. The directness of the dynamics allows us to interpret the stable sand surfaces as world sheets of fluctuating interfaces in one lower dimension. In our specific case, the interface growth dynamics belongs to the Kardar-Parisi-Zhang (KPZ) universality class. We formulate relations between the critical exponents of the various avalanche distributions and those of the roughness of the growing interface. The nonlinear nature of the underlying KPZ dynamics provides a nontrivial test of such generic exponent relations. The numerical values of the avalanche exponents are close to the conventional KPZ values, but differ sufficiently to warrant a detailed study of whether avalanche-correlated Monte Carlo sampling changes the scaling exponents of KPZ interfaces. We demonstrate that the exponents remain unchanged, but that the traces left on the surface by previous avalanches give rise to unusually strong finite-size corrections to scaling. This type of slow convergence seems intrinsic to avalanche dynamics.

2.1 Introduction

Avalanche phenomena are common in nature. Examples range from accumulating snow on mountain slopes, slow shearing between continental plates [21], rerouting in river networks, to creeping magnetic flux lines in super conductors [8]. Following the work by Bak *et al.* [5], physicists aim to capture the essential aspects of such dynamical systems with simple automaton processes, commonly referred to as sandpile models and self-organized criticality (SOC). Impressive successes have been achieved, like reproducing power-law distributions in avalanche events similar to those observed in nature, and the start of a classification

scheme of such processes in terms of so-called universality classes [13]. Unfortunately most of these are numerical in nature. Analytical exact results remain rare.

Directed avalanche phenomena form a subclass of these SOC processes. Dhar and Ramaswamy introduced the first directed sandpile model and solved it exactly [32]. This was possible because in their model the avalanche propagation is governed solely by its two edges, and those two follow independent random walk dynamics. Tadić and Dhar introduced a directed model in which particles are allowed to pile up beyond the critical height, by replacing the automaton's deterministic toppling rule by a stochastic one [107]. The density of critical sites tunes itself and at distances far from the driving edge the propagation of active sites approaches the directed percolation [68] threshold. The scaling properties of the avalanche distributions are thus linked to the critical exponents characterizing the DP universality class. Another example of a stochastic directed avalanche process is the model introduced and studied numerically by Pastor-Satorras and Vespignani [95]. Similar as in the above model by Dhar and Ramaswamy, the stable landscape configurations (between avalanche events) lack internal correlations in the stationary state. This allowed Paczuski and Bassler [91] and also Kloster *et al.* [69] to link this dynamic process to so-called Edwards-Wilkinson [35] (EW) interface growth and to derive the exact scaling exponents of the avalanche distributions.

This novel world-sheet-type connection between avalanche dynamics and interface growth is particularly promising, because interface dynamic processes such as EW and Kardar-Parisi-Zhang [64] (KPZ) growth are very well understood, in particular, in 1+1 dimensions (1+1D) where the scaling properties are known exactly. However, the above models that are linked to EW-type growth are rather poor examples, because EW growth is described by a simple linear stochastic (diffusion-type) Langevin equation; correlations factorize, and important caveats in the relation to avalanche dynamics can be obscured by this simplicity.

We set out to generalize this approach to nonlinear interface dynamic processes, and recently introduced a directed unloading sandbox model [23] in which the two-dimensional (2D) avalanche dynamics relates to 1+1D KPZ-type interface growth. We derived exponent relations between the avalanche and interface growth scaling properties, which are generic, and valid beyond our specific model. Our numerical results for the avalanche distributions

(for length, width, depth, and mass) follow indeed these exponent relations. Moreover, the avalanche critical exponents obey the predicted KPZ values within a few percent, an accuracy typical to avalanche simulations. However, our numerical accuracy is better than that; mostly because of a careful finite-size scaling (FSS) analysis. The exponents seem to converge to values that are slightly different from the KPZ values.

This left us with a puzzle. What is the origin of these small deviations? Is this a fundamental effect; or do the exponents ultimately converge to the KPZ values, but with unusually large corrections to scaling. In this chapter, we address these issues. We also provide a more detailed discussion of these world-sheet-type relationships between avalanche and interface growth dynamics.

The fundamental difference between conventional KPZ interface growth and avalanche dynamics arises from the averaging process over KPZ-type space-time world sheets. In normal Monte Carlo (MC) simulations of interface growth the distribution functions are determined in terms of ensemble averages over a set of totally uncorrelated space-time MC runs. In contrast, the avalanche dynamics gives rise to KPZ world sheets that are strongly correlated. Two subsequent MC runs are identical except inside a single avalanche area. This difference in averaging, uncorrelated versus avalanche-correlated MC runs, therefore emerges as a key issue for understanding the scaling properties of avalanche dynamics. This issue did not arise in the earlier EW-type avalanche models due to the linear nature of the EW process. However for nonlinear dynamics, such as KPZ, avalanche-correlated-type sampling could well lead to novel interface scaling exponents.

Speaking against a shift in the values of the exponents, are arguments that: the KPZ stationary state, i.e., the sand surface profile far away from the driving edge, can not be affected by the avalanche-correlated-type averaging, because large avalanches that span the entire width of the box occur periodically. These completely refresh the surface far away from the driving edge regularly, and thus wipe out all correlations between MC runs. This suggests that we are only dealing with much larger than usual corrections to scaling. The details are more complex than this simple argument, but we will establish that indeed the exponent values do not change.

This chapter is organized as follows. In the following section, we present the unloading

sandbox model. In Sec. 2.3, we comment on how directed avalanche dynamics can be linked to interface growth in one lower dimension. Next, in Sec. 2.4, we show that in the interface growth interpretation our specific model belongs to the KPZ universality class. In Sec. 2.5, we derive the generic exponent relations between interface growth and directed avalanche dynamics, and in Sec. 2.6 we test this numerically for our specific model.

In the second half of this chapter, we address the small deviations in the numerical values of the exponents from those of conventional KPZ growth. In Sec. 2.7, we present numerical results detailing how the traces left on the surface profile by previous avalanches influence both the avalanche exponents and the interface growth ones. These scars in the rough surface enhance the surface roughness. We cast this enhanced interface roughness in terms of corrections to scaling, and determine what value the critical dimension of the corresponding irrelevant operator $O_{\rm sc}$ (in the sense of renormalization theory) should have. Next, in Sec. 2.8, we identify the geometric meaning of $O_{\rm sc}$, starting with a study of the one dimensional version of our model where a similar phenomenon takes place. In 1D the interface growth process is a simple random walk, and the avalanche-correlated sampling relates to the scaling properties of merging random walkers. $O_{\rm sc}$ represents the distribution of avalanche end points in the 1D surface, and can be studied directly from the rounding of the surface profile near the driving edge. In Sec. 2.9, we return to the full 2D case. The scars of previous avalanches form lines on the surface. We identify $O_{\rm sc}$ with the angle these lines make with respect to the direction perpendicular to the driving edge, and confirm with an analytic argument that the critical dimension of $O_{\rm sc}$ is equal to $x_{\rm sc} = -z$ with z the KPZ dynamic exponent. Finally, we summarize our results in Sec. 2.10.

2.2 An unloading sandbox

Imagine a box filled with granular material, as illustrated in Fig. 2.1. One of its four retaining walls is slowly lowered, such that the sand spills out from that side, and thus slowly unloads the box and establishes a sloped surface. In the quasistatic limit, the wall moves slow enough that the unloading events can be described as distinct avalanches. The box can be three dimensional, leading to 2D avalanche dynamics on a 2D surface, or can be

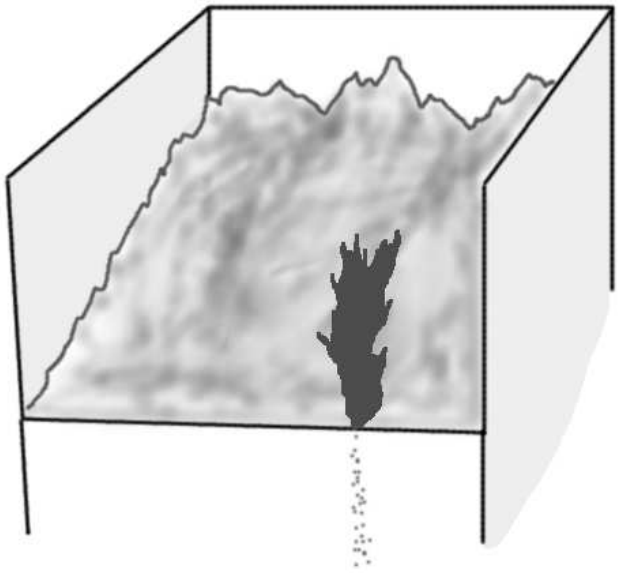

Figure 2.1: Sandbox with a slowly lowering retaining wall.

2D (like in a very narrow box) giving rise to 1D avalanches on a 1D surface.

Inspired by this we consider a so-called solid-on-solid model defined on a 2D lattice. Height variables $h(\mathbf{r})$ are defined on a square lattice. We will consider two versions of the model. In the continuous height version, the heights are real numbers. In the discrete model, the heights are integers $h(\mathbf{r}) = 0, \pm 1, \pm 2, \ldots$. The former corresponds to a continuous material without internal structure, but strong cohesion up to a specific length scale s_c, while the latter corresponds to layered material where the surface height is quantized.

The 2D lattice is rotated diagonally such that the propagation direction of the avalanche is along the diagonal direction denoted by y. This is the direction in which the avalanche will run. Throughout this chapter the coordinate perpendicular to y will be denoted by x. Figure 2.2 illustrates this geometry.

The configurations are subject to the following stability condition. The column of particles on site $\mathbf{r} = (x, y)$ is supported by the two columns $\mathbf{r}_l = (x-1, y-1)$ and $\mathbf{r}_r = (x+1, y-1)$ directly below it and is stable when its height is less than the minimum of the heights at

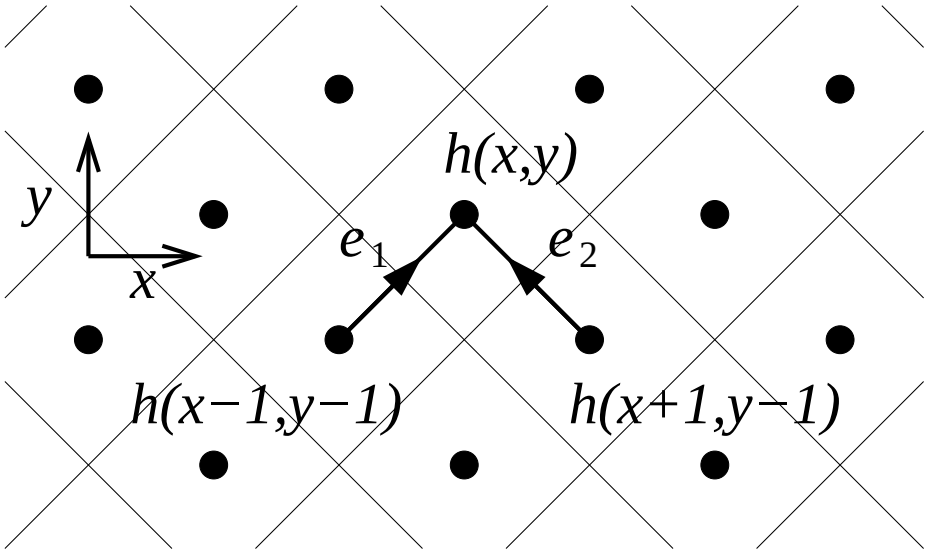

Figure 2.2: Lattice structure of sandbox model in 2D.

these two supporting sites increased by a fixed amount:

$$h(\mathbf{r}) \leq \min\left[h(\mathbf{r}_l), h(\mathbf{r}_r)\right] + s_c, \tag{2.1}$$

where s_c is a constant. In the version of our model where the heights are continuous variables, s_c represents the only length scale in the h direction and can be set equal to 1 without the loss of generality. Throughout this chapter we will also set $s_c = 1$ in the discrete h model.

Consider a stable configuration, after $\tilde{t}-1$ avalanches. The $\tilde{t}$th avalanche is triggered at the highest site $\mathbf{r} = (\mathbf{x}_{\tilde{t}}, 0)$, on the $y = 0$ driving boundary (or, in the discrete height model, by randomly choosing one of the highest sites) and reducing its height by a random amount $0 < \eta_{\tilde{t}} \leq s_c$. This likely creates unstable sites in the next $y = 1$ row. Those are updated by replacing their height by an amount equal to the lowest of the two supporting columns in the previous row and then adding an uncorrelated random amount $0 \leq \eta(\mathbf{r}) \leq s_c$ with uniform distribution, as

$$h(\mathbf{r}) \rightarrow \min\left[h(\mathbf{r}_l), h(\mathbf{r}_r)\right] + \eta(\mathbf{r}). \tag{2.2}$$

This updating continues row by row until all the sites are stable again. Only after that the

next avalanche is started. The toppling of a site only affects the stability of the two sites immediately above it in the next y row. Therefore we can update the system row by row in increasing order of y.

Direct experimental realizations of this unloading sandbox model are not our immediate concern (the focus is on establishing a generic theoretical relationship between avalanche dynamics and interface growth), but we expect that this model is applicable to actual experimental unloading sandboxes. One of the most important issues in this context is the row-by-row nature of the toppling rule. This is a crucial feature for our purposes, allowing the identification with KPZ interface growth (in the following section). In real unloading sandboxes the sand removed from row y rolls down hill and likely disturbs the already stabilized lower surface levels. Experimental realizations can avoid this from happening, e.g., by choosing very light grains (compared to the cohesion forces). Note that our dynamic rule does not allow the buildup of any pockets (deeper than s_c) on the surface that might trap such downward rolling grains.

Conservation laws are crucial to avalanche dynamics. Unlike most avalanche processes, our model does not conserve mass while the avalanche propagates. That might raise the specter of our model not being (self-organized) critical. The connection to KPZ growth (an intrinsic critical process) dispels this phantom. Moreover, the global slope of the surface is preserved during each avalanche run, and conservation of steps in the profile plays the role analogous to conservation of mass.

In a typical SOC process, the quasistatic limit must be taken such that the surface regains full stability before a new grain is being removed at the driving edge. Since avalanches of all sizes appear, this means that the velocity of the lowering wall should be inversely proportional to the size $L_x \times L_y$ of the box. Our process, however, is Markovian, i.e., row by row in the y direction. Removal of particles in row y does not affect the stability of the lower levels. In that case the lowering velocity needs only be inversely proportional to L_x.

The analysis of the dynamics involves distribution functions of various characteristic features of the avalanches, The common examples are: length, width, depth, and mass. The avalanche length l will be defined throughout this chapter as the maximum distance y the avalanche travels from the driving edge; the width w as the maximum departure of the x

coordinate (perpendicular to the propagation direction) from the trigger point x coordinate; the depth δ as the maximum height change the avalanche creates at any of the affected sites; and the mass m as the total amount of material removed by the avalanche. All the above are dimensionless quantities measuring the numbers of lattice spacings (or multiples of s_c in the h direction) in our numerical presentations.

2.3 Avalanches versus epitaxial interface growth

The focus of this chapter is on how the above avalanche dynamics relates to interface growth in one lower dimension. Each stable sloped surface configuration of a directed sandpile can be reinterpreted as a world sheet (space-time configuration) of an interface in one lower spatial dimension. The direction in which the avalanches propagate plays the role of time and the perpendicular coordinates the role of space. Our 2D unloading sandbox is equivalent to a 1D growing interface. Such an interpretation makes sense only when the stability condition and the avalanche dynamic rule is directional and local in space time, such that causality is not violated in the interface growth interpretation. The stability condition (2.1) and toppling rule (2.2) of our model are row by row in nature and therefore indeed Markovian in this sense.

Every stable configuration of the sandpile represents a possible interface growth lifeline (space-time-evolution interface world sheet). The conventional procedure for determining the scaling properties of growing interfaces is to average over a large set of completely independent MC runs. This would mean, in sandbox language, an ensemble average over completely refreshed surfaces, each totally uncorrelated from the previous one (except typically for the initial condition in row $y = 0$). The toppling rule (2.2) is applied to all sites in every row, and repeated row by row, instead of only the unstable sites created by toppling only the highest site in the initial row.

In avalanche dynamics, however, two subsequent growing interface lifelines in this ensemble differ only inside the avalanche area. From the interface growth perspective this represents a rather peculiar and dangerous correlated-type MC run averaging procedure. The MC runs of KPZ space-time configuration are strongly correlated, and this raises the

specter of a change in the interface roughness scaling properties. The numerical evidence, presented below is sufficiently ambiguous that this issue will preoccupy us in the second half of this chapter.

2.4 KPZ growth

In this section, we demonstrate that the interface growth model conjugate to the unloading 2D sandbox belongs to the 1+1D KPZ universality class. The time evolution of the interface is governed by the toppling rule of the sand model with y in Eq. (2.2) representing time t,

$$h(x, t+1) = \min\left[h(x+1, t), h(x-1, t)\right] + \eta(x, t). \tag{2.3}$$

In the conventional global-type interface evolution (i.e., totally refreshing non-avalanche-type uncorrelated MC runs) every site in row $t+1$ is updated according to this rule.

Figure 2.3 illustrates the interface dynamics for one time step, $t \to t+1$. Conceptually, the time step can be split into two parts; the deterministic min[ ] operator part and the stochastic random deposition η part.

Note that because of the diagonal orientation of the square lattice (see Fig. 2.2), the lattice sites are not "stationary in time." The conceptually easiest interpretation to resolve this flip-flopping is to first double the number of lattice sites and then to require them to be paired alternately with their right or left neighbors at even and odd times; at even times sites $2n$ and $2n+1$ are fused to be at equal heights and at odd times the $2n-1$ and $2n$ sites.

The upper panel shows the deterministic first half of the update (from the drawn to the dash line). The partners switch and the min[ ] operation equalizes their heights by choosing the lowest of the two, so this step always removes material.

This can be interpreted also in terms of a movement of the steps in the interface. All up steps move to the right and all down steps to the left; while up and down steps merge when they meet at one site.

The lower panel illustrates the second half of the update. The height of each fused pair increases by a random amount $0 \leq \eta \leq s_c$.

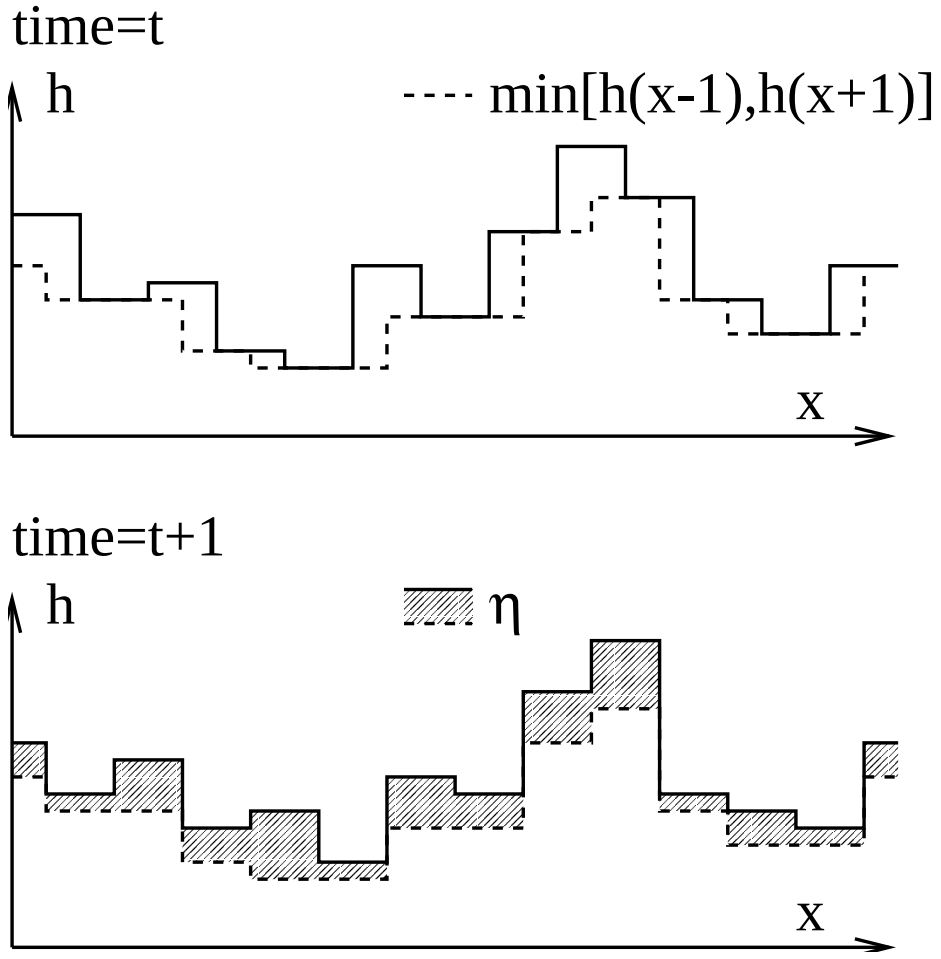

Figure 2.3: The interface growth dynamics described by Eq. (2.3) with upper panel showing movement of steps (from the drawn to dashed line) and lower panel random depositions (shaded area) to the interface.

Deposition-type interface dynamics like this typically belongs to the KPZ universality class [64]. Indeed, Eq. (2.3) can be rewritten as

$$\begin{aligned} h(x,t+1) &= \frac{1}{2}\left[h(x+1,t)+h(x-1,t)\right] \\ &- \frac{1}{2}\left|h(x+1,t)+h(x-1,t)\right| + \eta(x,t), \end{aligned} \tag{2.4}$$

and from this it can be easily identified to be a discrete form of the KPZ Langevin equation,

$$\frac{\partial h}{\partial t} = \nabla^2 h - \frac{\lambda}{2}\left|\boldsymbol{\nabla} h\right|^2 + \eta. \tag{2.5}$$

The crucial point is that the coefficient of the nonlinear term λ is clearly present. There is no hidden special symmetry of some kind that makes it vanish by accident. At $\lambda = 0$, the KPZ equation would reduce to EW growth.

To confirm the KPZ nature and make sure that the λ is large enough that corrections to scaling from the EW point ($\lambda = 0$) are not obscuring the KPZ scaling, we perform MC simulations on the interface dynamics as illustrated in Fig. 2.3. The MC runs are completely independent.

We measure the time evolution of the interface width W defined as

$$W^2(L_x,t) \equiv \langle \overline{(h-\bar{h})^2} \rangle \tag{2.6}$$

with over bars (angle brackets) indicating average over x (ensemble). Starting from, e.g., a flat initial condition it should scale as

$$W \sim t^{\beta} \tag{2.7}$$

at intermediate times $0 \ll t \ll L_x^z$, and saturate at

$$W \sim L_x^{\alpha} \tag{2.8}$$

for $t \gg L_x^z$; with L_x the length of the 1D interface. The exponents for the KPZ universality class in 1+1D are known exactly with $\alpha = 1/2$, $\beta = 1/3$, and $z \equiv \alpha/\beta = 3/2$.

The numerical results are shown in Fig. 2.4. The values of $\alpha(L_x)$ are obtained from the saturated interface widths by imposing the scaling form (2.8) at adjacent values of the system size L_x. Similarly, the values of $\beta(t)$ are obtained from the transient interface

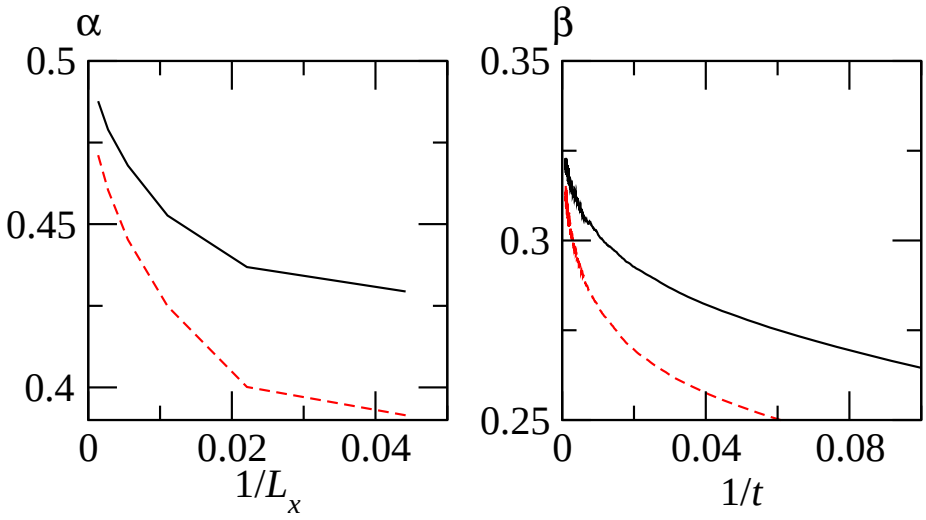

Figure 2.4: MC results for the global interface width: left, finite-size (L_x, in the unit of lattice spacing) estimates for the saturated surface width exponent α; right, finite-time (t, in MC time steps) estimates for the transient interface width exponent β from a flat initial configuration. The solid (dashed) curves are for continuous (discrete) height model.

widths by imposing the scaling form (2.7) at nearby times t. We like to remind the reader that simple log-log plots of W versus L_x and t look typically impressively straight, but are notoriously inaccurate. The construction of effective exponents, in the above manner might at first glance look less impressive (the data appears noisier), but this brings the analysis to a higher level where the leading corrections to finite-size and finite-time scaling become visible.

The approach to $L_x \to \infty$ in Fig. 2.4 is consistent with the leading correction to scaling exponent $y_{\rm ir} = -1/2$ expected from the EW term $\nabla^2 h$ in Eq. (2.5). The corrections to FSS are stronger when the height variables are discrete than when they are continuous. This is consistent with the smaller growth rate in the discrete height interface, and the fact that the growth rate is typically proportional to the nonlinear term λ. On average, more material is removed during the first deterministic part of the update process when the surface heights are discrete.

2.5 Scaling properties of 2D avalanches

In this section, we derive the exact relations between the scaling properties of the avalanches and 1+1D KPZ interface growth. However, in the latter the world sheets are sampled in the correlated manner as outlined in Sec. 2.3.

The characteristic feature of SOC is the lack of typical avalanche length, width, depth or mass scales. The probability distributions follow power laws. For example, the distribution of avalanche widths scales as

$$P_w \sim w^{-\tau_w} \tag{2.9}$$

with scaling exponent τ_w. Similarly, the avalanche length, depth, and mass distributions scale as power laws with exponents τ_l, τ_δ and τ_m. We can summarize this in a metadistribution function $P(l, w, \delta)$; the probability to find an avalanche of a specific width w, length l, and depth δ obeys the scaling relation

$$P(l, w, \delta) = b^{-\sigma} P(b^{-z} l, b^{-1} w, b^{-\alpha} \delta) \tag{2.10}$$

with b an arbitrary scale parameter. The exponents σ, z, and α are expected to be robust with respect to details of the dynamic rule, and thus are characteristic of the universality class to which this avalanche dynamics belongs. Single parameter distributions, such as P_w, follow by integrating out the other variables. This implies the following expressions for the τ exponents:

$$\tau_l = \frac{\sigma - 1 - \alpha}{z},\ \tau_w = \sigma - z - \alpha,\ \tau_\delta = \frac{\sigma - 1 - z}{\alpha}, \tag{2.11}$$

or inverted,

$$z = \frac{\tau_w - 1}{\tau_l - 1},\ \alpha = \frac{\tau_w - 1}{\tau_\delta - 1},\ \sigma = \tau_w + z + \alpha. \tag{2.12}$$

Let us presume that the avalanches are compact, i.e., that the inside and the boundaries of an avalanche are well defined and distinguishable (unlike in certain fractal structures), and that the sizes of the holes (unaffected regions) inside the avalanche do not scale with the avalanche size. This can be checked visually from typical simulation configurations, and both assumptions are indeed satisfied in our dynamics at least qualitatively. In that case, the mass of the avalanche must scale as $m \sim lw\delta$, such that the critical exponent of the

distribution of avalanche masses $P_m \sim m^{-\tau_m}$ obeys the identity

$$\tau_m = \frac{\sigma}{1+z+\alpha}. \tag{2.13}$$

There is one more relation between these critical exponents (leaving only two independent ones). The avalanche is initiated by lowering the bar at the driving edge of the box. In the stationary state the average surface profile is invariant, and therefore it shifts down at the same rate as the lowering bar. Thus we know how much mass drops out of the box on an average.

To be more precise, during each avalanche event, the height of only one single boundary site at $y = 0$ is lowered by, on average, an amount $s_c/2$. For a sandbox of width L_x the boundary row is lowered by $s_c/2$ after L_x avalanches. In the stationary state, the entire surface matches this lowering speed, such that the amount of removed sand is on average equal to $L_x L_y s_c/2$. Therefore, the average mass of each avalanche must be equal to

$$\langle m \rangle = \frac{1}{2} s_c L_y. \tag{2.14}$$

The scaling properties of the mass distribution function tie into this because

$$\langle m \rangle = \int m' P_m(m') dm', \tag{2.15}$$

which can be evaluated using the metadistribution function as

$$\begin{aligned} \langle m \rangle &\sim \int_0^{L_y} dl \int_0^\infty dw \int_0^\infty d\delta \, lw\delta P(l,w,\delta) \\ &+ m_{L_y} \int_{L_y}^\infty dl \int_0^\infty dw \int_0^\infty d\delta \, P(l,w,\delta). \end{aligned} \tag{2.16}$$

This equation incorporates finite-size effects. The box is presumed to be wide and deep enough, such that the length L_y of the box (in the direction perpendicular to the driving edge) is the only limiting finite-size factor. The first term in the above equation accounts for all avalanches that fit inside the box and the second term for the ones that reach the L_y edge, and thus are prematurely terminated. The first integral scales as $L_y^{(-\sigma+2+2z+2\alpha)/z}$ for large L_y. The second term scales with the same power because the second integral scales as $L_y^{(-\sigma+1+z+\alpha)/z}$, while the mass factor in front of it scales as $m \sim lw\delta \sim L_y^{(1+z+\alpha)/z}$. The result

$$\langle m \rangle \sim L_y^{(-\sigma+2+2z+2\alpha)/z}, \tag{2.17}$$

when compared to Eq. (2.14), yields the exponent identity

$$\sigma = 2 + z + 2\alpha. \tag{2.18}$$

The validity of these exponent identities goes well beyond our KPZ-type unloading sandbox. For example, the EW-type directed avalanche models by Paczuski and Bassler [91] and Kloster *et al.* [69] obey our Eq. (2.11) when we substitute for z and α the EW values ($z = 2$, $\alpha = 1/2$). The scaling exponents of the original Dhar-Ramaswamy model can be described by the same equations with $z = 2$, $\alpha = 0$ as well.

2.6 Numerical results for 2D sandbox avalanches

The discussion of the previous section leaves us with two independent avalanche critical exponents, α and z. The notation anticipates their identification with the scaling properties of a rough interface in interface growth. There, α is the scaling exponent of the interface width and z the dynamic critical exponent. Indeed, the interface width relates to the depth of the avalanche, and time to the length of the avalanche. We expect therefore that α and z take same values as in 1+1D KPZ growth, $\alpha + z = 2$ and $\alpha = 1/2$.

We perform MC simulations on the sandbox avalanche model and measure the avalanche metadistribution function $P(l, w, \delta|L_y)$ [see Eq. (2.10)]. The sandbox is always taken wide and deep enough such that the box length L_y acts as the only FSS-type limiting factor. We average over 2^{31} avalanches. The reduced distributions, such as $P_l \sim l^{-\tau_l}$, follow from the metadistribution from, e.g., summation over w and δ.

Figure 2.5 shows FSS approximates for the τ exponents. They are constructed as follows. Power-law-decaying objects such as $P_l \sim l^{-\tau_l}$ are almost always subject to crossover-scaling-type effects, i.e., subdominant additional power-law terms. In the language of renormalization theory they originate from so-called irrelevant scaling fields and also from nonlinear scaling field effects. This is well documented in equilibrium critical phenomena, but most recent nonequilibrium scaling studies ignore this systematic effect, e.g., by simply making a log-log plot of P_l as function of l and drawing a least-square-fitting-type straight line through the data. Such results show very little statistical noise, but can give rise to significant systematic errors. An example of the importance of corrections to scaling, was the

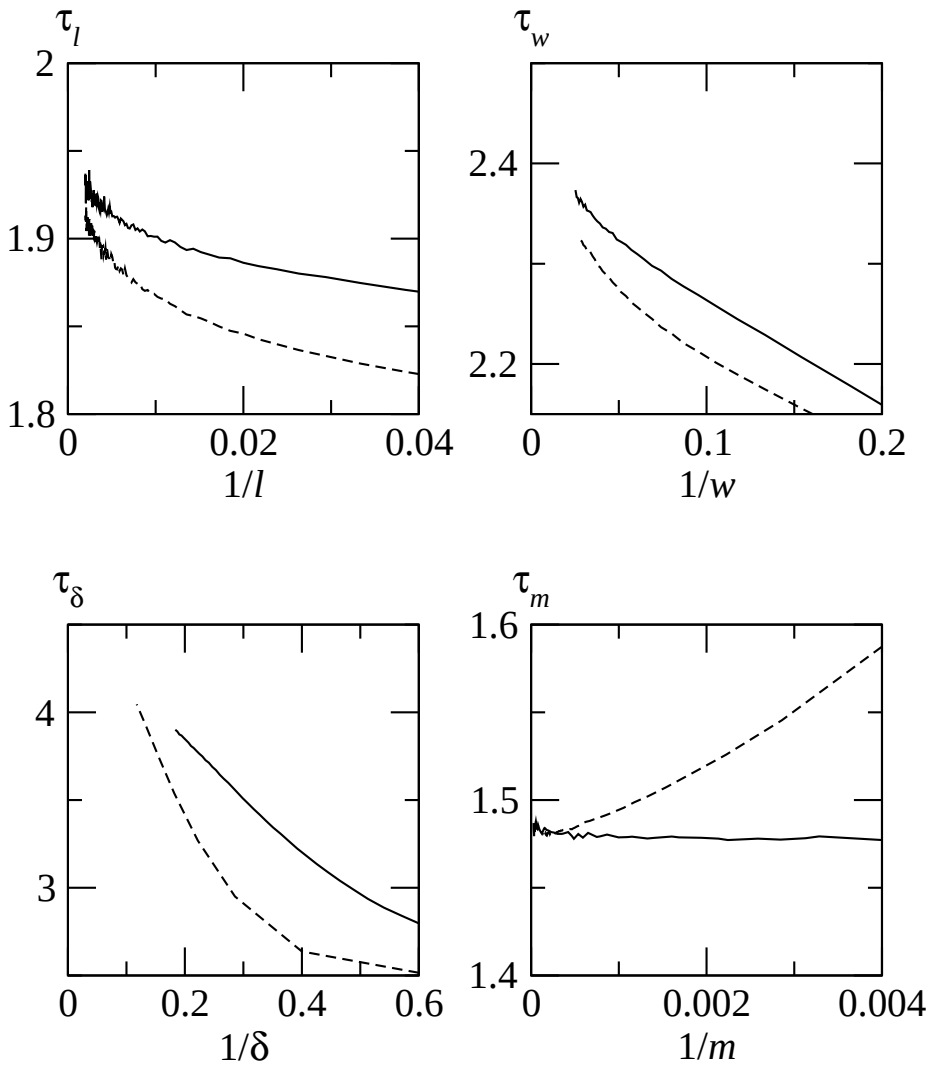

Figure 2.5: FSS plots for the τ exponents of 2D sandbox model. The solid (dashed) lines are for continuous (discrete) height model.

large spread in reported values of the stationary state roughness exponent α between various 2D KPZ-type-growth lattice models, which was resolved using a similar FSS analysis as presented here [24].

In the limit of large l the subdominant additional power-law terms fade away. So, more weight must be put on the large l part of the data than on the short l section. However, it is a balancing act, because at large l the results become noisier, since few avalanches reach that far.

The total number of avalanches that reach beyond y scales as

$$Q_l(y) = \int_y^\infty P_l(l)dl \simeq \frac{A}{\tau_l}\, y^{-\tau_l+1}, \tag{2.19}$$

if the fraction of avalanches of length y scales as $P_l \simeq A\ y^{-\tau_l}$ (these are only the leading terms). We construct a y dependent approximate for the exponent τ_l from the ratio of these two quantities, as

$$\tau_l(y) = \frac{lP_l(y)}{Q_l(y)} \tag{2.20}$$

The results are shown in Fig. 2.5. (We do the same for the other distributions.) Plots such as this are intrinsically noisier than conventional simple log-log type of plots of the distributions, but they contain much more information. The variation with y reflects the leading corrections to scaling. The statistical noise at large y could be suppressed by running the MC simulation longer. The simulation time is the only limiting factor. We used 2^{31} avalanches and in that case, $L_y = 512$ is the optimal box size.

In Fig. 2.6, we replot the same data in terms of α, z, and σ, following Eq. (2.12) and using the same type of FSS analysis. From the trend of the curves, we conclude that $\alpha = 0.46 \pm 0.01$, $z = 1.52 \pm 0.02$, $\sigma = 4.43 \pm 0.05$, and $\tau_m = 1.48 \pm 0.01$. This means that the exponent relations (2.13) and (2.18) are satisfied well within the statistical noise limitations, i.e., within a few percent.

Surprisingly, the actual values for z and α, although close, differ significantly from the exactly known 1+1D KPZ values, $\alpha = 1/2$ and $z = 3/2$. They deviate more than warranted from statistical noise alone, and do not converge smoothly if the KPZ values are correct. The approximates for α actually undershoot the KPZ value $\alpha = 1/2$, and those for z overshoot $z = 3/2$. This systematic effect needs to be explained. It could be that the exponents

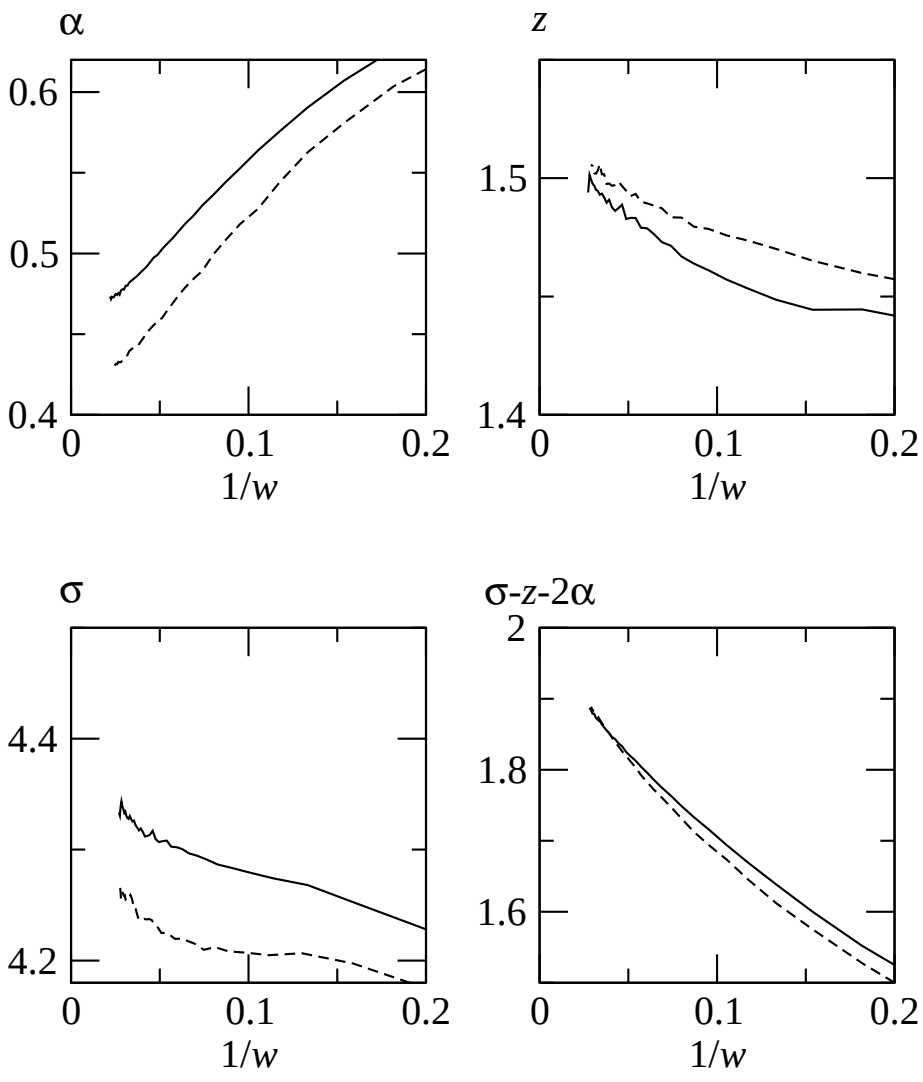

Figure 2.6: Effective scaling exponents derived from stationary avalanche distributions of sandbox systems. The solid (dashed) lines are for continuous (discrete) height model.

differ in a fundamental manner from the conventional KPZ values, or that we are looking at unusually large and slow corrections to FSS. The smallness of the deviations makes the latter more likely (except when this happens to be a continuously varying exponents scenario).

We will blame the correlated MC averaging feature for this, but it should be noted that avalanche distributions are intrinsically more sensitive to FSS effects than global interface features. Many avalanches in the ensemble are small compared to the global box size, and therefore sample and average the KPZ scaling properties over much smaller lengths and shorter time scales than in a conventional global interface roughness analysis at a comparable space-time box size.

One option is to push the run button on the computer and out perform all corrections to FSS. Unfortunately, it would require extremely long MC times to create large numbers of such large avalanches. It is doubtful that we would be able to get far enough in a reasonable time span. Moreover this approach is intellectually unappealing. We prefer to search for the origin of the deviations in the exponents.

2.7 Avalanche-correlated MC runs

The basic premise of our exponent identities is that avalanches are like any other fluctuation on a 1+1D KPZ-type world sheet. Initially flat KPZ interfaces (the sand surface next to the driving edge) roughen in time (moving away from the driving edge) in such a manner that at (KPZ) time y the stationary state roughness is established within a length scale $l_x \sim y^{1/z}$. This defines a so-called spreading cone. The avalanches are expected to follow the same pattern. However, the avalanche cone seems to spread slightly faster, since the above avalanche value for z slightly exceeds the conventional KPZ value, and inside the avalanche the surface seems to be slightly less rough, since the avalanche value for α is slightly smaller.

In this and the following section, we will establish that this is caused by correlations with previous avalanches. The new avalanche does not run its course on a pristine fresh KPZ interface world sheet but on an aged one scarred by previous avalanches.

There are two obvious tests to address the effects of these scars. The first one is to

determine the avalanche distributions for only the first avalanche on a fresh KPZ world sheet (the initial condition), i.e., to refresh the entire surface completely after each avalanche. The results are shown in Fig. 2.7. The first avalanches likely follow normal KPZ exponents: z converges now smoothly towards $z = 3/2$; while the FSS approximates for α, although still too small, start to turn towards $\alpha = 1/2$, and do not cross that value anymore. It should be noted that the FSS corrections are expected to be larger, and that the data is noisier than in Fig. 2.6, because although we ran the same number of avalanches (2^{31}), the fraction of large avalanches is smaller, leading to smaller and noisier amplitudes in the power-law tails of the distributions.

The second test of the role of the scars is to measure the global interface roughness for avalanche-type correlated MC runs instead of completely refreshing MC runs. The upper panel of Fig. 2.8 shows the global interface width W^2 as function of time for several L_x's. The drawn lines correspond to avalanche-correlated MC runs and the dashed line to conventional uncorrelated MC averaging. The drawn lines have bumps, i.e., the avalanche-correlated runs lead to rougher interfaces at intermediate times.

This enhanced interface roughness is caused by the scars left by earlier avalanches. The scars vanish at very large y because avalanches reaching that far span the entire system in the x direction. Figure 2.9 shows a typical configuration of scars. The lines are the traces of previous avalanches, i.e., their edges. Latter avalanches wipe them out partially.

For finite system sizes, the stationary state interface width follows from the plateaus at large times. There the avalanche-correlated and uncorrelated MC curves coincide. This is to be expected, because the large avalanches that span the entire system (in the x direction at large y) occur at regular MC time intervals, such that the large y part of the surface (i.e., the stationary state of the growth process) is completely refreshed periodically and therefore sampled effectively like in uncorrelated MC runs. As a result, the roughness exponent α, defined by Eq. (2.8), is the same for the both cases.

Most avalanches do not extend into that large y part of the surface. They terminate in the scarred part of the surface. Therefore, we define an alternative roughness exponent α^*,

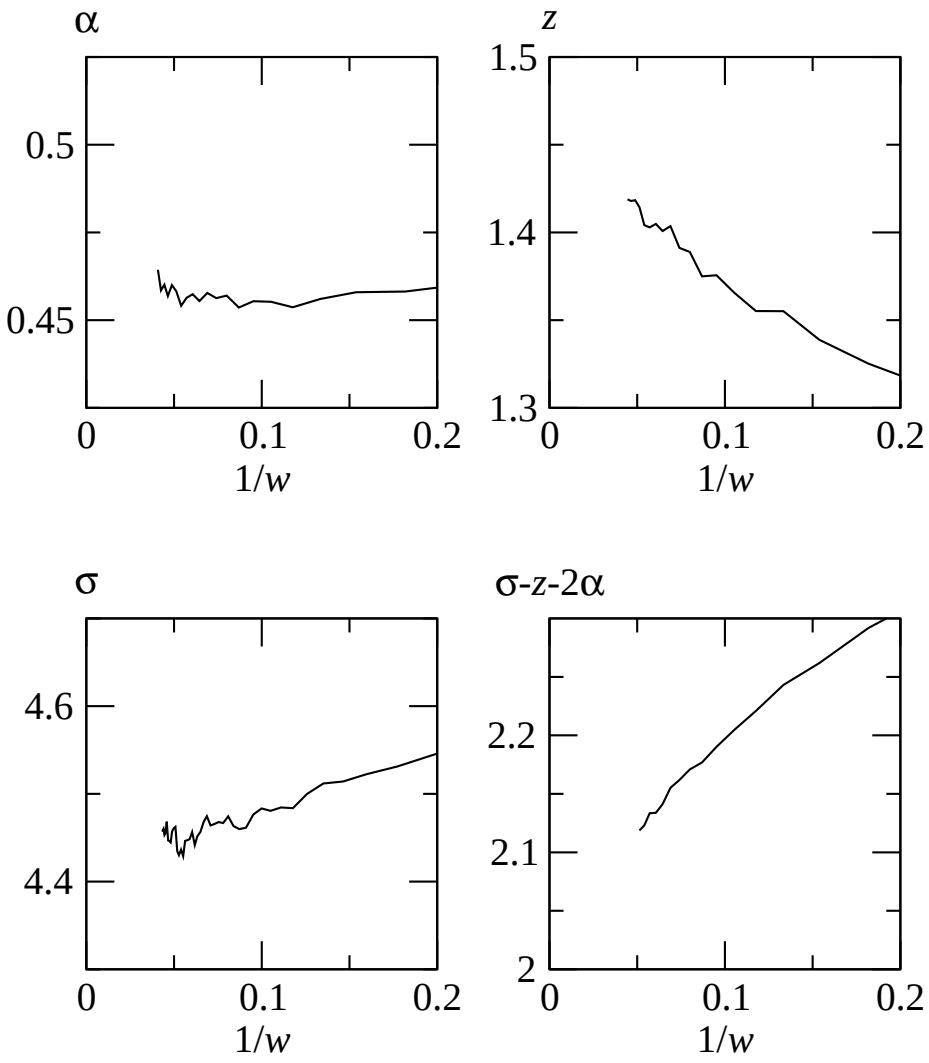

Figure 2.7: Effective scaling exponents derived from the distributions of first avalanches on fresh sandbox surface for the continuous height model.

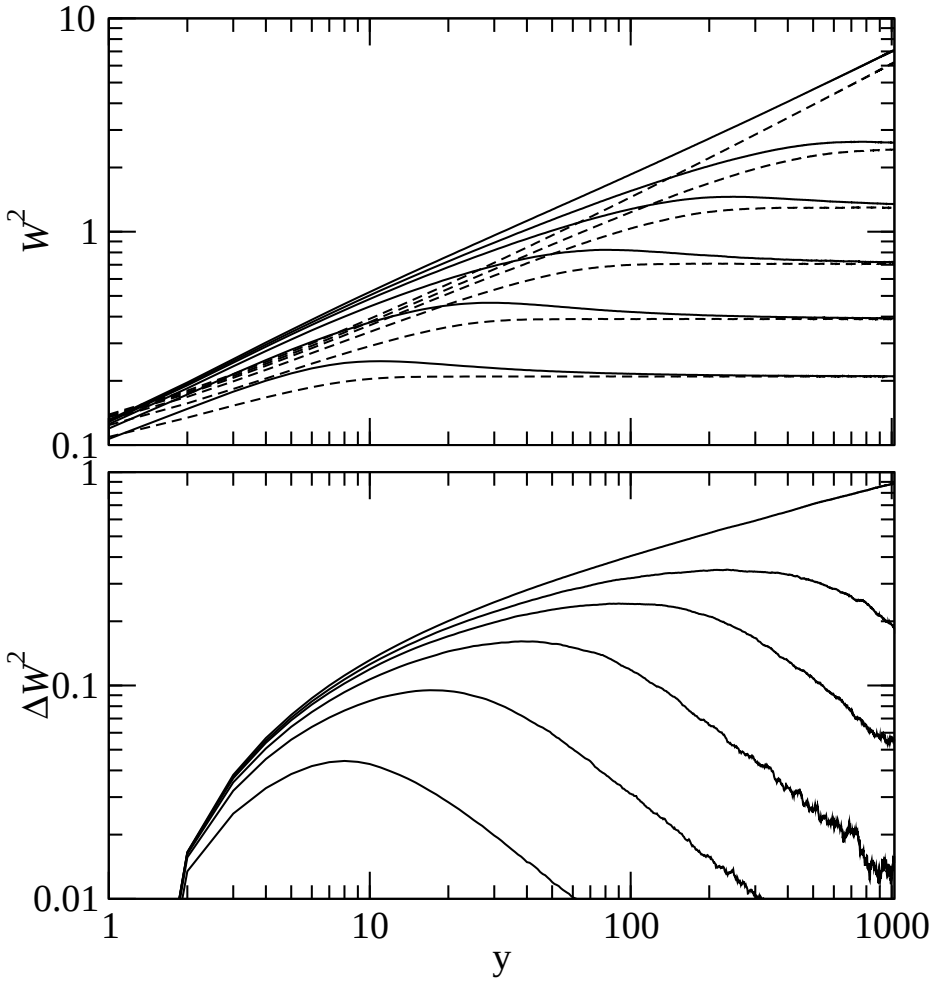

Figure 2.8: Upper panel: The interface width (squared) for sandbox surface (solid lines) and the same for an ensemble of fresh surface (dashed lines); Lower panel: The difference between the two, with $L_x = 8$, 16, 32, 64, 128 and ∞ (from bottom up) the box size in the direction parallel to the driving edge.

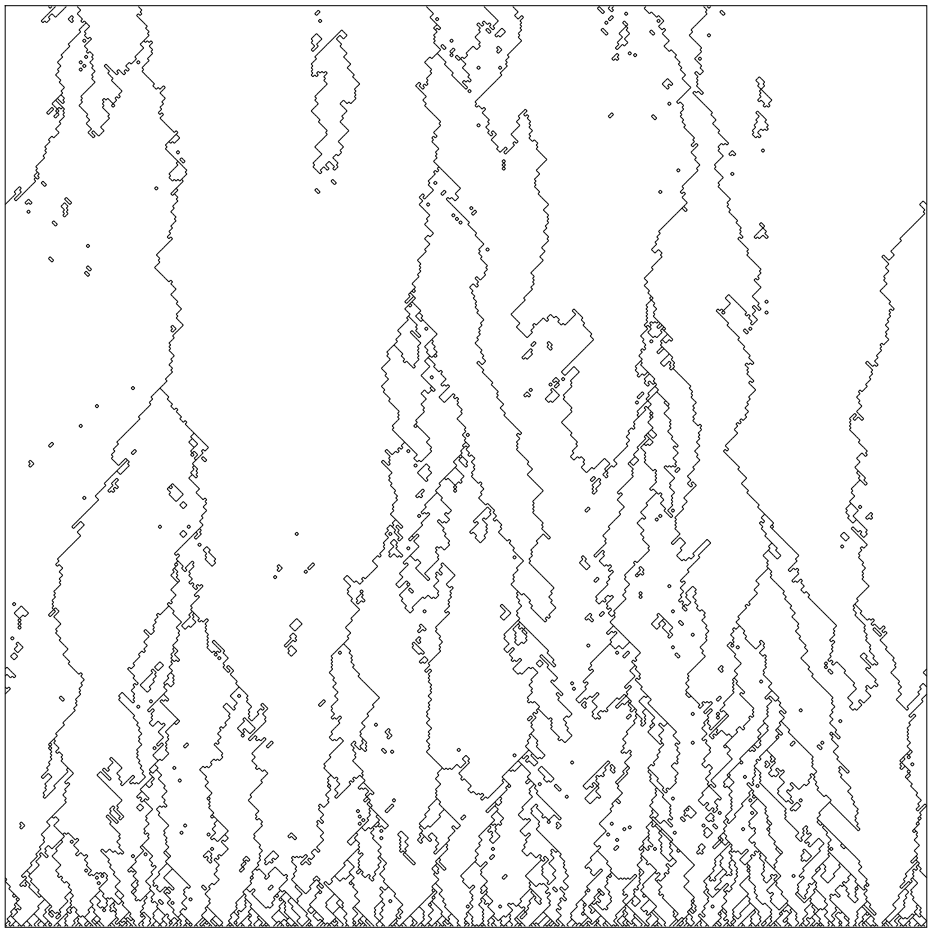

Figure 2.9: A typical configuration of the scars on the sandbox created by the avalanches. The driving edge is located at the bottom of the graph while avalanches propagate upward in the y (or t) direction. The system sizes are $L_x = 256$ and $L_y = 512$.

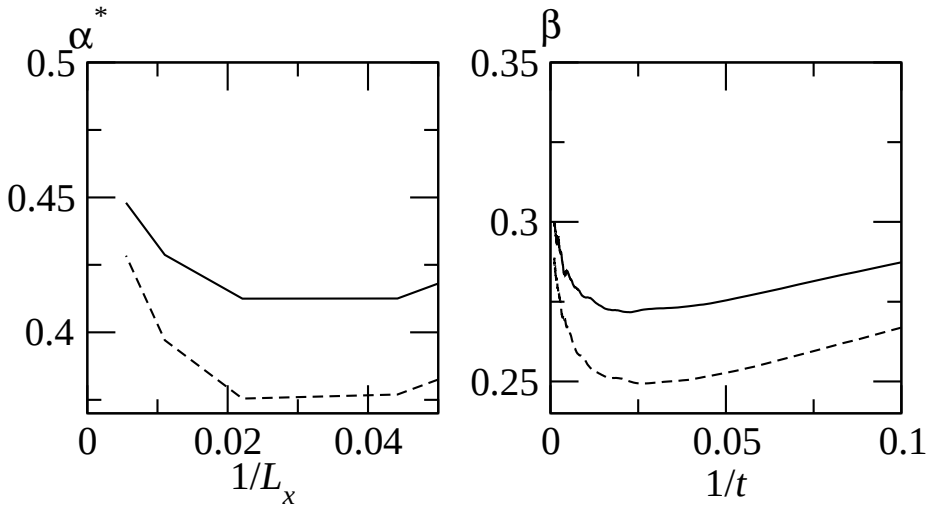

Figure 2.10: Finite-size approximates of the scaling exponents for stationary surface of sandbox (or correlated MC runs for the interface model) with α^* defined by Eq. (2.21) and β by Eq. (2.7). The solid (dashed) curves are for the continuous (discrete) height model.

associated with the scaling of the bumps, in terms of the maximized width

$$W^* \equiv \max_y W(L_x, y) \sim L_x^{\alpha^*} \tag{2.21}$$

more relevant for the avalanche scaling properties. Note that for uncorrelated MC runs, $\alpha^* = \alpha$, since the interface width increases monotonically in time.

The conventional method for measuring the exponent β, involves the slope at times $y < L_x^z$, and thus is sensitive to the bumps in W as well. The results are shown in Fig. 2.10. Compared to those in Fig. 2.4, they clearly converge less smoothly, with larger corrections to scaling and we should wonder if they converge to the conventional exact KPZ values, $\alpha = 1/2$ and $\beta = 1/3$, at all.

In the lower panel of Fig. 2.8 we plot ΔW^2 as function of time, the difference between the squared widths of avalanched-correlated MC runs (the drawn lines in the upper panel) and completely uncorrelated MC runs (the dashed lines in the upper panel). For infinite system size, ΔW^2 scales as $\Delta W^2 \sim y^s$ with an exponent that numerically is very close to $s \simeq 1/3$. Since the width itself scales as $W^2 \sim y^{2/3}$, it follows that the bumps in the width

curves are a transient FSS effect.

This settles our basic issue at the numerical level; the avalanche-correlated nature of the MC runs does not change the interface scaling exponents, but only gives rise to slow corrections to FSS. In the next two sections we will identify these corrections to scaling with the scars on the surface left behind by previous avalanches.

We start this analysis here by casting the deviations into the framework of corrections to scaling from a so-called irrelevant operator in the sense of renormalization theory. Let $O_{\rm sc}(x)$ be that irrelevant operator and u be its scaling field. This amounts to presuming that the avalanche correlation between MC runs can be represented effectively by adding to the KPZ Langevin equation (2.5), a term $uO_{\rm sc}(x)$. We will have to determine below how $O_{\rm sc}(x)$ is related to the density of scars on the interface space-time world sheet left by previous avalanches. According to scaling theory, the presence of such a term to the Langevin equation leads to corrections to scaling in the interface width as

$$W^2(L_x, y, u) = b^{2\alpha} W^2(b^{-1}L_x, b^{-z}y, b^{y_{\rm sc}}u), \tag{2.22}$$

i.e., in the infinite-size limit, $L_x \to \infty$, to

$$W^2(y, u) = y^{2\alpha/z} S(y^{y_{\rm sc}/z}u), \tag{2.23}$$

and by expanding the scaling function S, while assuming that $y_{\rm sc} < 0$, such that $u = 0$ is a stable fixed point, and the argument $y^{y_{\rm sc}/z}u$ is a small parameter, to

$$W^2(y, u) = y^{2\alpha/z}\left[S(0) + y^{y_{\rm sc}/z}uS'(0) + \cdots\right]. \tag{2.24}$$

The critical exponent $y_{\rm sc}$ of this irrelevant scaling field must take the value $y_{\rm sc} = -\alpha$ to account for the $\Delta W^2 \sim y^{1/3}$ corrections in the interface width we found above. Moreover the operator must scale as

$$O_{\rm sc}(x) \sim b^{-x_{\rm sc}} \tag{2.25}$$

with critical dimension $x_{\rm sc} = z$, since the KPZ equation (2.5), implies that the terms $uO_{\rm sc}(x)$ and $\partial h/\partial t$ must scale alike. In the following two sections we will trace down the geometric identity of this mysterious operator $O_{\rm sc}$, starting with the 1D version of the model.

2.8 Surface rounding in the 1D unloading sandbox

The 1D version of the unloading sandbox shows the same type of differences between uncorrelated and avalanche-type correlated MC runs as the 2D version. We determined numerically the difference between the interface width for avalanche-correlated and uncorrelated MC runs, and found that it diverges as a power law $\Delta W^2 \sim y^{1/2}$, with an exponent which is again (like in 2D) half the size of that for $W^2 \sim y$ itself. According to the corrections to scaling formalism (2.24), the scaling dimension of $O_{\rm sc}$ must therefore be equal to $x_{\rm sc} = z$, just as in 2D.

The underlying interface dynamics becomes a zero-dimensional growth model, i.e., a simple random walk in the h direction with a nonzero drift velocity to account for the net tilt of the surface. The exponents of the various avalanche distribution functions must obey the same type of relations as in Sec. 2.5:

$$\tau_l = \frac{\sigma - \alpha}{z}, \quad \tau_\delta = \frac{\sigma - z}{\alpha}, \quad \tau_m = \frac{\sigma}{\alpha + z}, \tag{2.26}$$

and

$$\sigma = z + 2\alpha. \tag{2.27}$$

Without loss of generality we can set $\alpha = 1$ (measure all lengths in terms of δ). These identities are satisfied exactly, and the exponents are the same for uncorrelated and avalanche-correlated runs. From the interface dynamics perspective, a single directed random walker, the diffusion equation character of the dynamics implies that $z = 2\alpha = 2$. The values of all the other exponents follow from this, and are consistent with their values from the avalanche perspective. There, we are dealing with the statistics of merging random walkers. The number of walkers at a given "time" y is equal to the number of avalanches of a length l equal or larger than y in the ensemble of MC runs. The density of the walkers decays as $\rho(y) \sim y^{-1/2}$ [58], such that the distribution of avalanche lengths obeys the form

$$P_l(l) = \left[-\frac{\partial}{\partial y} \rho(y) \right]_{y=l} \sim l^{-3/2}, \tag{2.28}$$

and therefore that $\tau_l = 3/2$. The depth of the avalanche follows from the maximum separation between two subsequent walkers, and scales as $\delta \sim l^{1/2}$, i.e., $\alpha/z = 1/2$. The mass scales as $m \sim l\delta \sim l^{3/2}$, i.e., $(\alpha + z)/z = 3/2$ and $\tau_m = 4/3$.

This can be compared directly with the exponents of other 1D sandpile models, e.g., with results by Paczuski and Boettcher [92] on the so-called Oslo sandpile model, where $\tau \equiv \tau_m \approx 1.55$ and $D \equiv (\alpha + z)/z \approx 2.23$.

Let us turn our attention now to the central issue, the difference between uncorrelated versus avalanche-correlated MC runs. Adding a term like $uO_{\rm sc}$ to the diffusion equation of motion creates a correction to the drift velocity of the random walk. This suggests we can identify the geometric meaning of $O_{\rm sc}$ directly by studying the deviations of the slope near the driving edge of the surface from its asymptotic value.

The average surface slope does not show any deviations (near the driving edge) from $s_c/2$ when we run the dynamics as a conventional random walk, which amounts to "completely refreshing" the surface after each MC run (uncorrelated MC runs). The avalanche-correlated runs do show a rounding of the surface near the driving edge,

$$s(y) \simeq Ay^{-\kappa} + \frac{1}{2}s_c. \tag{2.29}$$

The numerical results for the exponent yield $\kappa = 0.98 \pm 0.03$. This confirms our corrections to scaling picture, because it predicts that $x_{\rm sc} = z$ from the interface width since $\kappa = x_{\rm sc}/z$ and $z = 2$ for random walks.

This rounding originates from the distribution of termination points of the avalanches. A new random walk starts below the previous one and propagates until it meets the previous trajectory and terminates. The avalanche is the space between the trajectory of that new random walk and the already existent surface. The amount of rounding of the slope near the driving edge is proportional to the distribution $\rho(y)$ of merging points on the surface. These merging points represent the scars left from previous avalanches. Each random walker by itself does not contribute to the rounding, i.e., on average each has a constant slope $s_c/2$. However every new walk lies below the previous surface, such that down stream from every avalanche end point the surface is systematically lower than beyond it. This upward bias across the avalanche merging points (by an amount, e.g., $s_c/2$, on an average, in the discrete h version of our model) gives rise to the surface rounding and yields that the latter is proportional to $\rho(y)$.

The entire process and the set of subsequent stable sand surfaces (Fig. 2.11) is therefore

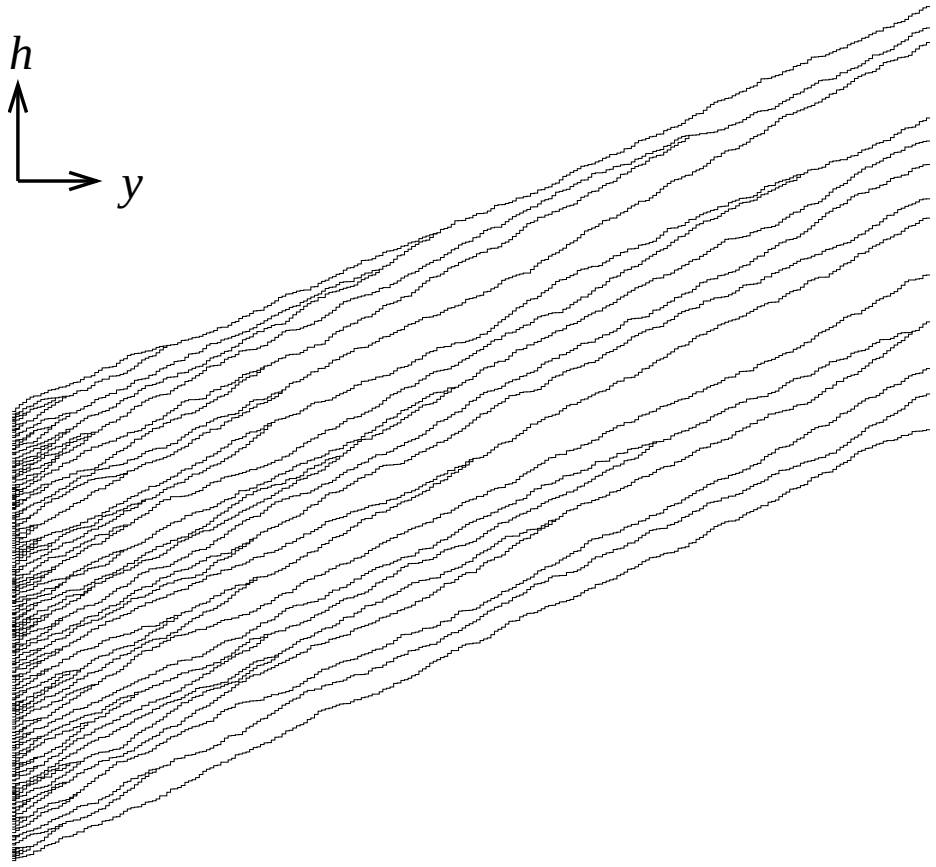

Figure 2.11: Traces of stable sand surface over 256 avalanches for 1D sandbox model with $L_y = 256$. The system is driven from the left at $y = 0$.

equivalent to a system of merging random walkers obeying the rule $A + A \rightarrow A$. That type of dynamics has received extensive attention recently and its various scaling properties are known exactly [58]. There is little doubt that our 1D unloading sandbox is exactly soluble, using absorbing-wall-type random-walk mathematics. However, we will refrain from pursuing this path here.

The critical dimension of $O_{\rm sc} \sim \rho(y)$ can be estimated (for intuition building purposes) as follows. After adding a term $uO_{\rm sc}$ to the KPZ equation, we should also write down an equation of motion for $O_{\rm sc}$ itself, to close the equations. The latter is not trivial, because the scars on the surface build up slowly in time, such that the equation of motion for $O_{\rm sc}$ is

highly nonlocal. On the other hand, the linear nature of the diffusion equation allows one to be somewhat frivolous with the order in which averages are taken, (without losing the essential physics, nor even the correct critical exponents).

Let $\rho_{\tilde{t}}(y)$ be the end-point distribution after $\tilde{t}$ avalanches (MC time steps). During the last MC time step, one avalanche runs through the system. It refreshes the entire surface before its termination point $y = l_{\tilde{t}}$, such that $\rho_{\tilde{t}}$ at site y does not change if the avalanche terminates before y; $\rho_{\tilde{t}}(y) = 1$ if it terminates at y; and $\rho_{\tilde{t}}(y) = 0$ if it extends beyond y:

$$\frac{\partial \rho_{\tilde{t}}(y)}{\partial \tilde{t}} = P_l(y) - \rho_{\tilde{t}}(y) \int_y^\infty P_l(l) dl \tag{2.30}$$

with $P_l(l)$ the probability that the avalanche terminates at distance l from the driving edge. The stationary state end-point profile therefore takes the form

$$\rho(y) = \frac{P_l(y)}{\int_y^\infty P_l(l) dl}, \tag{2.31}$$

and $P_l(l) \sim l^{-\tau_l}$ yields

$$\rho(y) = \frac{1}{\tau_l - 1} y^{-1}. \tag{2.32}$$

In other words, the surface curvature scales as $\Delta s \sim y^{-x_{\rm sc}/z}$ with $x_{\rm sc} = z$, in agreement with the above results. Interestingly, this result is independent of the actual value of the scaling exponent τ_l, provided that $\tau_l > 1$, which has to be true for P_l to be normalizable.

In conclusion, in 1D we identified the crossover scaling operator with the density of avalanche end points. These represent indeed the scars on the surface, the memory of previous avalanches.

2.9 Avalanche rounding near the driving edge in 2D

As in the 1D model, the surface slope is modified by the iterated avalanche process. However, unlike in 1D, the average slope near the edge is not constant already in conventional interface dynamics (where the entire surface is being refreshed during each MC run). The surface slope is related to the growth rate of the underlying interface, and the rounding of the slope near the driving edge represents the transient growth rate of the KPZ interface from the

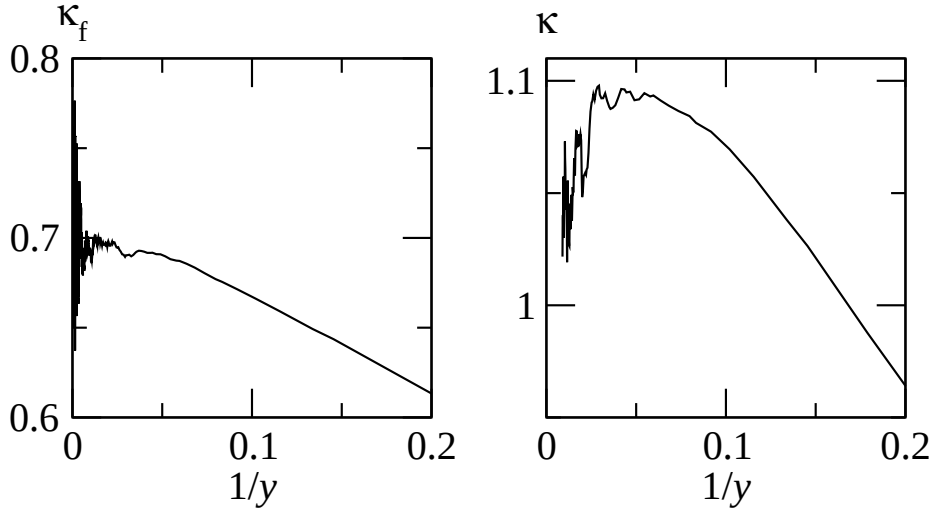

Figure 2.12: Scaling exponent for boundary correction to the local slope of fresh 2D sandbox surface (or, in the interface language, transient growth rate from a flat interface), $s_f(y) - s_f(\infty) \sim y^{-\kappa_f}$, and its correction due to the iterated avalanche process, $\Delta s = s(y) - s_f(y) \sim y^{-\kappa}$.

initial configuration, e.g., a flat one:

$$s_f(y) \simeq v_0 + cy^{-\kappa_f} \tag{2.33}$$

with y playing the role of time and the subscript, f, denoting that the entire surface is refreshed. By direct numerical simulation of uncorrelated interface dynamics we find $\kappa_f \approx 0.7$ (the left panel of Fig. 2.12). This is consistent with conventional KPZ scaling and power counting

$$s \sim h/y \sim y^{\alpha/z-1} \sim y^{-2/3}, \tag{2.34}$$

suggesting $\kappa_f = 2/3$.

We evaluate the surface slope profile $s(y)$ in avalanche-correlated dynamics MC runs, in terms of the difference with respect to the uncorrelated case,

$$\Delta s(y) = s(y) - s_f(y) \sim y^{\kappa}. \tag{2.35}$$

The FSS analysis for the exponent κ (the right panel of Fig. 2.12) yields $\kappa = 1.05 \pm 0.07$.

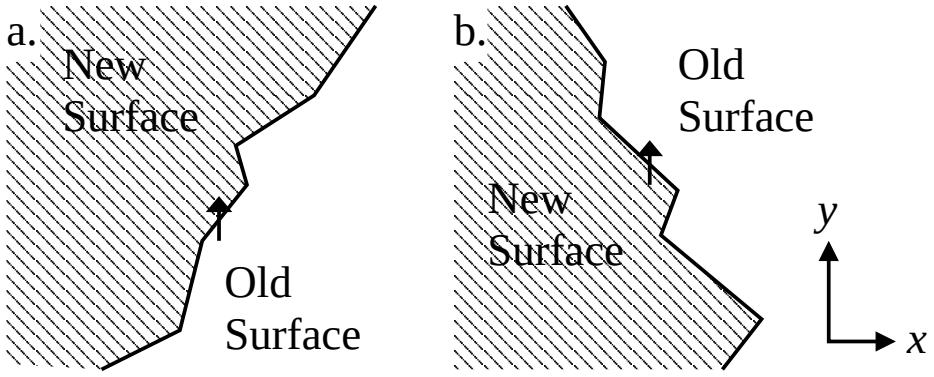

Figure 2.13: Two possible cases at a boundary of an avalanche cluster (the shaded area): (a) avalanche expands; (b) avalanche shrinks. The local slopes along the arrow marks is reduced in (a) while increased in (b).

This is in agreement with $x_{\rm sc} = z$ and $\kappa = x_{\rm sc}/z$ implied by the corrections to scaling formalism (2.24).

Inside the bulk of an avalanche the interface is fully refreshed, and scales as in uncorrelated KPZ dynamics. At the avalanche boundaries, the slope of the surface is biased upwards, because of the merging with previous MC runs (which are on average shifted upwards by an amount $s_c/2L_x$ each time an avalanche is triggered). This means that the Δs is proportional to the density of scars in the surface. In 1D, the scars are pointlike objects, the end points of the avalanches; but in 2D the avalanche boundaries are line objects. This nonscalar aspect makes that most line-segment contributions, when integrated along the boundaries of an avalanche, cancel out against each other.

To be more precise, $s(y)$ represents only the component of the slope in the y direction, and the magnitude of those jumps depends on the local angle θ the boundary makes with the y axis. This is an odd function, $\Delta(\theta) = -\Delta(-\theta)$, as illustrated in Fig. 2.13. The slope change is negative when the avalanche opens up and positive when it narrows down. The latter also implies that $\Delta(\theta)$ has opposite sign for the left and right boundary of each avalanche. Notice that, while in the lattice model θ takes only two discrete values, it renormalizes to a continuous variable at larger length scales.

Let us estimate the change in surface slope due to these scars in the same spirit as we did successfully in 1D. Consider one specific surface, and let $s_{\tilde{t}}(y)$ be the surface slope in a slice of the surface at distance y from the driving edge, averaged over all x, after $\tilde{t}$ avalanches (MC time $\tilde{t}$). The last avalanche changes this as follows. Let $w_{\tilde{t}}(y')$ be the width of this avalanche, which terminates at $y = l_{\tilde{t}}$, in slice y'. The inside area of the avalanche is completely refreshed and therefore has the same average slope $s_f(y)$ as in ordinary KPZ dynamics (totally refreshed subsequent world sheets). This leads to the following equation of motion:

$$\frac{\partial s_{\tilde{t}}(y)}{\partial \tilde{t}} = [\Delta(\theta_L) - \Delta(\theta_R)] + w_{\tilde{t}}(y)[s_f(y) - s_{\tilde{t}}(y)]. \tag{2.36}$$

The first term on the right hand side represents the creation of the two new avalanche edges, and the second term represents the refreshed surface inside the new avalanche. Note that $\partial s_{\tilde{t}}(y)/\partial \tilde{t} = 0$ when this latest avalanche does not reach slice y, and that this is automatically taken care of because in that case $\theta_L = \theta_R = 0$ and $\Delta(0) = 0$, while $w_{\tilde{t}}(y) = 0$ for $y > l_{\tilde{t}}$. In the stationary state, after averaging over all possible avalanches, Eq. (2.36) leads to

$$\overline{w_{\tilde{t}}(y)\,[s_f(y) - s_{\tilde{t}}(y)]} = \overline{\Delta(\theta_L) - \Delta(\theta_R)}. \tag{2.37}$$

Next, we perform an heuristic coarse-graining renormalization-type transformation. At large length scales, the average angle θ remains small, such that the right hand side can be approximated as

$$\overline{\Delta(\theta_L) - \Delta(\theta_R)} \simeq a\ \overline{\theta_L - \theta_R} \simeq a\ \frac{\partial \overline{w_{\tilde{t}}(y)}}{\partial y}. \tag{2.38}$$

Finally, we presume that in the stationary state it is not too bad to treat the KPZ height fluctuations deep inside the bulk of an avalanche and those near its edge as decoupled (at least in lowest order) such that

$$\Delta s(y) = \overline{s_f(y) - s_{\tilde{t}}(y)} = a\ \frac{\partial}{\partial y} \ln\left[\overline{w_{\tilde{t}}(y)}\right]. \tag{2.39}$$

This yields $\Delta s(y) \sim y^{-1}$, exactly the power-law decay we are looking for, and consistent with all the above numerical results.

The only requirement for the latter is that $\overline{w_{\tilde{t}}(y)} \sim y^{-\xi}$ decays as a power law. Again, like in Eq. (2.32) for 1D, the value of the critical exponent ξ does not matter. $\overline{w_{\tilde{t}}(y)}$ is equal

to the average avalanche width in slice y averaged over all avalanches. It is reasonable to expect, and we confirmed numerically, that this quantity scales with the same exponent as the average width of all avalanches longer than y, i.e., as

$$\int_y^\infty w(l)P(l)dl \sim y^{1/z-\tau_l+1} \tag{2.40}$$

which yields $\xi \simeq 1/3$.

We are now ready to represent the crossover scaling operator $O_{\rm sc}(x)$ in terms of the scars on the surface. Consider time slice y. $O_{\rm sc}(x) = 0$ when no scar line runs through site x, and otherwise is proportional to the angle the scar line makes with respect to the y axis. However, the sign also flips depending on whether this represents a left or right boundary of the original avalanche. The latter can be denoted by an arrow along the avalanche scar line. Alternatively, we can associate an age field $g(x, y)$ to the entire surface, representing the age of the surface segments (how many MC time steps ago site x was updated),

$$O_{\rm sc} \sim \frac{\hat{e}_y \cdot \boldsymbol{\nabla} g}{|\boldsymbol{\nabla} g|} \tag{2.41}$$

with $\hat{e}_y$ a unit vector in the y direction. The denominator arises because the magnitude of the age jump across the scar line $|\boldsymbol{\nabla} g|$ does not play a role.

2.10 Summary

In this chapter, we studied a directed avalanche model inspired by the unloading of a sandbox by means of a slowly lowering wall, and the wish to setup an avalanche dynamic rule belonging to the same universality class as KPZ-type interface growth. The 2D sand surface represents the world sheet of the 1+1D growing interface.

The scaling exponents of the avalanche distributions are directly related to the dynamical and stationary state roughness exponents z and α of KPZ growth in 1+1D [Eq. (2.11)]. However, we encounter one crucial difference. From the avalanche perspective, the conventional uncorrelated MC runs correspond to completely refreshing the surface, i.e., an ensemble average over all possible initial conditions, without ever running an avalanche. From the KPZ perspective, the avalanche dynamics represents an unusual MC ensemble averaging procedure where subsequent interface world sheets only differ inside the single

avalanche. This avalanche-correlated-type averaging enhances the interface roughness at time scales $y < L_x^z$, due to the scars of previous avalanches. It required a careful study, combining numerical and analytical tools, presented in the second half of this chapter, to establish that these scars give rise only to larger than usual corrections to scaling and not to fundamentally different values of the global roughness scaling exponents z and α.

The effect of the scars can be represented by introducing an additional age field $g(x, y)$ to the height variables $h(x, y)$, that keeps track of how many MC runs ago site (x, y) participated in an avalanche. This age-field couples into the KPZ equation (2.5) as an additional term of the form $uO_{\rm sc}$. The operator $O_{\rm sc}$ is proportional to the angle a scar makes with respect to the time-axis, and can be expressed in terms of the age field as shown in Eq. (2.41). We establish that the coupling of this age field to the KPZ equation is irrelevant in the sense of renormalization theory, both numerically and by writing down approximate equations of motion for $uO_{\rm sc}$. The scaling field u renormalizes with exponent $y_{\rm sc} = -\alpha$ and $O_{\rm sc}$ scales with critical dimension $x_{\rm sc} = -z$.

We believe that the results of our work presented here can be generalized to most "Markovian" avalanche dynamic systems with local row-by-row-type toppling rules, and that this is a promising route to improve our understanding of the scaling properties of avalanche dynamics in general.

Chapter 3

DEEPENING TRANSITION OF AVALANCHES

In this chapter, we will use the discrete-height of the sandbox models introduced in the previous chapter with a control parameter p representing the cohesiveness to investigate the transition between the avalanches in cohesive granular materials and noncohesive granular materials. From the previous chapters, we know the avalanche dynamics of the model can be mapped to interface growth model. For the DHSB model, there is a continuous phase transition which separates the rough phase and the flat phase of the underlying interface growth dynamics. In the avalanche system, this corresponds to a transition from deep avalanches to shallow avalanches. We will verify that the scaling exponents of the avalanches follow those of the interface growth in both phases and at the transition point. However, we will also show that the mass hyperscaling relation is broken at the transition point. This is likely due to the fractal property in a hierarchy of critical directed percolation processes taking place at the transition point.

3.1 Introduction

Granular avalanches have received much attention since the sandpile models were used as the paradigm of the so-called self-organized criticality by Bak *et al.* [5]. However, the observations of critical distribution of avalanches in real physical systems are still rare apart from the rice pile experiments by Frette *et al.* [42]. It was suggested by Christensen *et al.* [25] that the anisotropy in the rice grains allows more packing configurations in a stable granular pile and could be what leads to the successful observation of criticality. Some of the recent attentions have been drawn to the avalanches in cohesive granular materials with the premise that cohesion will also allow the sand more packing configurations and thus increase the likelihood of observing critical scaling behavior. While the goal of finding criticality in cohesive sandpiles remains to be fulfilled even after the experimental work by

Quintanilla *et al.* [99], the effect of cohesion in granular avalanche represents an interesting direction for a theoretical study.

In this chapter, we'll use the discrete height version of the sandbox (DHSB) model introduced in [23] to understand the effects of cohesion in directed avalanche systems. In the following section, we'll discuss how we can model the cohesiveness in avalanche systems. In Sec. 3.3, we'll review the DHSB model with a cohesion parameter. In Sec. 3.4, we describe the step-flow random-deposition (SFRD) interface growth model underlying the DHSB model and the directed percolation (DP) roughening transition of the SFRD model. In Sec. 3.5, we focus on the two deterministic limits of the model and present the exact solution at the upper limit. In Sec. 3.6, we present the numerical results for the avalanches in the flat phase of the interface model. In Sec. 3.7, we investigate the scaling behavior at the transition point where the interface roughness increases logarithmically in time. We show the avalanche-scarred sand surface, while being rougher than nonscarred one, retains the same scaling exponent of the roughness in the thermodynamic limit. However, we'll also show that at the transition point, the violation of mass hyperscaling relation spoils the two-independent-exponent picture established in [22]. We'll summarize in Sec. 3.8.

3.2 Tunable parameter for cohesion

One interesting character of cohesion in sand is that it possesses certain hysteresis behavior. Consider building a sand castle on a beach. It's common sense that we'll need to add water to the sand before we can shape it into a standing castle. However, the sand castle can somehow maintain its shape even after it dries out afterward [59]. The moisture in sand increases the cohesion between the sand particles [89] and allows one to manipulate the sand into a stable shape that, while not as attainable, is more or less an equally valid stable shape for the dry sand.

In accounting for this standing-sand-castle effect, we'll use the same stability condition for all cohesiveness of the sandbox. While, in reality, the space of possible stable configurations for wet and dry sand might not be identical, in this article, we shall ignore this distinction to avoid considering a more complicated rule set.

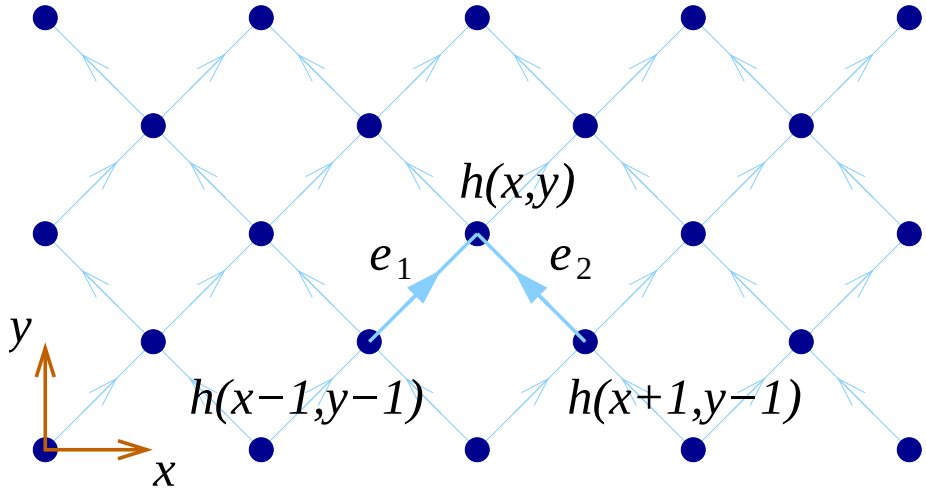

Figure 3.1: Lattice structure of the two dimensional discrete-height sandbox model.

On the other hand, the way an unstable sand surface topples surely depends on the cohesiveness. In the DHSB model, there are only two possible final stable states for any toppling site. We'll call them the minimal stable state and the maximal stable state. These two states are similar to the angle of repose and maximal stable angle in a real sandpile. However, those two states in sandbox model are microscopic states while the "angles" of a real sandpile are macroscopic. We'll use the parameter p, a real number between 0 and 1, to represent the strength of cohesion. In the model, p is the probability for a toppling site of the sandpile to settle into the maximal stable state instead of the minimal one. For wet sand the p is large and for dry sand the p is small.

3.3 Discrete height sandbox model

With the discussion of the previous section in mind, let's review the dynamic rules of the discrete height sandbox model (DHSB). The surface of the sandbox is represented by an integer height variable h defined on a two-dimensional (2D) square lattice which is tilted at 45° as illustrated in Fig. 3.1. This is equivalent to considering only the lattice points whose integer x and y coordinates satisfy the condition that $x + y$ is an even number. The lowering wall that drives the system by creating unstable sites is located at the $y = 0$ row

and the activities in the system propagates only in the positive y direction. In our numerical simulations, the system is periodic in the x direction, which is parallel to the driving wall. The sizes of the system in the x and y directions are denoted by the numbers of sites L_x in each row and the number of rows L_y respectively.

As in most sandpile models, the dynamics of the sandbox model is defined by a stability condition, a toppling rule, and a driving method which we describe as follows. The stability condition of the DHSB is given by

$$h(x,y) \leq \min\left[h(x-1,y-1), h(x+1,y-1)\right] + s_c, \tag{3.1}$$

with $s_c = 1$ which represents the local maximal stable slope. The unstable sites in the system topple with the rule

$$h(x,y) \to \min\left[h(x-1,y-1), h(x+1,y-1)\right] + \eta, \tag{3.2}$$

where $\eta = 0$ with probability $1-p$ and $\eta = 1$ with probability p. This is the only place in the dynamics of the DHSB that the cohesion parameter p comes into play. The lowing wall which drives the system is implemented in the model by randomly picking one of the highest sites $(x_i, 0)$ on the $y = 0$ row and reducing its height by 1

$$h(x_i,0) \to h(x_i,0) - 1, \tag{3.3}$$

where i is the Monte Carlo time which also serves as an index of the avalanches.

A typical configuration of the DHSB before and after an avalanche is shown in Fig. 3.2. Since the toppling of a site on a given row y only affects the stability of the two sites immediately above it at the $y+1$ row, we choose to update the system in a row-by-row fashion. For each avalanche, the entire system is stabilized by such a single sweep of topplings from $y = 0$ to $y = L_y$.

3.4 Underlying interface dynamics

The underlying interface dynamics of the sandbox models is given by the step-flow random-deposition (SFRD) models with a two-step growth rule [23, 22] as illustrated in Fig. 3.3. Models similar to this generally belong to the Kardar-Parisi-Zhang (KPZ) universality class

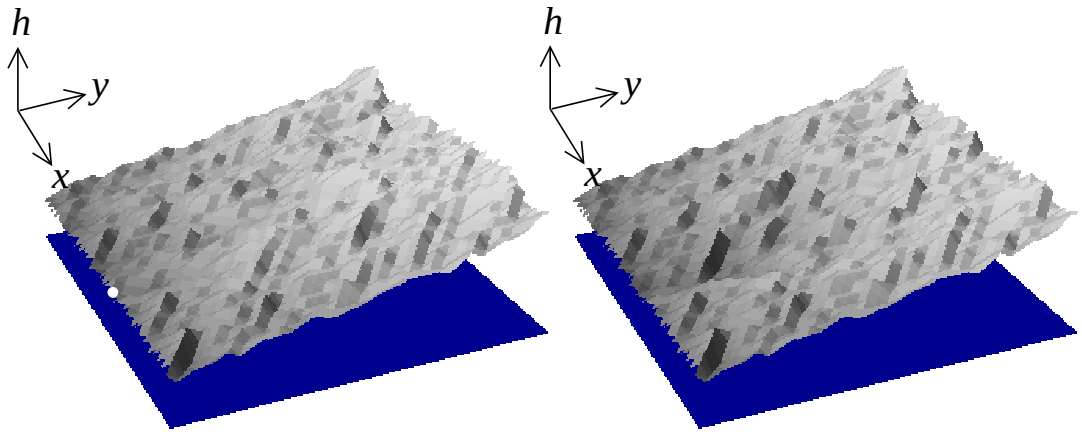

Figure 3.2: A typical configuration of the discrete-height sandbox model before (left) and after (right) a system spanning avalanche trigger at the boundary site marked by the white dot; The system size $L_x \times L_y$ is 32×64.

with the critical exponents $\alpha = 1/2$, $\beta = 1/3$, and $z = \alpha/\beta = 3/2$. Thus, from the mapping introduced in [23], the avalanche exponents are given by

$$\tau_l = \frac{\sigma - 1 - \alpha}{z} = 2, \tag{3.4}$$

$$\tau_w = \sigma - z - \alpha = \frac{5}{2}, \tag{3.5}$$

and

$$\tau_\delta = \frac{\sigma - 1 - z}{\alpha} = 4 \tag{3.6}$$

for the distribution functions of avalanche length l, width w, and depth δ. The σ in these expressions was eliminated with the mass hyperscaling relation

$$\sigma = 2 + z + 2\alpha. \tag{3.7}$$

obtained from the compactness of the avalanche clusters, i.e., assuming $m \sim lw\delta$.

However, the discrete height version of the SFRD model undergoes a DP roughening transition at $p = p_c \approx 0.294515$ similar to those studied by Kertész and Wolf [65] also Alon *et al.* [1]. The KPZ scaling behavior only applies when the value of the control parameter p

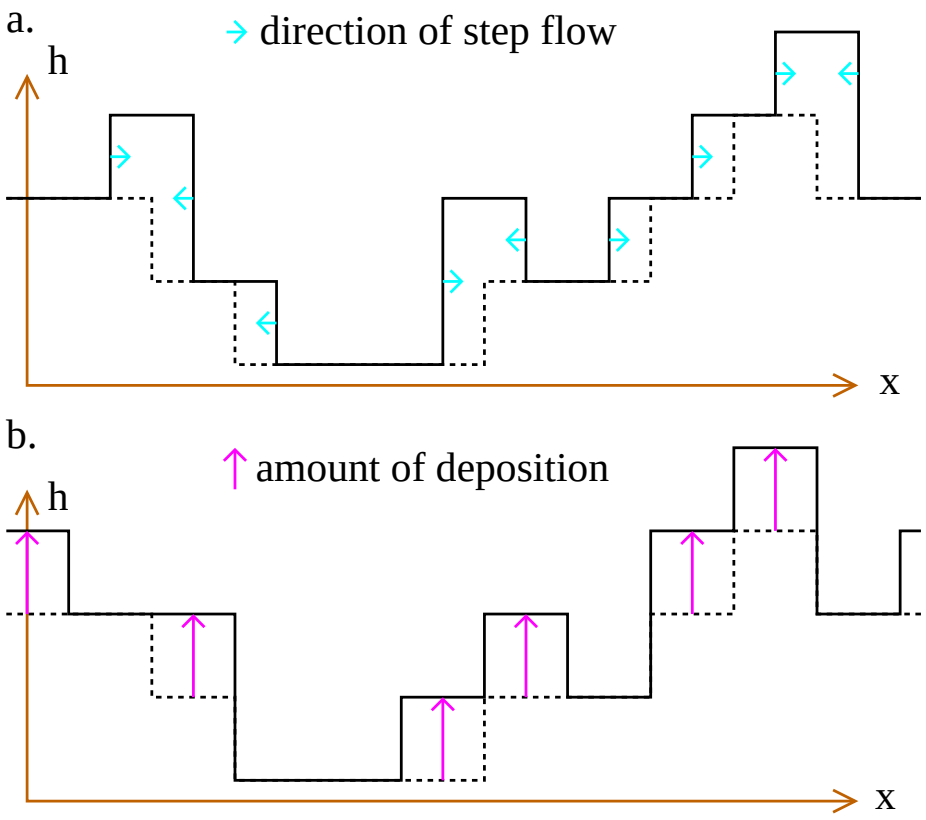

Figure 3.3: Two-step growth of the discrete-height step-flow random-deposition interface growth model; (a) Steps flow by one unit to the right (left) when its size Δh is negative (positive); (b) Each site increases by one unit with a probability p.

is greater than the critical value p_c. Below this transition point the interface is in a trivial flat state, where, for a stationary interface (interface time $y \to \infty$), the density of sites at the bottom $h = h_0$ layer is finite. The interface is thus *pinned* at this level and its growth rate becomes zero.

At the transition point $p = p_c$, the roughness of the interface

$$W^2 \equiv \overline{(h - \bar{h})^2} \tag{3.8}$$

diverges only logarithmically in time

$$W^2 \sim (\ln t)^{\gamma}, \tag{3.9}$$

with the exponent $\gamma \approx 1$ similar to that of the Kertész and Wolf's model as well as the restricted version of the models by Alon *et al.*.

3.5 Deterministic limits

At the two limits, $p = 1$ and $p = 0$, the toppling process of the avalanches becomes deterministic and the sand surface goes down layer by layer. The only randomness of the system comes from the driving method (3.3), where we randomly choose one of the highest sites at the $y = 0$ row to trigger an avalanche. The typical avalanche scar configurations at these two limits are shown in Fig. 3.4. These are the edges of avalanche clusters left on the surface, some of which are partially wiped out by newer avalanches.

3.5.1 Domain walls at $p = 0$

The $p = 0$ limit runs into the complication that in the bulk of the system ($y > 0$) the sand surface goes down by two units at a time. Since $\Delta h \equiv h(x, y) - \min[h(x - 1, y - 1), h(x + 1, y - 1)] = 1$ is stable according to the stability condition (3.1) and the sites on the $y = 0$ row always goes down by 1 each time according to the driving method (3.3), the sites on the $y = 1$ row will only topple when their highs are 2 higher than the triggering sites and they alway go down by 2 to the same height of the triggering site according to the toppling rule (3.2). All the sites at higher rows will be locked into the same even-oddness as the

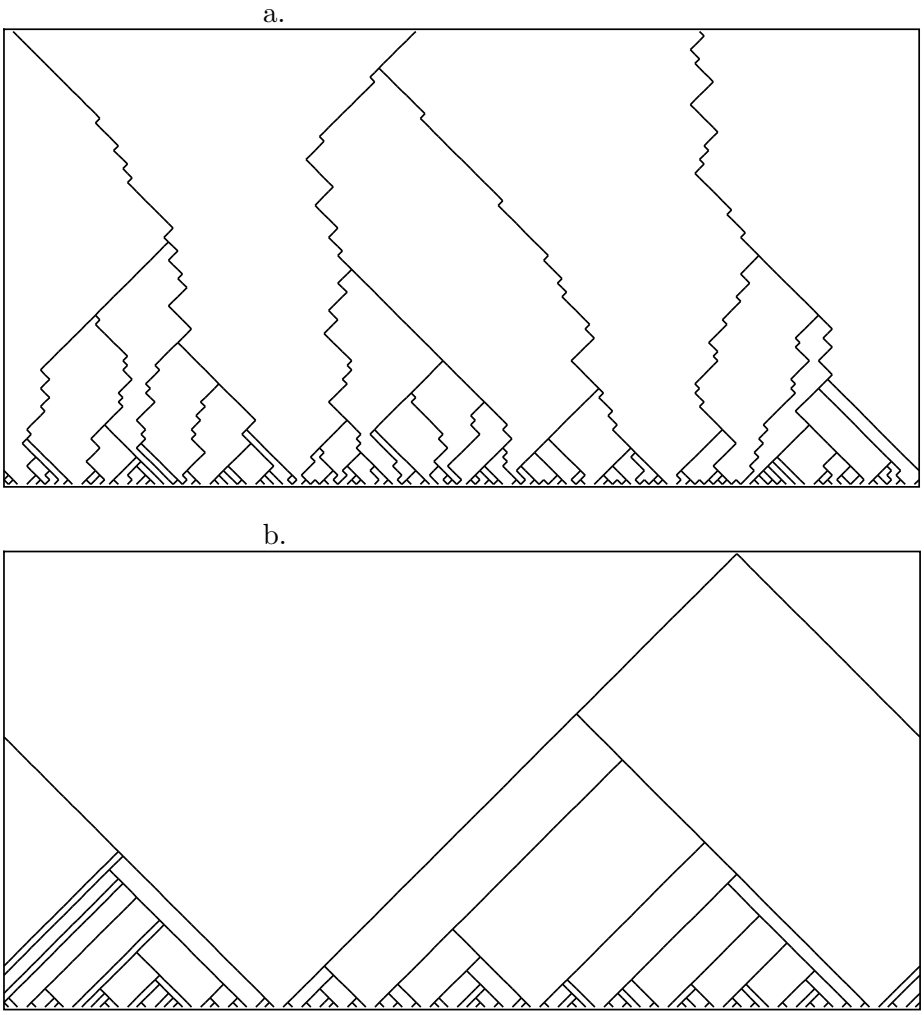

Figure 3.4: Scar (edge lines of avalanche clusters) configurations of DHSB avalanches at the two deterministic limits; (a) $p = 0$; (b) $p = 1$.

sites triggering their toppling. Therefore, after all sites have participated in at least one avalanche, their even-oddness will be fixed for all subsequent topplings. This means the even-oddness of a site is preserved by the toppling process. Therefore, the lines separating the even and odd sites thus form impenetrable domain walls for the avalanches (see Fig. 3.5). This hinders the applicability of the same analysis for the $p = 1$ situation we will present below.

3.5.2 Exact solution at $p = 1$

The $p = 1$ limit has a nice solution. Since the sites in the bulk topple from $\Delta h = 2$ to $\Delta h = 1$, the sand surface indeed goes down one layer at a time without the complication discussed previously. An exact solution can be obtained by considering the avalanches taking place in such one single layer. For a brand-new layer, the two boundaries of the first avalanche opens up linearly until it spans the system in the x direction and leave two scar lines on the surface. The two boundaries of the second avalanche expand until they meets the scar lines created by the first avalanche. Then, they turn and follow those scar lines until they meet with each other and terminate the avalanche. Subsequent avalanches follow the same scenario. The maximum distance an avalanche cluster can expand from its triggering point to each side in the x direction is exactly half the distance from the nearest triggering point of the previous avalanches in the same layer on that side. As the triggering points are chosen at a noncorrelated way, the maximum width w of an avalanche should follow Poisson's distribution

$$P_w(w) = \frac{\mu^w e^{-\mu}}{w!} \tag{3.10}$$

if the number of previous avalanches in the same layer is fixed so that μ is the average distance between the triggering points of the previous avalanches in the same layer. However, the avalanche under consideration could be any one of the avalanches happening in the same layer. Thus, we need to average over the number of avalanches n happening before this one in the same layer. For system of transverse size L_x, $n = L_x/\mu$. The integral can be carried out explicitly and gives

$$\int_0^\infty \frac{\mu^w e^{-\mu}}{w!} d\frac{1}{\mu} = \frac{(w-2)!}{w!} \sim w^{-2}, \tag{3.11}$$

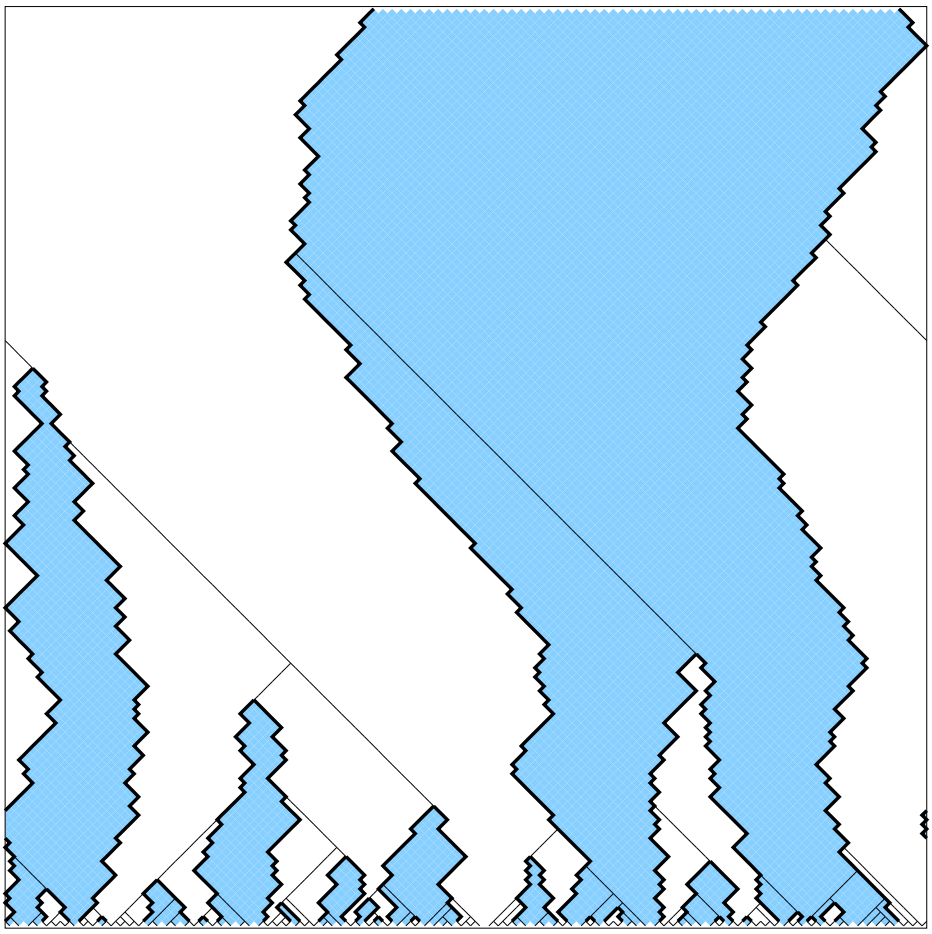

Figure 3.5: The domains of odd (shaded region) and even (light region) sites on a DHSB surface at $p = 0$, separating them are domain walls that no avalanche will penetrate at this deterministic limit.

which results in

$$\tau_l = \tau_w = 2. \tag{3.12}$$

The same results can also be derived from Eq. (3.4) and (3.5) by assuming $z = 1$ and $\alpha = 0$. Since the avalanches are compact the hyperscaling relation (3.7) and the derivations in [23] hold.

3.6 Shallow-avalanche phase

Below the transition point, the underlying interface model is in a flat phase where the bottom layer percolates with finite density. All the information of the initial configuration of the interface (the $y = 0$ row next to the wall) is wiped out at a time scale proportional to the sizes of the islands above bottom layer in the initial state. (Without deposition, the size of these islands decrease linearly in time.) While the underlying interface model is in a trivial phase, much like the uncorrelated stationary state of the system in Dhar and Ramaswamy's directed sandpile model [32], the avalanche distributions of the system may still exhibit power-law scaling. The numerical values of the scaling exponents shown in Fig. 3.6 confirm the power-law scaling of the distributions and they are similar to those values found at the $p = 1$ fixed point following $z = 1$ and $\alpha = 0$. While an exact solution is not available in this phase, we can understand that the scaling exponent $z = 1$ comes from the perspective that the DP clusters triggered from a single seed in the percolating phase open up linearly and also that roughness exponent $\alpha = 0$ comes from that the interface here is in a flat phase. However, a difference is that while $p < p_c$ represents an entire phase of shallow avalanches which should be controlled by an attractive fixed point, the $p = 1$ fixed point is unstable in the sense that the scaling behavior falls back to the KPZ universality class for any small deficiency in the cohesiveness p from the value 1.

3.7 DP roughening transition

At the transition point $p = p_c$, the interface roughness diverges logarithmically thus both the α and β exponent are zero. Nonetheless, the dynamic exponent z has a nontrivial value $z_{\mathrm{DP}} \approx 1.582$ coming from the DP nature of the bottom-layer dynamics. However, at

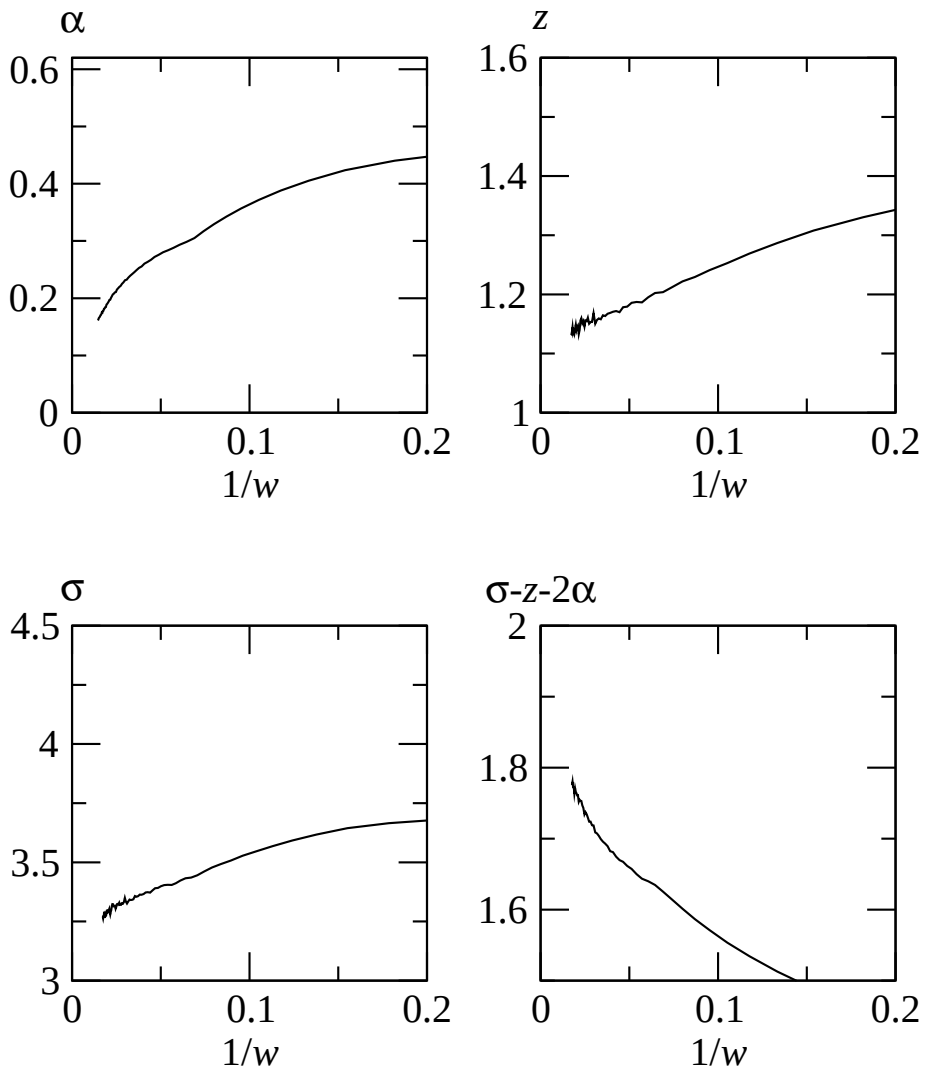

Figure 3.6: Finite-size scaling (FSS) estimates of the scaling exponents versus inverse width ($1/w$) of avalanche clusters for the DHSB avalanches in the shallow-avalanche phase (measured at $p = 0.1$). They are consistent with $\alpha = 0$ and $z = 1$.

the transition point, the avalanche clusters loss their compact shapes (see Fig. 3.7) and we should not expect the derivation in [23] for the avalanche exponents nor the calculation in [22] for the correction to scaling to remain valid. In this section we will show the break down of mass hyperscaling relation (3.7) and how the avalanches affect the roughness of the sand surface.

3.7.1 Breakdown of mass hyperscaling

At the transition point, the bottom layer of an avalanche cluster follows the critical DP dynamics therefore we should expect from the fractal DP cluster shape, the density of sites at the lowest $h = h_0$ level goes to zero in the thermodynamic limit for large avalanches. However, the overall shape of an avalanche consists of, in addition, sites at $h_0 + 1, h_0 + 2$, ... levels. The higher-level sites that participate in the avalanche fill into the holes and voids next to the bottom layer cluster and more or less bring the avalanche cluster back to a compact shape. We can verify this compactness of the avalanche cluster by a direct measurement of the ratio $a/(lw)$, with a being the area of (or, the number of sites participate in) an avalanche. The result is shown as the solid line in Fig. 3.8. The approach to a finite value on the vertical axis shows the compactness of the avalanche clusters by the existence of a finite area density ≈ 0.2 in the thermodynamic limit. The FSS estimates are plotted against $1/\ln y$ instead of $1/y$ since the roughness of the surface diverges only logarithmically in y, which we will elaborate later.

Contrary to a finite area density, as also shown in Fig. 3.8, the mass density $m/(lw\delta)$ (the dashed line) goes to zero in the thermodynamic limit. The nonexistence of a finite mass density breaks the scaling

$$m \sim lwd, \tag{3.13}$$

which was assumed in [23] for the derivation of the mass hyperscaling relation (3.7). The plot of the combined exponent $\sigma - z - 2\alpha$ in Fig. 3.9 shows the violation of Eq. (3.7) where the FSS estimates approaches ≈ 1.72 which is much lower than the expected value 2.

Also shown in Fig. 3.9 are the plots for the α, z, and σ exponents. They are consistent with $z = z_{\rm DP}$ and more or less with $\alpha = 0$. This confirms that the scaling behavior of the

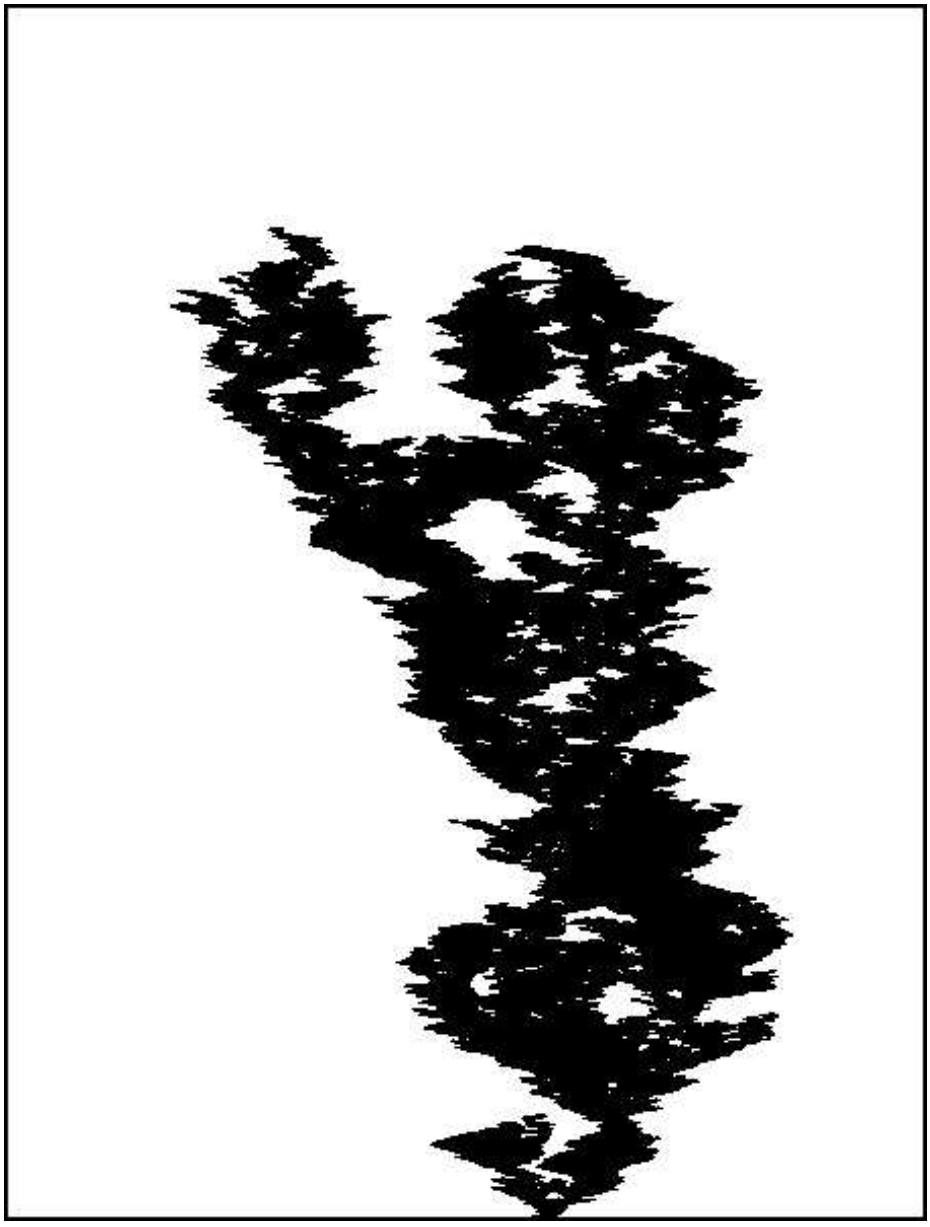

Figure 3.7: A typical large avalanche cluster for DHSB at the DP transition point; The size of the box is $L_x \times L_y = 455 \times 10000$.

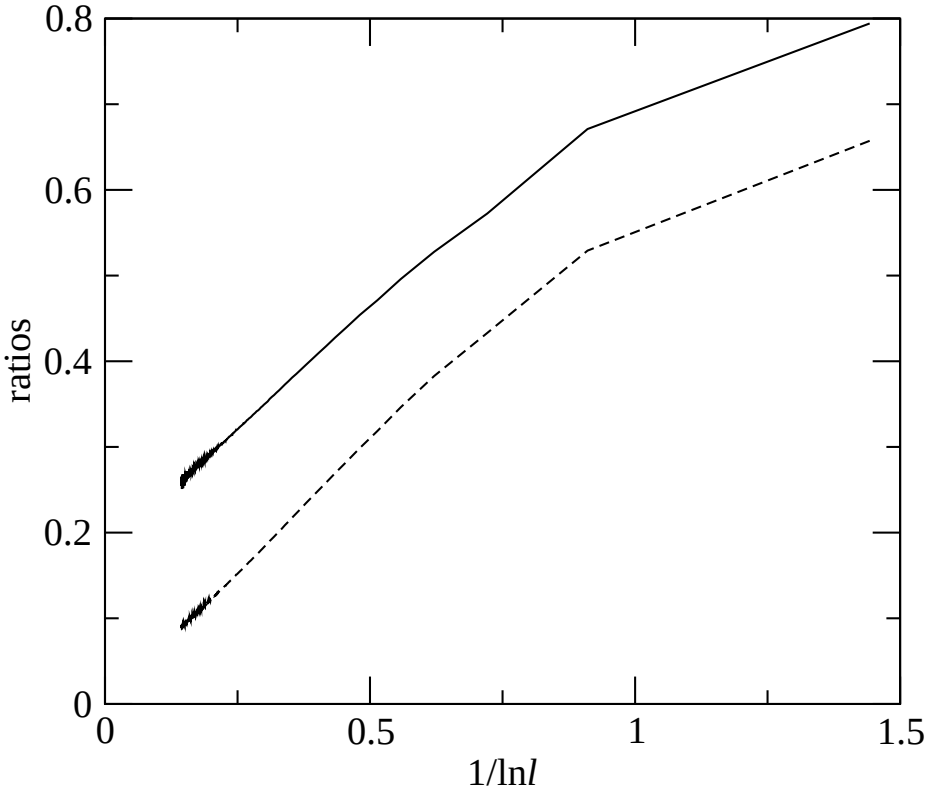

Figure 3.8: The FSS plot of the area density $a/(lw)$ (solid line) and the mass density $m/(lw\delta)$ (dashed line) versus inverse length $(1/l)$ for the avalanche clusters at the DP transition point. While the area density converges to a finite value at the thermodynamic limit, the mass density converges to 0.

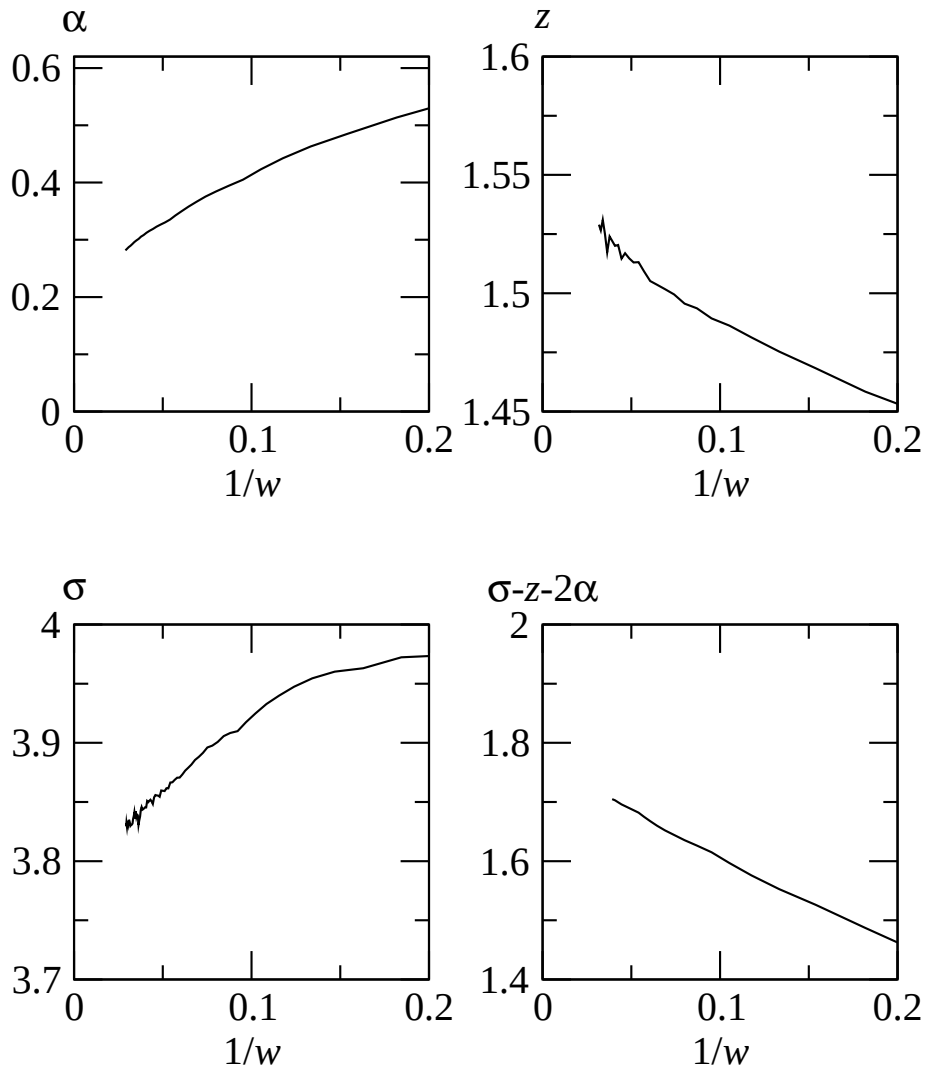

Figure 3.9: FSS estimates of the scaling exponents derived from the avalanche exponents τ_l, τ_w, τ_δ for the discrete height sandbox model versus the inverse width $(1/w)$ at the DP transition point. The z exponent is consistent with dynamic exponent of DP universality class $z_{\rm DP} \simeq 1.582$. The combination $\sigma - z - 2\alpha < 2$ indicates a violation of mass hyperscaling relation (3.7).

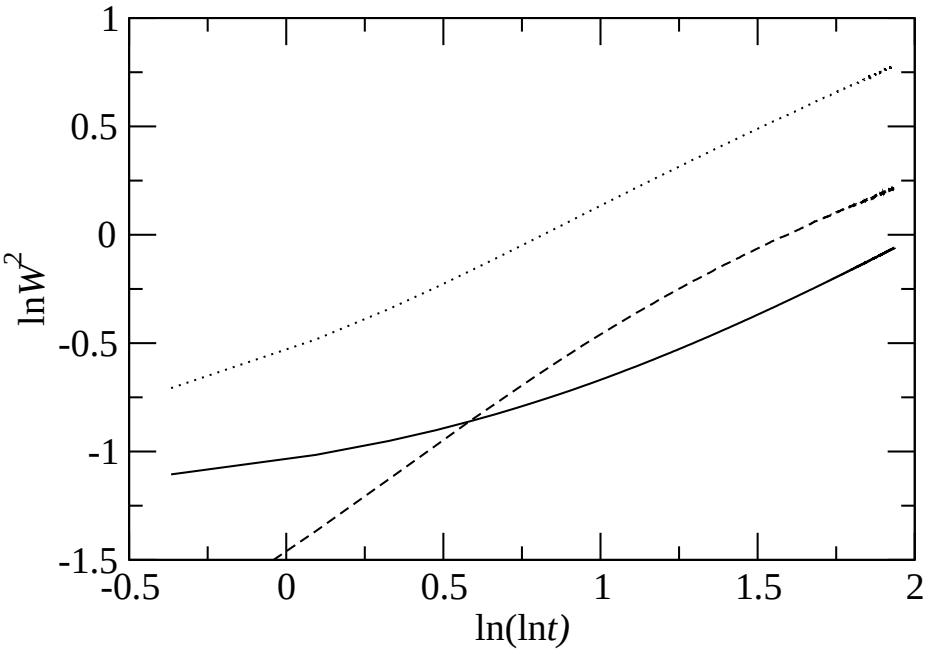

Figure 3.10: The roughness of a stationary DHSB surface(dotted line) compared with the roughness of the SFRD model (solid line) versus the double logarithm of time t at the DP transition point. The iterated avalanche process makes the surface rougher. The dashed line shows the increase of the roughness by the iterated avalanche process.

avalanches follows those of the SFRD interface. The slow convergence of α is to be expected from the logarithmic divergence of the interface roughness.

3.7.2 Interface roughness

The remaining question is how the scaling behavior of the roughness will be changed by the iterated avalanche process. We approach this by looking at the change of the roughness itself and compare the scaling of this change to the scaling of the original interface roughness as what was done in [22]. The results are shown in Fig. 3.10. The change in the roughness ΔW^2 scale as $(\ln t)^\gamma$ with $\gamma \approx 0.4$ as shown in Fig. 3.11 which is less than $\gamma \approx 1$ for the SFRD model. Therefore, in the thermodynamics limit, the DHSB should retain the same γ exponent as the SFRD model.

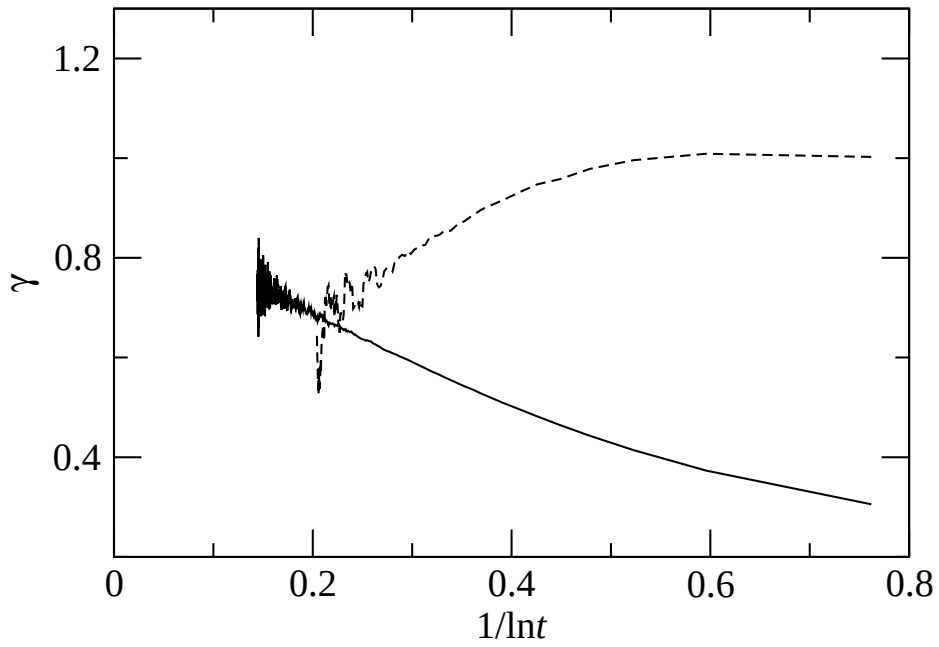

Figure 3.11: FSS of the γ exponents of the logarithmic scaling of SFRD roughness (solid line) and $\Delta W^2 \equiv W^2_{\rm DHSB} - W^2_{\rm SFRD}$ (dashed line), assuming the scaling form $(\ln t)^\gamma$, versus the inverse of the logarithm of time. The change in roughness ΔW^2 scales with a smaller exponent than the scaling exponent of W^2.

3.8 Summary

In this chapter, we introduced the DHSB as a model for the avalanches in granular materials with variable cohesiveness. This model exhibits a deepening transition from a shallow-avalanche phase where avalanches only involve a couple of surface layers of the granular material, into a deep avalanche phase where the depths of avalanches increase with power laws of their lengths or widths. In the deep avalanche phase, the scaling behavior of the avalanches belongs to the KPZ universality class: The avalanche clusters scale anisotropically with $l \sim w^{3/2}$ and depth increase as $\delta \sim w^{1/2}$. In the flat phase, the avalanche clusters scale isotropically $l \sim w$ with finite depths.

In both phases, the mass hyperscaling relation (3.7) based on the compactness (3.13) of the avalanche holds. On the other hand, at the transition point, the hierarchical DP structure studied by Tauber *et al.* [110] for each level of the toppling sites break this scaling in a subtle way. While the mass density $m/(lw\delta)$ of the avalanche clusters goes to zero in the thermodynamic limit, the area density $a/(lw)$ remains finite. However, the exact scaling behavior of the systems at this DP roughening transition point remains a mystery even without the iterated avalanche in the DHSB model [2, 75, 44].

While we are not aware of any experimental study on how the avalanche behavior of a system will vary with a gradual change in the cohesiveness of the grains, the cohesiveness in granular system is known to depend on moisture [89] and grain sizes [111, 99]. We thus expect experimental studies in this direction not to be meet with too much difficulty. However, the DHSB model represents a system with layered structure where the heights are discrete and the DP nature of the deepening transition relies heavily on a well defined bottom layer or minimal stable configuration of the systems. It thus wouldn't be a surprise if the exact DP scaling were not to be observed in the avalanches of most regular sandpiles.

Nonetheless, the breakdown of the mass hyperscaling relation (3.7) comes from the fractal aspect of the hierarchical DP clusters. It would serve as a hallmark to the existence of such a transition if it's to be observed experimentally.

BIBLIOGRAPHY

[1] U. Alon, M. R. Evans, H. Hinrichsen, and D. Mukamel. Roughening transition in a one-dimensional growth process. *Physical Review Letters*, 76:2746–2749, 1996.

[2] U. Alon, M. R. Evans, H. Hinrichsen, and D. Mukamel. Smooth phases, roughening transitions, and novel exponents in one-dimensional growth models. *Physical Review E*, 57:4997–5012, 1998.

[3] Thomas Andrews. The bakerian lecture: On the continuity of the gaseous and liquid states of matter. *Philosophical Transactions of the Royal Society of London*, pages 575–590, 1869.

[4] Per Bak and Kim Sneppen. Punctuated equilibrium and criticality in a simple model of evolution. *Physical Review Letters*, 71(24):4083–4086, 1993.

[5] Per Bak, Chao Tang, and Kurt Wiesenfeld. Self-organized criticality: An explanation of $1/f$ noise. *Physical Review Letters*, 59:381–384, 1987.

[6] Per Bak, Chao Tang, and Kurt Wiesenfeld. Self-organized criticality. *Physical Review A*, 38:364–374, 1988.

[7] Albert-László. Barabási and H. Eugene Stanley. *Fractal Concepts in Surface Growth*. University Press, Cambridge, 1995.

[8] Kevin E. Bassler and Maya Paczuski. Simple model of superconducting vortex avalanches. *Physical Review Letters*, 81:3761–3764, 1998.

[9] Kevin E. Bassler, Maya Paczuski, and George F. Reiter. Braided rivers and superconducting vortex avalanches. *Physical Review Letters*, 83:3956–3959, 1999.

[10] R. Bausch, V. Dohm, H. K. Janssen, and R. K. P. Zia. Critical dynamics of an interface in 1+ ϵ dimensions. *Physical Review Letters*, 47:1837–1840, 1981.

[11] A. Ben Hur, R. Hallgass, and V. Loreto. Renormalization procedure for directed self-organized critical models. *Physical Review E*, 54:1426–1432, 1996.

[12] Asa Ben-Hur and Ofer Biham. Universality in sandpile models. *Physical Review E*, 53:R1317–R1320, 1996.

[13] Asa Ben-Hur and Ofer Biham. Universality in sandpile models. *Physical Review E*, 53:R1317–R1320, 1996.

[14] G. Bianconi, M. A. Mu noz, A. Gabrielli, and L. Pietronero. Renormalization-group study of one-dimensional systems with roughening transitions. *Physical Review E*, 60:3719–3726, 1999.

[15] Michael Bretz, Jevne B. Cunningham, Peter L. Kurczynski, and Franco Nori. Imaging of avalanches in granular materials. *Physical Review Letters*, 69:2431–2434, 1992.

[16] J. M. Burgers. *The nonlinear diffusion equation : asymptotic solutions and statistical problems.* Riedel, Boston, 1974.

[17] R. Burridge and L. Knopoff. Model and theoretical seismicity. *Bulletin of the Seismological Society of America*, 57(3):341–371, 1967.

[18] Florence Cantelaube, Yann Limon-Duparcmeur, Daniel Bideau, and G.H Ristow. Geometrical analysis of avalanches in a 2d drum. *Journal de Physique I France*, 5:581–596, 1995.

[19] J. L. Cardy and R. L. Sugar. Directed percolation and reggeon field theory. *Journal of Physics A: Mathematical and General*, 13:L423–L427, 1980.

[20] John Cardy. *Scaling and Renormalization in Statistical Physics*. University Press, Cambridge, 1996.

[21] J. M. Carlson and J. S. Langer. Properties of earthquakes generated by fault dynamics. *Physical Review Letters*, 62:2632, 1989.

[22] Chun-Chung Chen and Marcel den Nijs. Directed avalanche processes with underlying interface dynamics. *Physical Review E*, 66:01xxxx, 2002.

[23] Chun-Chung Chen and Marcel den Nijs. Interface view of directed sandpile dynamics. *Physical Review E*, 65:031309, 2002.

[24] Chen-Shan Chin and Marcel den Nijs. Stationary-state skewness in two-dimensional kardar-parisi-zhang type growth. *Physical Review E*, 59:2633–2641, 1999.

[25] Kim Christensen, Àlvaro Corral, Vidar Frette, Jens Feder, and Torstein Jøssang. Tracer dispersion in a self-organized critical system. *Physical Review Letters*, 77:107–110, 1996.

[26] Kim Christensen and Zeev Olami. Sandpile models with and without an underlying spatial structure. *Physical Review E*, 48:3361–3372, 1993.

[27] Zoltán Csahók and Tamás Vicsek. Kinetic roughening in a model of sedimentation of granular materials. *Physical Review A*, 46:4577–4581, 1992.

[28] Gianaurelio Cuniberti, Angelo Valleriani, and José Luis Vega. Effects of regulation on a self-organized market. *Quantitative Finance*, 1(3):332–335, 2001.

[29] S. Das Sarma and P. Tamborenea. A new universality class for kinetic growth: One-dimensional molecular-beam epitaxy. *Physical Review Letters*, 66:325–328, 1991.

[30] Deepak Dhar. Self-organized critical state of sandpile automaton models. *Physical Review Letters*, 64:1613–1616, 1990.

[31] Deepak Dhar. The abelian sandpile and related models. *Physica A*, 263:4–25, 1999.

[32] Deepak Dhar and Ramakrishna Ramaswamy. Exactly solved model of self-organized critical phenomena. *Physical Review Letters*, 63:1659–1662, 1989.

[33] Eytan Domany and Wolfgang Kinzel. Equivalence of cellular automata to ising models and directed percolation. *Physical Review Letters*, 53:311–314, 1984.

[34] Murray Eden. A probabilistic model for morphogenesis. In Hubert P. Yockey, editor, *Symposium on Information Theory in Biology*. Pergamon Press, New York, 1958.

[35] S. F. Edwards and D. R. Wilkinson. The surface statistics of a granular aggregate. *Proceedings of the Royal Society of London. Series A, Mathematical and Physical Sciences*, 381:17–31, 1982.

[36] Albert Einstein. *Investigations on the theory of the Brownian movement*. Dover, New York, 1956.

[37] J. W Essam, A. J. Guttmann, I. Jensen, and D. TanlaKishani. Directed percolation near a wall. *Journal of Physics A: Mathematical and General*, 29:1619–1628, 1996.

[38] Pierre Evesque. Analysis of the statistics of sandpile avalanches using soil-mechanics results and concepts. *Physical Review A*, 43:2720–2740, 1991.

[39] Fereydoom Family. Scaling of rough surfaces: effects of surface diffusion. *Journal of Physics A: Mathematical and General*, 19(8):L441–L446, 1986.

[40] Fereydoon Family and Tamás Vicsek. Scaling of the active zone in the eden process on percolation networks and the ballistic deposition model. *Journal of Physics A: Mathematical and General*, 18(2):L75–L81, 1985.

[41] Dieter Forster, David R. Nelson, and Michael J. Stephen. Large-distance and long-time properties of a randomly stirred fluid. *Physical Review A*, 16:732–749, 1977.

[42] V. Frette, K. Christensen, A. Malthe-Sorenssen, J. Feder, T. Jossang, and P. Meakin. Avalanche dynamics in a pile of rice. *Nature*, 379:49–52, 1996.

[43] Per Fröjdh, Martin Howard, and Kent Bækgaard Lauritsen. Directed percolation with a wall or edge. *Journal of Physics A: Mathematical and General*, 31:2311–2320, 1998.

[44] Yadin Y. Goldschmidt, Haye Hinrichsen, Martin Howard, and Uwe C. Täuber. Nonequilibrium critical behavior in unidirectionally coupled stochastic processes. *Physical Review E*, 59:6381–6408, 1999.

[45] P. Grassberger and A. de la Torre. Reggeon field theory (schlögl's first model) on a lattice: Monte carlo calculations of critical behaviour. *Annals of Physics*, 122:373–396, 1979.

[46] P. Grassberger and K. Sundermeyer. Reggeon field theory and markov processes. *Phys. Lett. B*, 77(2):220–222, 1978.

[47] Peter Grassberger. Some further results on a kinetic critical phenomenon. *Journal of Physics A: Mathematical and General*, 22(23):L1103–L1107, 1989.

[48] Peter Grassberger, Hugues Chaté, and Guillaume Rousseau. Spreading in media with long-time memory. *Physical Review E*, 55:2488–2495, 1997.

[49] Peter Grassberger, Friedrich Krause, and Tassilo von der Twer. A new type of kinetic critical phenomenon. *Journal of Physics A: Mathematical and General*, 17(3):L105–L109, 1984.

[50] D. G. Green, A. M. Gill, and I. R. Noble. Fire shapes and the adequacy of fire-spread models. *Ecological Modelling*, 20(1):33–45, 1983.

[51] Beno Gutenberg and C. F. Richter. Seismicity of the earth. *Geological Society of America, Special Papers*, (34):1–131, 1941.

[52] Timothy Halpin-Healy and Yi-Cheng Zhang. Kinetic roughening phenomena, stochastic growth, directed polymers and all that. aspects of multidisciplinary statistical mechanics. *Physics Reports*, 254:215–414, 1995.

[53] Jeff Hasty and Kurt Wiesenfeld. Renormalization group for directed sandpile models. *Physical Review Letters*, 81:1722–1725, 1998.

[54] G. A. Held, D. H. Solina, H. Solina, D. T. Keane, W. J. Haag, P. M. Horn, and G. Grinstein. Experimental study of critical-mass fluctuations in an evolving sandpile. *Physical Review Letters*, 65:1120–1123, 1990.

[55] Chu heng Liu, H. M. Jaeger, and Sidney R. Nagel. Finite-size effects in a sandpile. *Physical Review A*, 43:7091–7092, 1991.

[56] H. Hinrichsen and H.M. Koduvely. Numerical study of local and global persistence in directed percolation. *European Physical Journal B*, 5:257–264, 1998.

[57] Haye Hinrichsen and Géza Ódor. Roughening transition in a model for dimer adsorption and desorption. *Physical Review Letters*, 82:1205–1208, 1999.

[58] Haye Hinrichsen, Vladimir Rittenberg, and Horatiu Simon. Universality properties of the stationary states in the one-dimensional coagulation-diffusion model with external particle input. *Journal of Statistical Physics*, 86:1203–1235, 1997.

[59] D. J. Hornbaker, R. Albert, I. Albert, A.-L. Barabási, and P. Schiffer. What keeps sandcastles standing? *Nature*, 387:765–766, 1997.

[60] Eugene V. Ivashkevich, Alexander M. Povolotsky, Alessandro Vespignani, and Stefano Zapperi. Dynamical real space renormalization group applied to sandpile models. *Physical Review E*, 60:1239–1251, 1999.

[61] H. M. Jaeger, Chu heng Liu, and Sidney R. Nagel. Relaxation at the angle of repose. *Physical Review Letters*, 62:40–43, 1989.

[62] Iwan Jensen. Critical exponents for branching annihilating random walks with an even number of offspring. *Physical Review E*, 50:3623–3633, 1994.

[63] Iwan Jensen. Low-density series expansions for directed percolation on square and triangular lattices. *Journal of Physics A: Mathematical and General*, 29(22):7013–7040, 1996.

[64] M. Kardar, G. Parisi, and Y.-C. Zhang. Dynamic scaling of growing interfaces. *Physical Review Letters*, 56:889–892, 1986.

[65] János Kertész and Dietrich E. Wolf. Anomalous roughening in growth processes. *Physical Review Letters*, 62:2571–2574, 1989.

[66] Mann Ho Kim and Hyunggyu Park. Critical behavior of an interacting monomer-dimer model. *Physical Review Letters*, 73:2579–2582, 1994.

[67] W. Kinzel and J. M. Yeomans. Directed percolation: a finite-size renormalisation group approach. *Journal of Physics A: Mathematical and General*, 14:L163–L168, 1981.

[68] Wolfgang Kinzel. Directed percolation. In G. Deutscher, R. Zallen, and J. Adler, editors, *Percolation Structures and Processes, Annals of the Israel Physical Society*, volume 5, pages 425–445, Bristol, 1983. Hilger.

[69] Morten Kloster, Sergei Maslov, and Chao Tang. Exact solution of stochastic directed sandpile model. *Physical Review E*, 63:026111, 2001.

[70] Sungchul Kwon, WonMuk Hwang, and Hyunggyu Park. Dynamic behavior of driven interfaces in models with two absorbing states. *Physical Review E*, 59:4949–4952, 1999.

[71] J. S. Langer. Instabilities and pattern formation in crystal growth. *Rev. Mod. Phys.*, 52:1–28, 1980.

[72] Kent Bækgaard Lauritsen, Per Fröjdh, and Martin Howard. Surface critical behavior in systems with absorbing states. *Physical Review Letters*, 81:2104–2107, 1998.

[73] Kent Bækgaard Lauritsen, Kim Sneppen, Maria Markošová, and Mogens H. Jensen. Directed percolation with an absorbing boundary. *Physica A*, 247:1–9, 1997.

[74] David R. Lide, editor. *CRC Handbook of Chemistry and Physics*. CRC Press LLC, 3rd electronic edition, 2001.

[75] Juan M. López and Henrik Jeldtoft Jensen. Nonequilibrium roughening transition in a simple model of fungal growth in 1 + 1 dimensions. *Physical Review Letters*, 81:1734–1737, 1998.

[76] S. Lübeck, B. Tadić, and K. D. Usadel. Nonequilibrium phase transition and self-organized criticality in a sandpile model with stochastic dynamics. *Physical Review E*, 53:2182–2189, 1996.

[77] Thomas Lux and Michele Marchesi. Scaling and criticality in a stochastic multi-agent model of a financial market. *Nature*, 397:498–500, 1999.

[78] S. Majumdar and D. Dhar. Equivalence between the abelian sandpile model and the q to 0 limit of the potts model. *Physica A*, 185:129–145, 1992.

[79] Benoit Mandelbrot. How long is the coast of britain? statistical self-similarity and fractional dimension. *Science*, 156(3775):636–638, 1967.

[80] Benoit B. Mandelbrot. *The fractal geometry of nature*. W. H. Freeman, San Francisco, 1983.

[81] S S Manna. Two-state model of self-organized criticality. *Journal of Physics A: Mathematical and General*, 24(7):L363–L369, 1991.

[82] Mitsugu Matsushita and Hiroshi Fujikawa. Diffusion-limited growth in bacterial colony formation. *Physica A*, 168:498–506, 1990.

[83] S. Matsuura and S. Miyazima. Self-affine fractal growth front of aspergillus-oryzae. *Physica A*, 191:30–34, 1992.

[84] J. Maunuksela, M. Myllys, O.-P. Kähkönen, J. Timonen, N. Provatas, M. J. Alava, and T. Ala-Nissila. Kinetic roughening in slow combustion of paper. *Physical Review Letters*, 79:1515–1518, 1997.

[85] P. Meakin and R. Jullien. Restructuring effects in the rain model for random deposition. *Journal de Physique*, 48:1651–1662, 1987.

[86] Paul Meakin, P. Ramanlal, L. M. Sander, and R. C. Ball. Ballistic deposition on surfaces. *Physical Review A*, 34:5091–5103, 1986.

[87] Ernesto Medina, Terence Hwa, Mehran Kardar, and Yi-Cheng Zhang. Burgers equation with correlated noise: Renormalization-group analysis and applications to directed polymers and interface growth. *Physical Review A*, 39:3053–3075, 1989.

[88] M. Myllys, J. Maunuksela, M. Alava, T. Ala-Nissila, J. Merikoski, and J. Timonen. Kinetic roughening in slow combustion of paper. *Physical Review E*, page 036101, 2001.

[89] Steven T. Nase, Watson L. Vargas, Adetola A. Abatan, and J. J. McCarthy. Discrete characterization tools for cohesive granular material. *Powder Technology*, 116:214–223, 2001.

[90] John Neergaard and Marcel den Nijs. Crossover scaling functions in one dimensional dynamic growth models. *Physical Review Letters*, 74:730–733, 1995.

[91] Maya Paczuski and Kevin E. Bassler. Theoretical results for sandpile models of soc with multiple topplings. *Physical Review E*, 62:5347–5352, 2000.

[92] Maya Paczuski and Stefan Boettcher. Universality in sandpiles, interface depinning, and earthquake models. *Physical Review Letters*, 77:111–114, 1996.

[93] Giorgio Parisi and Zhang Yi-Cheng. Field theories and growth models. *Journal of Statistical Physics*, 41:1–36, 1985.

[94] S. Park and B. Kahng. Nonequilibrium roughening transition in an interface growth model with two species of particles. *Physical Review E*, 60:6160–6163, 1999.

[95] Romualdo Pastor-Satorras and Alessandro Vespignani. Critical behavior and conservation in directed sandpiles. *Physical Review E*, 62:6195–6205, 2000.

[96] Romualdo Pastor-Satorras and Alessandro Vespignani. Universality classes in directed sandpile models. *Journal of Physics A: Mathematical and General*, 33(3):L33–L39, 2000.

[97] L. Pietronero, A. Vespignani, and S. Zapperi. Renormalization scheme for self-organized criticality in sandpile models. *Physical Review Letters*, 72:1690–1693, 1994.

[98] V. B. Priezzhev, D. V. Ktitarev, and E. V. Ivashkevich. Formation of avalanches and critical exponents in an abelian sandpile model. *Physical Review Letters*, 76:2093–2096, 1996.

[99] M. A. S. Quintanilla, J. M. Valverde, A. Castellanos, and R. E. Viturro. Looking for self-organized critical behavior in avalanches of slightly cohesive powders. *Physical Review Letters*, 87:194301, 2001.

[100] Jean Rajchenbach. Flow in powders: From discrete avalanches to continuous regime. *Physical Review Letters*, 65:2221–2224, 1990.

[101] Robert Savit and Robert Ziff. Morphology of a class of kinetic growth models. *Physical Review Letters*, 55:2515–2518, 1985.

[102] F. Schlögl. Chemical reaction models for non-equilibrium phase transitions. *Zeitschrift für Physik A: Atoms and nuclei*, 253(2):147–161, 1972.

[103] J. A. Shapiro. Organization of developing escherichia-coli colonies viewed by scanning electron-microscopy. *Journal of Bacteriology*, 169(1):142–156, 1987.

[104] D. Sornette and Y.-C. Zhang. Nonlinear langevin model of geomorphic erosion processes. *Geophysical Journal International*, 113:382–386, 1993.

[105] D. N. Sutherland. Comment on vold's simulation of floc formation. *Jouranl of Colloid and Interface Science*, 22:300–302, 1966.

[106] B. Tadic, U. Nowak, K. D. Usadel, R. Ramaswamy, and S. Padlewski. Scaling behavior in disordered sandpile automata. *Physical Review A*, 45:8536–8545, 1992.

[107] Bosiljka Tadic and Deepak Dhar. Emergent spatial structures in critical sandpiles. *Physical Review Letters*, 79:1519–1522, 1997.

[108] Bosiljka Tadić and Vyatcheslav Priezzhev. Scaling of avalanche queues in directed dissipative sandpiles. *Physical Review E*, 62:3266–3275, 2000.

[109] Chao Tang, Kurt Wiesenfeld, and Per Bak. Phase organization. *Physical Review Letters*, 58:1161–1164, 1987.

[110] Uwe C. Täuber, Martin J. Howard, and Haye Hinrichsen. Multicritical behavior in coupled directed percolation processes. *Physical Review Letters*, 80:2165–2168, 1998.

[111] Jose Manuel Valverde, Antonio Castellanos, Antonio Ramos, and P. Keith Watson. Avalanches in fine, cohesive powders. *Physical Review E*, 62:6851–6860, 2000.

[112] T. Vicsek, M. Cserzö, and V. K. Horváth. Self-affine growth of bacterial colonies. *Physica A*, 167:315–321, 1990.

[113] Marjorie J. Vold. Computer simulation of floc formation in a colloidal suspension. *Journal of Colloid Science*, 18(7):684–695, 1963.

[114] Yi-Cheng Zhang. Scaling theory of self-organized criticality. *Physical Review Letters*, 63:470–473, 1989.

[115] Robert M. Ziff, Erdagon Gulari, and Yoav Barshad. Kinetic phase transitions in an irreversible surface-reaction model. *Physical Review Letters*, 56:2553–2556, 1986.

Appendix A

ACTIVE WIDTH AT A SLANTED ACTIVE BOUNDARY IN DIRECTED PERCOLATION

It is shown in this appendix that the width W of the active region around an active moving wall in a directed percolation process diverges at the percolation threshold p_c as $W \simeq A\epsilon^{-\nu_\parallel} \ln(\epsilon_0/\epsilon)$, with $\epsilon = p_c - p$, ϵ_0 a constant, and $\nu_\parallel = 1.734$ the critical exponent of the characteristic time needed to reach the stationary state $\xi_\parallel \sim \epsilon^{-\nu_\parallel}$. The logarithmic factor arises from screening the statistically independent needle shaped subclusters in the active region. Numerical data confirm this scaling behavior.

A.1 Introduction

Directed percolation (DP) has emerged as one of the generic absorbing-state-type dynamic processes. It describes epidemic processes, e.g., forest fires and various types of surface catalysis processes [68, 102, 45, 46, 115]. Such processes include a so-called absorbing state, typically the vacuum, from which it cannot escape. The relevant tunable parameter is the propagation probability p. The system undergoes a phase transition from the absorbing phase at small p, where the stationary state is the absorbing state, into an active stationary phase at large p, where the system refuses to die. The scaling properties at DP dynamic phase transitions have been known for almost two decades, and it's now realized that DP critical behavior is the generic universality class for dynamic absorbing-state-type processes [68].

At DP-type critical points, the equilibration time $\xi_\parallel$ diverges. It scales as $\xi_\parallel \sim \xi_\perp^z$ compared to the spatial correlation length $\xi_\perp$, with dynamic exponent $z = 1.581$ [63]. For example, starting from a single seed, the survival probability obeys the scaling form

$$P_s(\epsilon, t) = b^{-x_s} P_s(b^{1/\nu_\perp}\epsilon, b^{-z}t) \tag{A.1}$$

with $\epsilon = p_c - p$ the distance from the critical point. This leads to

$$P_s \sim \epsilon^{\beta} \exp(\frac{-t}{\xi_{\|}}), \tag{A.2}$$

with exponent $\beta = x_s \nu_{\perp}$. The exponential factor reflects that deep inside the absorbing phase P_s decays exponentially in time. The equilibration time diverges at the DP critical point as $\xi_{\|} \sim \epsilon^{-\nu_{\|}}$ with $z = \nu_{\|}/\nu_{\perp}$. At p_c the survival probability decays as a power law, $P_s(t) \sim t^{-\delta}$ with $\delta = x_s/z = \beta/\nu_{\|}$.

A recent direction of research in this topic concerns the scaling properties near boundaries [37, 43, 72, 73]. Those studies address absorbing and reflective walls. The scaling properties are modified by surface-type critical exponents. In particular, the survival probability for a seed near the boundary obeys the same scaling form as above, but with a new interface critical exponent x, and therefore a modified value for β.

In this appendix, we discuss the scaling properties near active boundaries. Consider a stationary active vertical wall in the system. All sites in the wall are alive. The critical exponent β is not an issue, because the system remains active near the wall for all p. However, in the absorbing phase the cloud of active sites near the wall has a specific stationary state width, which is expected to diverge as $W \sim \xi_{\perp} \sim \epsilon^{-\nu_{\perp}}$. Widths like this diverge with bulk exponents.

Assume that this wall is slanted, with an arbitrary angle $\theta \neq 90^{\circ}$ with respect to the horizontal direction (see Fig. A.1). In the space-time interpretation of the configurations, the wall moves with a constant velocity. It acts as a slanted active curtain rod. A curtain of active sites hangs down from it as illustrated in Fig. A.1. For $p < p_c$, the curtain has a finite width $l_{\perp}$ and length $l_{\|} = l_{\perp} \tan(\theta)$.

In this appendix, we address how the stationary state width of this slanted curtain scales near the DP critical point. Naively this seems a simple question. One would expect that the curtain width diverges with the same exponent as the equilibration time scale, $W \sim \epsilon^{-\nu_{\|}}$, i.e., with the same exponent as the length of a curtain hanging down from an horizontal curtain rod ($\theta = 0$) [48, 70]. The latter is equivalent to asking for the survival probability in the setup without any walls where all sites are active in the initial state.

This expectation is based on the anisotropic scaling properties. Consider a system with a

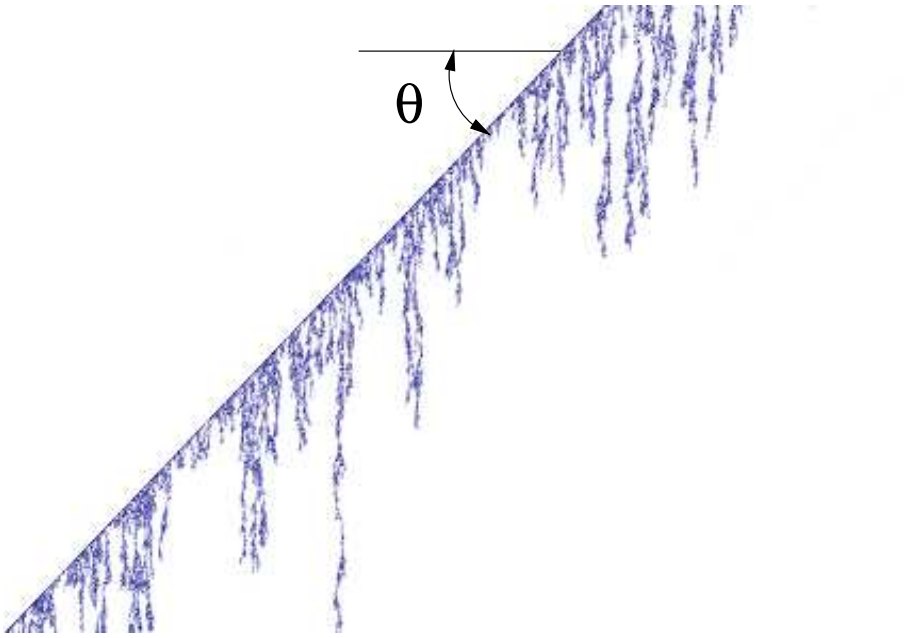

Figure A.1: The curtain of active sites at the active slanted boundary.

rod at angle $\theta \neq 0$. The horizontal and vertical bulk lengths diverge with different exponents, as $\xi_{\parallel} \sim \xi_{\perp}^{z}$. Therefore, a system at $p_c - p = \epsilon$ and wall angle θ is equivalent by renormalization to a system with a smaller wall angle θ' at $\epsilon' = b^{-1/\nu_{\perp}}\epsilon$ with $\tan(\theta') \simeq b^{z-1}\tan(\theta)$. The scaling properties of W should not depend on the angle θ, since the rod renormalizes towards the horizontal position. We should expect the same scaling behavior as at $\theta = 0$. However, a recent numerical study [70] seems to contradict this.

Kwon *et al.* [70] studied a model with two absorbing states. It undergoes a dynamic phase transition which belongs to directed Ising (DI) universality class when the two absorbing states are symmetric, and belongs to the directed percolation universality class when a symmetry breaking field is introduced. They studied the interface dynamics of the active domain between two asymmetric absorbing states. As one absorbing state dominates over the other, the interface is driven into the unpreferred absorbing region with a constant velocity. Therefore they expected the width of the active domain to scale like the horizontal width of the active curtain in the above setup for ordinary DP models. A simple power-law

fit of their data suggests that the active domain width scales as $W \sim \epsilon^{-x}$ with $x \simeq 2.00(5)$, which does not agree with the DP exponent $\nu_{\|} \approx 1.734$.

In this appendix, we address the same issue more directly. We insert a slanted active wall into the most basic model for DP, the one studied originally by Kinzel and coworkers [67, 33] (see Sec. A.2). We find a similar anomalous value for the width exponent. $W \sim \epsilon^{-x}$ scales as $x \simeq 1.95(5)$. In Sec. A.3, we develop a qualitative scaling theory. It predicts that the curtain width scales with the conventional exponent $\nu_{\|}$ but with an additional logarithmic factor as $W \simeq A\epsilon^{-\nu_{\|}} \ln(\epsilon_0/\epsilon)$. In Sec. A.4, we show that the numerical Monte Carlo data fits this form well. In Sec. A.5, we illustrates how DP-type processes with slanted walls can be studied in the master equation formalism. Our finite-size-scaling (FSS) results, using exact numerical enumeration of the eigenvalue spectrum, show that at p_c, the width of the slanted curtain diverges as $W \sim L^z$ with system size. This confirms the absence of a new independent exponent. The logarithmic factor arises only in the ϵ dependence.

A.2 Numerical results for the curtain width

Consider the square space-time lattice shown in Fig. A.2. All bonds run under 45°. The black (open) circles represent the active (inactive) sites. Time evolves from top to bottom in half units $t \to t + 1/2$. Bonds between nearest neighbor sites at t and $t \to t + 1/2$ are being created with probability p but only if the upper site is active. Each bond activates the lower site. Kinzel studied this model in detail with master-equation-type FSS in the early 1980s [67]. The critical exponents and the location of the DP transition are known quite accurately. For example, the latest series expansion results put the DP phase transition at $p_c \approx 0.6447$ [63].

We modify the boundary conditions in this model to accommodate an active wall. The lattice is semi-infinite, bound to the left by the wall, which runs away under $\theta = 45°$ as shown in Fig. A.2. 45° is its natural angle for the curtain rod for this specific lattice. We can restrict ourselves to this angle because the scaling properties of the curtain width should not depend on the angle according to the anisotropic scaling argument outlined above. Moreover, the angle is a continuous parameter in the model by Kwon *et al.* [70] and

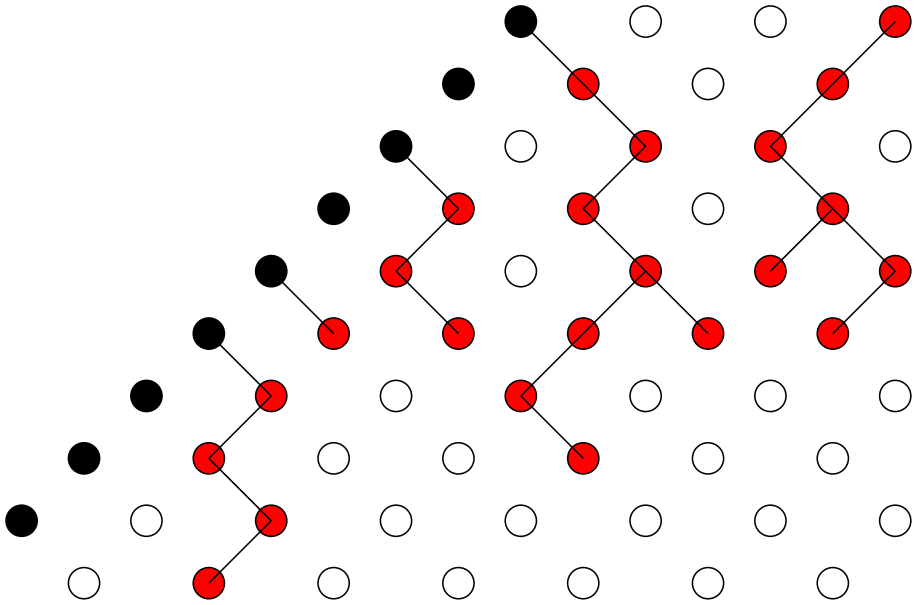

Figure A.2: Lattice structure near the active boundary.

their results show no angle dependence.

We perform Monte Carlo simulations with, as initial configuration, an active wall in an inactive bulk. The horizontal curtain width is defined as the distance of the last active site from the rod in each time slice. For $p < p_c$, the width grows initially approximately linear in time, until it saturates at the stationary state value which varies with $\epsilon = p_c - p$. Figure A.3 shows the active width versus ϵ on a logarithmic scale. The line is quite linear over the two decades shown. The slope is clearly distinct from the expected value $\nu_{\|} \approx 1.734$ and close to the value found by Kwon *et al.* [70]. In Fig. A.4 we perform a more careful FSS analysis of the same data. We fit the numerical data from two nearby points, $\epsilon_2 = \sqrt{2}\epsilon_1$, to the form $W \simeq a\epsilon^{-x}$ and plot x as a function of ϵ, the exponent x appears to be around 1.95. This fit is remarkably stable, and shows virtually no power-law-type corrections to scaling. Taken out of context it is strongly suggestive of a new independent critical exponent. The other curves in Fig. A.4 relate to the FSS analysis assuming an additional logarithmic factor as discussed in the next two sections.

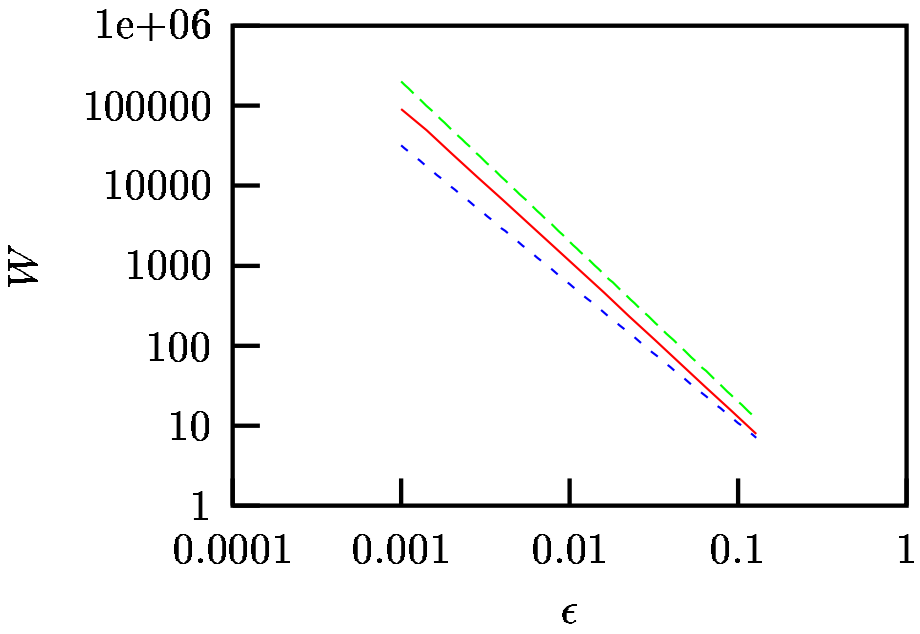

Figure A.3: Log plot of active width versus $p_c - p$ from straight Monte Carlo simulations on unlimited system sizes. The solid line represents the data. The dashed straight lines of slopes -2 and -1.734 are guides to the eyes.

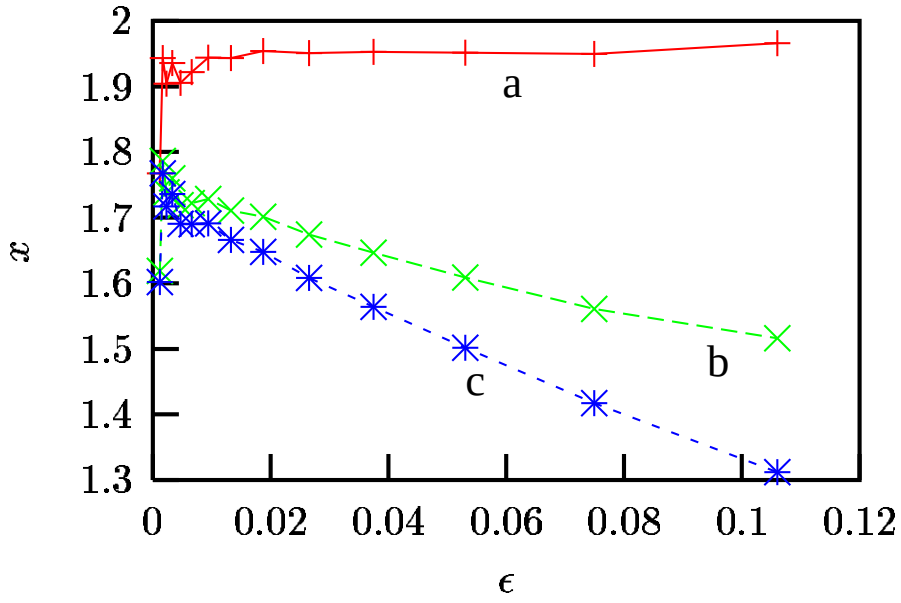

Figure A.4: Estimates for the active width exponent, x. In fit (a), W is assumed to scale as $W \sim \epsilon^{-x}$, in (b), as $W \sim \epsilon^{-x} \ln \epsilon$ and in (c), as $W \sim \epsilon^{-x}(\ln \epsilon + \ln 2)$.

A.3 Independent Cluster Approximation

Figure A.1 shows a typical curtain configuration in a Monte Carlo simulation at a p just below the percolation threshold p_c. The most striking features are the needles in the curtain. Isolated clusters are expected to be needlelike. The correlation length in the time direction diverges faster than in the spatial direction, as $\xi_\parallel \sim \xi_\perp^z$. Therefore, active clusters (when grown from a single seed) become needle shaped near the percolation threshold. Figure A.1 gives the impression that close to p_c, the curtain consists of a set of weakly interacting needle shaped clusters when viewed from length scales larger than $\xi_\perp$.

In this section, we pursue the implications of the assumption that such needles are completely uncorrelated. In that approximation, the probability that the curtain extends over a horizontal distance l is given by the probability that a needle longer than $\tau = l \tan(\theta)$ hangs down from the curtain rod vertically above that site. Let P be that probability. It must have the same form as the survival probability from a single seed [Eq. (A.2)]. The

actual value of the exponent β turns out to be irrelevant in this section, but it must be identical to the single seed value, according to a time reversal symmetry argument (following [19, 56]).

The spatial coordinate needs to be coarse grained, because the needles can only be uncorrelated beyond the horizontal correlation length $\xi_\perp \sim \epsilon^{-\nu_\perp}$. Define $n = x/\xi_\perp$ as the coarse-grained discrete spatial coordinate and recall that $t = x\tan(\theta)$ is the corresponding vertical distance from the curtain rod to the same point. The probability for the curtain to have width n factorizes in the independent needle approximation as

$$P_w(n) = P(n) \prod_{n'>n} \left[1 - P(n')\right]. \tag{A.3}$$

This equation can be rewritten into a derivative form

$$\frac{P_w(n+1) - P_w(n)}{P_w(n+1)} = \frac{P(n+1) - P(n)[1 - P(n+1)]}{P(n+1)}. \tag{A.4}$$

The maximum of the distribution obeys the relation

$$P_w(\tilde{n} - 1) = P_w(\tilde{n}) \tag{A.5}$$

and can be written as

$$\frac{1}{P(\tilde{n})} - \frac{1}{P(\tilde{n} - 1)} = 1. \tag{A.6}$$

Assume that P has the same asymptotic form as the single seed survival probability [in Eq. (A.2)] and that the maximum of the distribution occurs in this range of n. The transformation to the coarse-grained $n = x/\xi_\perp \sim x\epsilon^{\nu_\perp}$ variable changes the critical exponent inside the exponential factor

$$P \simeq B\epsilon^{\beta} e^{-bn\epsilon^{\Delta}}, \tag{A.7}$$

with $\Delta = \nu_\parallel - \nu_\perp$, and $b \sim \tan(\theta)$. Inserting this form into Eq. (A.6) leads to

$$1 - e^{-b\epsilon^{\Delta}} = B\epsilon^{\beta} e^{-b\tilde{n}\epsilon^{\Delta}}, \tag{A.8}$$

and after expanding the exponential on the left hand side, to

$$b\tilde{n}|\epsilon|^{\Delta} \simeq \ln\left(\frac{B}{b}\right) + (\beta - \Delta)\ln(\epsilon). \tag{A.9}$$

In original units this reads

$$\tilde{W} \simeq A\epsilon^{-\nu_\parallel} \ln\left(\frac{\epsilon_0}{\epsilon}\right). \tag{A.10}$$

The characteristic probability depends on the wall angle as $\epsilon_0 \sim 1/\tan(\theta)$. The most probable width $\tilde{W}$ scales with the expected exponent $\nu_\parallel$ but contains an additional logarithmic factor.

Asymptotically, the most probable and the average widths coincide. Equation (A.4) can be approximated in the continuum limit as

$$\frac{1}{P_w}\frac{dP_w}{dn} = 1 - \frac{P(n)}{P(n+1)} + P(n). \tag{A.11}$$

Close to p_c and for large n, where P obeys Eq. (A.7), we can integrate this

$$\begin{aligned} P_w(n) &\sim \exp\left((1-e^{b\epsilon^\Delta})n - \frac{B}{b}\epsilon^{\beta-\Delta}e^{-bn\epsilon^\Delta}\right) \\ &\sim e^{bn\epsilon^\Delta}\exp\left(-\frac{B}{b}\epsilon^{\beta-\Delta}e^{-bn\epsilon^\Delta}\right). \end{aligned} \tag{A.12}$$

This distribution decays exponentially on both sides of the most probable value and becomes sharp at the critical point, $\epsilon \to 0$. We checked explicitly that the most probable and the average coincide in this limit, and scale asymptotically with the same logarithmic factor, as in Eq. (A.10).

A.4 Logarithmic corrections to scaling analysis

The logarithmic factor in the independent needle approximation formula for the curtain width

$$W(\epsilon) \simeq A\epsilon^{-\nu_\parallel} \ln\left(\frac{\epsilon_0}{\epsilon}\right) \tag{A.13}$$

does not change the asymptotic exponent. It is still equal to $\nu_\parallel$. However the finite-size-scaling approach to this value is very singular. A conventional FSS analysis involves the construction of estimates for the critical exponent x by fitting the values of W at to nearby ϵ to a pure power-law form, $W \sim \epsilon^{-x}$. This is equivalent to defining $x(\epsilon)$ as a derivative and it yields the above logarithmic form

$$x = -\frac{\epsilon}{W}\frac{dW}{d\epsilon} = \nu_\parallel + \frac{1}{\ln(\epsilon_0/\epsilon)}. \tag{A.14}$$

This function approaches $\nu_{\|}$ in a singular manner. In the interval $0.01 < \epsilon/\epsilon_0 < 0.3$, x seems to converge convincingly with a linear correction to scaling term to an effective exponent which is about 0.2 too large. One would have to go to extremely small ϵ's to see the true convergence. The power-law fit in Fig. A.4 shows signs of this.

The two other curves in Fig. A.4 show the FSS estimates for the exponent $\nu_{\|}$ according to the form Eq.(A.13) with $\epsilon_0 = 1$ or $\epsilon_0 = 0.5$. ϵ_0 is unknown, but likely of order one. Both curves converge towards the conventional value $\nu_{\|} = 1.734$. This is strong evidence for the presence of the logarithmic factor.

A.5 Finite-size scaling at the percolation threshold

The logarithmic factor originates from the screening of independent needles. It should not play a role in the FSS at the percolation threshold itself, because there $\xi_{\perp}$ diverges, and the independent needle concept becomes meaningless.

So, the curtain width must scale as $W \sim L^z$ at p_c, if it is really true that no independent new exponent is involved. To confirm this, we present in this section numerical data from master-equation-type FSS using exact enumeration. We also performed Monte Carlo simulations but prefer to present our master-equation data since this method requires a technical novelty.

A moving wall is inconvenient in simulations. The lattice is finite by necessity and the moving wall requires a much bigger lattice than the one actually used by the process. This is a handicap in particular for master-equation calculations where one evaluates the rate at which the stationary state is being reached by letting time go to infinity at each lattice size L. Those systems' sizes are typically small ($L \leq 20$ in our case) because phase space scales exponentially with L. Compared to Monte Carlo simulations the master-equation method trades system size for numerical accuracy, and the ability to perform a detailed corrections to scaling analysis. The accuracy of the two methods is typically comparable, except for specific issues, such as the logarithmic factor in the previous sections, which requires intrinsic large lattice sizes.

The solution to the moving wall problem is to distinguish between the time and space

directions of the dynamic process, $\hat{e}_\perp$ and $\hat{e}_\parallel$, and the ones used in the master equation. There is no need for them to coincide. We choose a setup where the time and space directions of the master equation are redirected in the following manner. Lines of constant time are parallel to $\hat{e}_\parallel - \hat{e}_\perp$, such that the moving wall coincides with the $t = 0$ line. Lines of constant position are parallel to the x axis, which in the dynamic process represented lines of constant time.

The following skewed dynamic rule implements this pace-time rotation. Consider a square space-time lattice (Fig. A.2 rotated over 45 degrees). Each site in the master-equation time slice t is updated sequentially from right to left. The probability for site x at time τ to be active depends on whether site $x - 1$ was active at the previous time $t - 1$ and/or at this moment in time, t. This setup requires screwlike boundary conditions. The forest fire runs under an angle. In this new interpretation, the active wall represents a fully active initial configuration.

The energy gap in the spectrum of the time evolution operator (transfer matrix) is related to the curtain width in the following manner. Let $|I\rangle$ be the initial state of the master equation, $|0\rangle$ be the absorbing state, and $\hat{T}$ be the transfer matrix. The stochastic nature of the transfer matrix implies that the disordered state $|D\rangle$ is a left eigenvector with eigenvalue $\lambda_0 = 1$. Define $\hat{a}_x$ as the projection operator which returns one (zero) when site x active (inactive). The curtain width is associated with the probability distribution for site x to be active at time t but after that never again. This takes the form

$$P(x,t) = \lim_{t_F \to \infty} \langle D|[(1-\hat{a}_x)\hat{T}]^{t_F - t}\hat{a}_x\hat{T}^t|I\rangle. \tag{A.15}$$

The operator $(1 - \hat{a}_x)\hat{T}$ has $\lambda_0 = 1$ as largest eigenvalue since

$$(1-\hat{a}_x)\hat{T}]|0\rangle = |0\rangle, \tag{A.16}$$

and because attaching a projection operator to $\hat{T}$ cannot result in an eigenvalue larger than the largest one in $\hat{T}$. Let $\langle L_x|$ be the corresponding left eigenvector (which can be evaluated numerically). Inserting this leads to

$$P(x,t) = \langle L_x|\hat{a}_x\hat{T}^t|I\rangle \simeq \langle L_x|\hat{a}_x|\lambda_1\rangle\lambda_1^t\langle\lambda_1|I\rangle \sim \exp[-t/\xi_t], \tag{A.17}$$

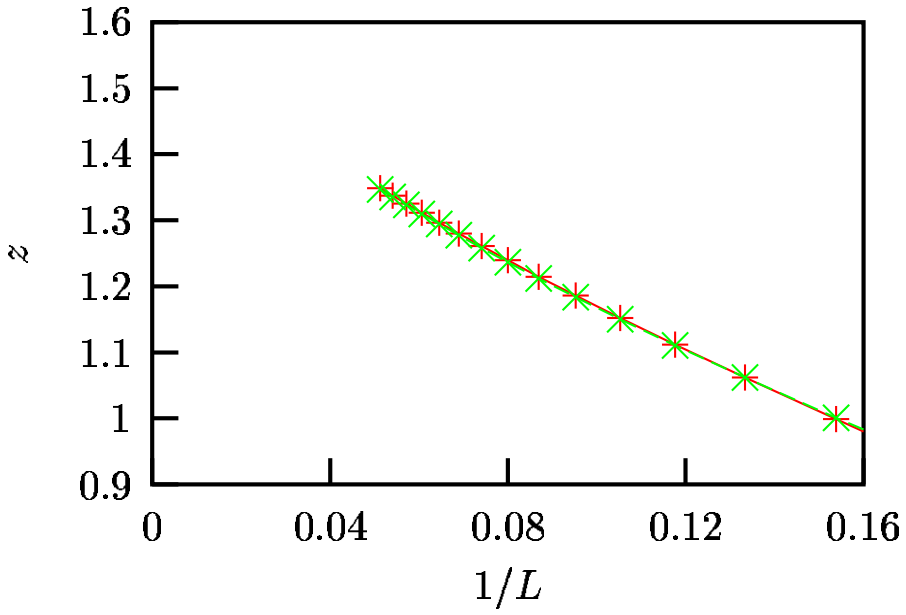

Figure A.5: Finite-size-scaling exponent z for ($\times$) the characteristic active width, $W \sim L^z$, and for ($+$) the time to reach the stationary state, $t \sim L^z$, at the percolation threshold in the transfer matrix setup. The data virtually coincide.

with $\xi_t = \ln(\lambda_1)$ and λ_1 the next largest eigenvalue of $\hat{T}$.

This illustrates that the curtain width scales in the same manner as the the characteristic time ξ_t needed to reach the stationary state, when the latter is measured in this space-time twisted coordinate system. Figure A.5 shows the FSS estimates for the dynamic exponent z according to $\xi_t \sim L^z$ and $W \sim L^z$. Both converge clearly to the DP dynamic exponent $z \approx 1.58$. This confirms that no new independent curtain width exponent is present.

A.6 Final Remarks

The analysis presented in this appendix explains the anomalous scaling of the width of the slanted curtain boundary in DP-type processes. The needles screen each other, and that leads to an extra logarithmic factor according to the independent needle approximation. Our numerical data confirm the validity of this assumption.

The same mechanism must apply to other dynamic processes, like directed-Ising-type absorbing state dynamics, and also to other quantities. Consider the following example. Directed percolation describes epidemic growth processes without immunization, where the probability to be sick at time $t+1$ requires that yourself or at least one of your neighbors is already sick at time t. Consider an initial condition that everybody is sick at time $t = 0$. A stationary local observer will conclude that below the percolation threshold the lifetime of the epidemic scales as $t \sim \epsilon^{-\nu_\parallel}$. A moving observer concludes it diverges faster, as $t \sim \epsilon^{-\nu_\parallel} \ln(\epsilon_0/\epsilon)$.

VITA

Chun-Chung Chen was born and raised in Taiwan. He entered the National Taiwan University in 1988 and graduated in 1992 with a Bachelor of Science degree in physics. After serving as a maintenance officer in the army in Taiwan, he came to the United States and started his graduate work in physics at the University of Washington in 1994. He received a Master of Science degree in 1996 and continued his study at the University of Washington. He earned his Doctor of Philosophy degree in physics in 2002.